Reliability Analysis of Soil Liquefaction using Truncated Distributions

by

SANKALP RAO YERRA

A thesis
submitted to the Faculty of Graduate Studies
in partial fulfilment of the requirements for the
Degree of Master of Science
in

Civil Engineering

Supervisor
Dr. Jian Deng
Associate Professor Dept. of Civil Engineering

Co-Supervisor
Dr. Eltayeb Mohamedelhassan
Professor & Chair Dept. of Civil Engineering

Lakehead University
Thunder Bay, Ontario
May, 2019

Author's Declaration

I hereby declare that I am the sole author of this thesis. This is a true copy of the thesis, including any required final revisions, as accepted by my examiners. I understand that my thesis may be made electronically available to the public.

Abstract

Soil liquefaction is a phenomenon caused by seismic activity in the ground which may result in surface settlement, the formation of sand boils, lateral spreading that ultimately damages the super-structure and loss of lives. This kind of natural disasters has been reported vastly from last few decades in different regions of the world. Soil Liquefaction triggering occurs in silty and sandy soils. The huge damage due to liquefaction at Niigata, Japan, and Alaska due to the earthquake that occurred in 1964, extensively grabbed the attention of many geotechnical researchers. SPT based empirical relationship is usually used to evaluate soil liquefaction. However, a few parameters involved in the analysis are associated with a great extent of uncertainties. A reliability-based analysis provides an approach to consider various uncertainties and provides the probability for the failure of the structure. Due to site conditions and other reasons, it is difficult to obtain complete information about a random variable. Therefore, very often we come across censored samples. It is important that we design an reliable engineering structure based on censored samples.

The primary objective of the research is to perform a reliability analysis based on censored samples. The research focuses on developing the deterministic, probabilistic and reliability-based models to calculate soil liquefaction resistance using historical liquefaction database based on the SPT. The principle of maximum entropy is incorporated to develop

probability density function that includes various uncertainties associated with soil and site parameters.

With the development of computing techniques like artificial intelligence, it is possible to frame the empirical relationship between the seismic load and resistance offered by the soil. Standard penetration test based database of soil liquefaction is used in the artificial neural network to predict the liquefaction index. Further, the developed liquefaction index model is utilized for modeling the empirical relationship between clean sand equivalence corrected standard penetration test-N count and cyclic resistance ratio. The deterministic model is developed, and the relationship for estimating the resistance offered by soil to liquefaction is established by identifying the best fit curve. Bayesian mapping theory is used for determining the function for liquefaction probability. With the knowledge about the expected values from the database, maximum entropy distributions are plotted for seismic, site and soil parameters. The developed probability density function of the random variables are utilized for performing the first order reliability analysis. Using sensitivity analysis, the degree of conservatism is identified and eliminated from performance function. Finally, the calibrated performance function is framed which can be used for performing reliability analysis on truncated samples.

The truncated normal and log-normal probability density function are developed using the information available on censored samples. The parameters of the truncated normal distribution are estimated using maximum likelihood method and Newton-Raphson's iterative procedure. When dealing with censored samples, the flow of iteration points has a limitation in reliability analysis. For this reason, a new algorithm is proposed to identify the reliability index for liquefaction potential based on global search.

Keyword: Soil liquefaction, standard penetration test, artificial neural network, Bayesian mapping, first order reliability analysis, censored samples, truncated normal & log-normal distribution.

Acknowledgements

This thesis becomes a reality and takes a wonderful shape with the kind of support and help of many individual. I would like to extend my sincere thanks to all of them.

I would like to express my special gratitude and thanks to my supervisor **Dr. Jian Deng**, Associate Professor, Department of Civil Engineering for sharing his knowledge and constant guidance throughout the research.

I am highly indebted to my co-supervisor **Dr. Eltayeb Mohamedelhassan**, Professor & Chair, Department of Civil Engineering for imparting his distinguished knowledge and providing excellent suggestions with endorsement in shaping thesis to such awful form.

I would like to express my special thanks of gratitude to the **Dr. Sultan Siddiqui**, Associate Professor, Department of Mechanical Engineering for reviewing my thesis and providing feedback.

I appreciate Sukdeep Singh, Navjoth Kanwar, Dhawan Joshi, Akshay Choudhary and other graduate fellow-mates for their enrich support throughout my master studies.

I would like to express special thanks to my friend Preethi.M for her continuous support at every moment during my hard times.

Finally, I would like to acknowledge with appreciation and gratitude to my parents for providing me with wonderful opportunity to

complete my graduate study and research without their support, I could not have fulfilled my dreams.

Dedicated to my father, ***Dr. Rama Mohan Rao Yerra*** *with love*

Table of Contents

List of Tables

List of Equations

List of Figures

FIGURE **Page**

Nomenclature

Roman

a_{max}	Horizontal peak ground acceleration
c	Modelling uncertainty
c_i	i^{th} central moment
D_r	Relative Density
h	Height of critical depth
g	Acceleration due to gravity
r_d	Stress reduction factor
$E(x)$	Function for expected values
f	Degree of freedom
f_T	Transformation function of the layer
$f(x)$	Probability density function of a continuous random variable
$F(x)$	Cumulative frequency function
F_s	Factor of safety
H	Shannon entropy of random variable
k	Distribution parameter
K_σ	Overburden stress correction factor
M	Magnitude of earthquake on Richter's scale
m_i	Moment of i^{th} order about origin
r	Epicenter distance of the site
R	Range of the random variable

N	SPT-N count
S	Jayne's entropy of random variable
N_1	Normalized SPT-N count
$(N_1)_{60}$	Normalised and corrected SPT-N count
$(N_1)_{60cs}$	Clean sand equivalent normalised and corrected SPT-N count
P_L	Probability of liquefaction
w_c	Water content
C_B	Borehole diameter correction factor
C_E	Energy ratio correction factor
C_N	Normalization factor
C_R	Rod length correction factor
C_S	Correction factor for sampling technique
$K-S$	Kolmogorov-Smirnov Test

Greek

α_1	Coefficient of skewness
α_2	Coefficient of kurtosis
β	Reliability Index
γ	Density of soil
σ	Standard deviation of normal random variable
σ'_{V_0}	Initial effective stress at the interested depth
σ'_v	Effective stress at the interested depth
σ_v	Total vertical stress at the interested depth
σ^2	Variance of the random variable
τ_{max}	Maximum earthquake-induced shear stress
μ	Mean of the random variable
Δu	Increase in pore-pressure

Abbreviation

LL	Liquid Limit
LI	Liquefaction indicator
PI	Plasticity Index
FC	Fineness Content
BPT	Becker Penetration Test
CPT	Cone Penetration Test
COV	Coefficient of Variance
CRR	Cyclic Resistance Ratio
CSR	Cyclic Stress Ratio
SPT	Standard Penetration Test
FCI	Fines Content Indicator
MSF	Magnitude Scaling Factor
PDF	Probability Density Function
PMF	Probability Mass Function
CDF	Cumulative Density Function
$FORM$	First Order Reliability Method
$SORM$	Second Order Reliability Method

Chapter 1

Introduction

Every year the earth experiences a large number of natural disasters like earthquake, tsunami, landslide, floods, cyclone, etc. which occurs around the world. They result in a devastating situations with massive loss of lives and properties, and adverse impact on the environment and economy. On the other hand, due to an increase in demands, shrinking of financial, natural and human resources, it is a more challenging job to maintain and rehabilitate the infrastructure.

According to the 2016 Annual Disaster Statistical report of Centre for Research on the Epidemiology by Guha-Sapir et al. (2016), there were 342 disasters registered in the year 2016, and about 8,733 people lost their lives, whereas 569.4 million people were affected. The estimated economic losses due to these natural disasters in the same year were US$ 153.9 billion, and the total financial loss in North America alone was about US$ 48.08 billion. For the period 2006-2015, the annual average 376.4 of natural disasters was recorded with an average human loss of 69,827 per year. The earthquake in Haiti during the year 2010 took away the life of 222,570 people.

It is crucially important to take effective measures to prevent the

hazard and loss caused by such natural disasters. Reliable engineering approaches can support to reduce the damages to the structure. Reliability-based design aspects can help society to build safe structures that could resist the stress produced by the natural disaster.

1.1 Soil Liquefaction

The phenomenon of soil liquefaction was first investigated by Terzaghi et al. (1996) to know the reason behind a sudden decrease in the strength of the loose sand. Soil liquefaction is a phenomenon in which the pore pressure of the soil increases rapidly than the effective pressure due to high ground acceleration at the time of seismic action leading to softening of the granular soil. Earthquake induces liquefaction by imposing dynamic loads on the saturated sandy soils. The shearing action that takes place in the soil layer tends the soil strata to lose its stiffness and strength because of transformation from solid medium to liquid consistency. i.e., due to the seismic shaking of the ground at a high rate, certain saturated soils transform from firm soil to suspended soil particle with water whose performance is similar to a viscous fluid. Hence it is easy for soil now to deform or flow laterally. In such a situation, the soil fails to support the overlying structure. The ground might displace vertically or horizontally, prevailing the possibilities for the occurrence of landslides or cracks in the ground. It results in a devastating disaster and causing damage to numerous structures.

Usually, the water particles present in the pores of the sandy or silt soil particles will resist the action of soil to consolidate. But at the time of shaking, the ground tends to change its volume by draining out the water from the pores, and therefore the pore pressure raises. The rising action of the water through the small gaps of the soil particle splits them apart. This makes the soil to lose its contact, that weakens the strength

of it. When the same action continues for a number of times, liquefaction starts. This is known as triggering of liquefaction. Effectively, identifying the triggering point for the occurrence of the soil liquefaction will partially solve the problem. If the triggering depth is located, then the engineering designs will support to avoid soil liquefaction.

Liquefiable soils are mostly frictional. They lose their strength when the contact force between the particles dissipates. The resistance to the deformation depends on how tight the soil particles placed. The bearing capacity of the soil is primarily governed by the effective pressure, which is equal to the total external stress less than the internal porewater pressure. The effective stress of the soil is related to the contact force between the internal particles of the soil. Usually, soils with high effective stress are stiff and strong, whereas the soils with low effective stress are soft and weak. Initially, soil resists the load acting on it, and the soil particles are in contact with each other. Therefore the density of the soil is high and the particles contract (decrease in volume, the soil profile is denser). The load action is being taken by the contact forces between the soil particles. It provides strength and stiffness. Shearing loads can modify the volume of soil depending upon the density, confining pressure and shear strain. At the time of high seismic loading (shearing), the load is carried by the granular particles to the pore water filling voids in individual soil particle.

On continuous shearing, the soil particles dilute (increase in volume, soil profile will be loose). With the cyclic increase in the load, the saturated particles cannot come in contract with each other due to the increase in pressure of water in pores. Because of it, the contact force decreases and increase the pore-water pressure. At this stage, the particles start suspending. Soil liquefaction is governed by the degree of saturation. For soil to liquefy, the degree of saturation should be equal

Figure 1.1: Soil liquefaction at Niigata (Vukobratovic and Ladjinovic, 2013)

to 100%. With continuous shearing of the saturated loose soil results in the following effects. They can cause serious damage like landslides, slope failure, structural collapse, the formation of sand buns, etc. The effects of soil liquefaction are as following,

- Strain softening
- Loss of bearing capacity of the soil
- Lateral spreading
- Ground settlement
- Ground oscillation

Soil Liquefaction created catastrophic failure due to the earthquake in Alaska and Niigata, Japan in 1964 (Fig. 1.1). Later in the

Figure 1.2: Building collapse at California due to soil liquefaction in 1989 (National Academies of Sciences et al., 2016)

year 1971, the large settlement of the land took place due to liquefaction that caused the over-topping of a dam. Hyogo-ken Nanbu earthquake in the year 1995 in Japan, damaged the citys port at the city Kobe by the action of soil liquefaction. Liquefaction was experienced at New Zealand by the people of Christchurch in the year 2010-2011 due to the earthquake of magnitude 6.2 (Fig. 1.3). The city had faced the loss of 15,000 single-family homes and hundreds of buildings in the highly commercial region [Guha-Sapir et al. (2016)].

It is important to know about the soil that is susceptible to soil liquefaction. Liquefaction is believed to occur in the loose sands and silts. But with experience of ground failure due to soil liquefaction in low plasticity silt and clay, reported by Chu et al. (2004) and Martin et al. (2006), it indicates that the high seismic loading can trigger the

Figure 1.3: Road damaged due to soil liquefaction at Christchurch, New Zealand (2011) (National Academies of Sciences et al., 2016)

development of strains with the loss in the strength in different kind of soils in wide range from sand to clay. Hence it is evident that the large magnitude earthquake can create liquefaction less prone clay to liquefaction. Based on their research, it is necessary to understand the plasticity behaviour of the fine gained saturated soils.

Before carrying out liquefaction potential evaluation of a region, it is significant to understand the liquefaction susceptibility criteria for silts and clay. Clay will undergo cyclic softening due to the large cyclic stress during ground shaking.

Conventionally, the criteria for the susceptibility of the soil to liquefy includes Chinese criteria which have been developed based on studying the behaviour of the site in China during high seismic action (Wang, 1979). Criteria were developed using Atterberg limits by

differentiated soil type based on United Soil Classification System to determine the ability to liquefy. According to the findings of Seed and Idriss (1982), clayey soils which are less than 15% finer than $5\mu m$ with Liquid Limit (LL) < 35 and water content (w_c) > 90% of LL are vulnerable to liquefaction. Findings of the Andrews and Martin (2000) showed that the soil is susceptible to liquefy if they are 10% finer than $2\mu m$ and LL less than 32, whereas the soil which is ≥ 10% finer than $2\mu m$ and LL ≥ 32 is not susceptible to liquefaction.

According to Boulanger and Idriss (2006), the potential to liquefy of fine-grained soils can be identified with the help of Atterberg limits, grain size characteristics, and natural water content. They can be used in correlations to determine the soil characteristics such as shear strength. This analysis can let us know whether the soil exhibits clay-like or sand-like behaviour. On relating the value of natural water content, the potential for strength loss can be analyzed. But the relation should not be taken as the ratio of w_c to LL.

1.2 Evaluation of Soil Liquefaction Potential

Liquefaction potential of saturated cohesion-less soils is mainly governed by four factors. They are intensity, duration of ground shaking, density and confining pressure of the soil. Evaluation of liquefaction potential of a soil can be performed by the cyclic stress-based approach.

1.2.1 Cyclic Stress Approach

The cyclic stress-based approach for measuring the liquefaction potential of soils was developed by Seed and Idriss (1967). Cyclic Stress Ratio (CSR) induced by the earthquake is compared with the Cyclic Resistance ratio offered by the soil strata at interested depth considered for evaluating the liquefaction potential. The earthquake loading of

shearing force on soil strata can be analyzed using the time-history ground response or using the cyclic stress ratio. The actual method to determine the earthquake-induced cyclic shear stress in soil strata is to perform dynamic response analysis at the site. But this way of estimating is expensive and requires a lot of resources, and hence an effective solution for this problem is "simplified procedure."

The simplified procedure for the determination of uniform cyclic stress ratio was proposed by Seed and Idriss (1971). All the components that influence the cyclic shear stress in the soil induced by earthquake ground motions are analyzes to frame a relationship. The cyclic shear stress ratio at a particular depth with the soil profile is expressed as

$$CSR = 0.65\tau_{max} \tag{1.1}$$

where τ_{max} = maximum earthquake-induced shear stress.

The uniform equivalent cyclic stress ratio is equal to 65% of the maximum cyclic stress ratio. The term τ_{max} is usually estimated from analysis of dynamic ground response. This method of calculating τ_{max} is not generally used because of the following reasons i) it is not economical and requires huge efforts ii) hard to obtain full ground response analyzed data and iii) not compatible to use with an empirical relationship with the in-situ methods. Eventually, simplified empirical relationships are necessary for engineering analysis and design as well as complete field evaluation of earthquake performance for case history analysis.

Vertical cyclic shear waves dominate the horizontal cyclic shear waves in the soil strata, shear stress induced by the earthquake at a particular depth is illustrated in Fig. 1.4. A soil element of the height h behaving as a rigid body is accelerated by the peak horizontal ground

motion a_{max}, then the maximum shear stress of a rigid body is given by

$$(\tau_{max})_{rigidbody} = \gamma h \frac{a_{max}}{g} \tag{1.2}$$

where γ is the unit weight of the soil, and g represents acceleration due to gravity.

Thus by using eq. (1.2), one can calculate the peak shear stress acted upon a rigid body. But of course, the behaviour of the soil is not going to be like a perfectly rigid body because of deformation in soil particles on shearing. Hence for this purpose, it is important to consider the actual mass of the soil which lesser than the theoretical rigid body mass, and this is also one of the reasons for the non-linear behaviour of the complete soil profile. To solve this issue, it is predominate for adjustment to be made in eq. (1.2) that will lead to estimating the actual shear stress acting on the soil profile. The actual shear stress can be represented as

$$(\tau_{max})_{deformablesoil} = r_d(\tau_{max})_{rigidbody} \tag{1.3}$$

where the term r_d is known as the stress reduction factor or nonlinear shear mass participation factor, and the concept is explained in Fig. 1.4 .

It is a function of site stratigraphy, soil properties and the characteristics of ground excitation. On the ground surface, the value of r_d is 1. A increase in depth, its value decreases, and the decrease in the value is not linear and smooth. For differing stiffness, the values of r_d have a vigorous jump. In short, the shear mass participation factor is a function of non-linear system response and harmonics. On establishing eq. (1.3) in terms of stress reduction factor, we get

$$r_d = \frac{(\tau_{max})_{deformable\ soil}}{(\tau_{max})_{rigid\ body}} \tag{1.4}$$

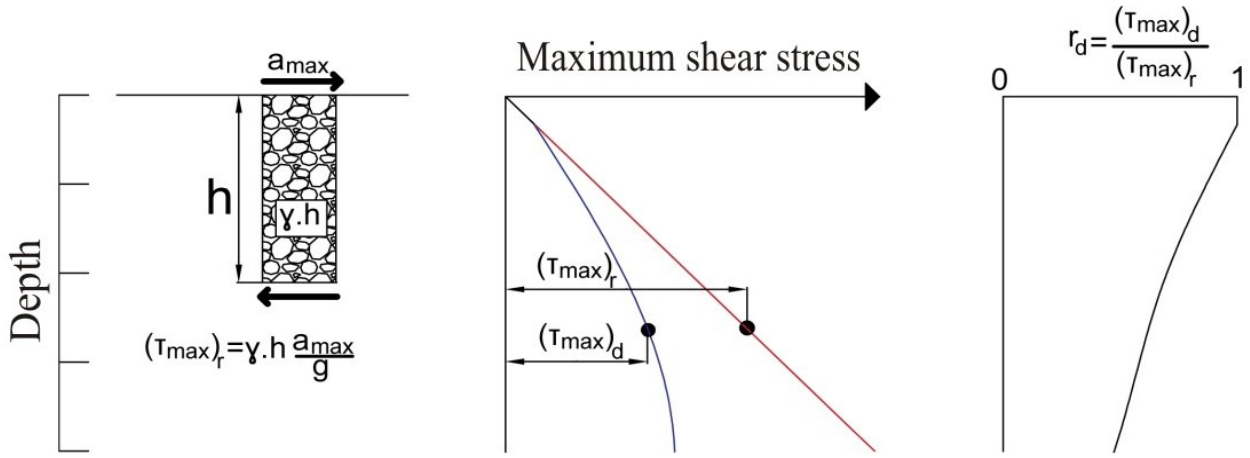

Figure 1.4: Schematic illustration of calculating maximum cyclic shear stress [reproduced based on the idea of Seed and Idriss (1971)]

The maximum shear stress in the soil strata can be written as

$$\tau_{max} = \frac{a_{max}}{g}\gamma h r_d \tag{1.5}$$

The equivalent uniform cyclic shear stress can be re-framed as

$$CSR = 0.65\gamma h \frac{a_{max}}{g} r_d \tag{1.6}$$

The cyclic shear stress of the soil strata can be determined at the laboratory using triaxial test techniques like cyclic triaxial shear, cyclic direct, simple shear, cyclic hollow cylinder torsional shear test, etc. These techniques can provide information about the factors that can cause liquefaction in the site. They are useful in determining the relationships for pore-pressure development before liquefaction and the post-liquefaction behaviour of the soil. In spite of many advantages, these techniques are less practiced by engineers. The following reasons will help in understanding the limitation of the laboratory test.

- It is practically difficult to collect the cohesion-less liquefiable soil samples that could represent the exact field condition.

- These techniques are sometimes time-consuming, and the results cannot be obtained easily.
- The soil samples recovered with thin-walled tubes should have enough plastic fines. In case of soils like fine sand and gravel, they do not have fine content in it. Therefore, they need techniques like ground freezing for sampling.
- The technique of ground freezing is based on the assumption that the unidirectional freezing of the soil pushes the porewater that expands on freezing without disturbing the soil sample, thus preventing the soil from damage and retaining the properties. On continuous freezing for a long time will cause the ice to expand in volume which in turns will cause the soil particles to expand. Therefore, this will require additional aging correction arrangements to be included, to determine the exact cyclic shear stress.
- Collecting the samples using ground freezing or other special techniques and laboratory test requires more funds. Therefore, the laboratory approach is limited to high-value projects.

The limitation of using laboratory procedures can be eliminated by using an in-situ technique like the Standard Penetration Test (SPT). The in-situ procedure for the evaluation of liquefaction potential of the soil proposed by Seed and Idriss (1971) is based on the limit state curve which represents the soil that can undergo liquefaction lie above the curve, and the non-liquefaction soil is found below the curve. The limit state concept provides an effective means for developing the relationship between the Cyclic shear Stress Ratio induced by the earthquake and the Cyclic Resistance Ratio (CRR) offered by the soil.

The resistance offered by the soil reflects the density and pore pressure parameters of the soil. The standard penetration test is the most common in-situ test used for evaluating the consistency of soil in many parts of the world. The idea for using the SPT test as a tool to determine the liquefaction potential of the soil can be seen in the histories right from 1971. Whitman (1971) framed the concept to determine the liquefaction potential of the soil by considering the following parameters: peak ground acceleration, depth of the groundwater table, depth of the critical layer, SPT-N count and the duration of the strong earthquake shaking of 13 different cases from 8 major earthquakes. Seed and Idriss (1971) came up with the simplified procedure based on 35 historical post-liquefaction cases in which 23 cases belongs to liquefied condition and 12 represents the non-liquefied state, for developing the limit state function that isolates the liquefied cases from non-liquefied cases.

Seed et al. (1983) made a modification by using CSR (τ_{av}/σ'_v) instead of maximum shear stress (τ_{max}) for measuring the seismic intensity and normalized SPT value (N_1) based on overburden pressure instead of relative density (D_r). The average cyclic shear stress is developed on the horizontal surface concerning the propagation of vertical shear waves is normalized by initial effective vertical stress σ'_v. Perhaps, geotechnical experts addressed that the different kinds of SPT equipment are being used across the world and hence the efficiency of the model would be varying. Seed et al. (1985) measured the resistance offered by the soil against soil liquefaction in terms of corrected and normalized standard penetration count ($N_{1,60}$). The driving energy in the drill rod is considered to be 60% of the free fall energy and normalization for overburden effect is applied. Liquefaction resistance curves for sands with different fines contents are proposed, which is considered to be more reliable than the previous curves expressed regarding mean grain size. Youd et al. (2001) presented a widely accepted procedure for evaluation of

soil liquefaction potential. Valid recommendations and correlations were developed based on the proposed method of Seed et al. (1985) with slight modification concerning the low cyclic stress ratio. The proposed cyclic stress ratio normalized with respect to vertical effective stress $\sigma'_v$is expressed as

$$CSR_{\sigma'_v} = 0.65\frac{\sigma_v}{\sigma'_v}\frac{a_{max}}{g}r_d \tag{1.7}$$

$$(N_1)_{60} = NC_NC_RC_SC_BC_E \tag{1.8}$$

where N denotes the SPT-N count, C_R represents correction factor for rod length, C_S resembles for correction factor for sampling technique, C_B stands for Borehole correction factor,C_E denotes correction for energy ratio. The values of the correction factors can be found in Table. 1.1. The values of C_R can be determined from the Fig. 1.5. The term C_N denotes normalization factor. Normalization of the SPT counts are made with respect to the effective initial overburden pressure. From eq. (1.8), the normalized and corrected SPT-N count $(N_1)_{60}$ can be calculated.

The CSR value of the soil is adjusted to equivalent CSR for an earthquake magnitude, M = 7.5 and the effect of overburden stress. Therefore, the CSR equaion is expressed as

$$CSR_{M=7.5,\sigma'_v=1atm} = 0.65\frac{\sigma_v}{\sigma'_v}\frac{a_{max}}{g}r_d\frac{1}{MSF}\frac{1}{K_\sigma} \tag{1.9}$$

where MSF stands for Magnitude Scaling Factor and K_σ denotes the overburden stress correction factor. According to Idriss and Boulanger (2006), the relation for determining MSF is given as

$$MSF = 6.9\exp\frac{-M}{4} - 0.058 \tag{1.10}$$

where M means earthquake's magnitude and the overburden stress correction factor is estimated by

$$K_\sigma = 1 - C_\sigma ln\frac{\sigma'_{vo}}{P_a} \leq 1.0 \tag{1.11}$$

Table 1.1: Corrections for SPT (Çetin et al., 2004)

Factor	Equipment Variable	Term	Correction
Overburden pressure	-	C_N	$(Pa/\sigma'_{vo})^{0.5}$
Overburden pressure	-	C_N	$\lim C_N \leq 1.6$
Energy Ratio	Donut Hammer	C_E	1.1-1.4
Energy Ratio	Donut Hammer	C_E	0.3-1.0
Energy Ratio	Safety Hammer	C_E	0.7-1.2
Energy Ratio	Automatic-trip Donut-type Hammer	C_E	0.8-1.4
Borehole Diameter	65-115 mm	C_B	1.0
Borehole Diameter	150 mm	C_B	1.05
Borehole Diameter	200 mm	C_B	1.15
Sampling Method	Standard sampler	C_S	1.0
Sampling Method	Sampler without liners	C_S	1.1-1.3

where

$$C_\sigma = \frac{1}{18.9 - 2.55\sqrt{(N_1)_{60}}} \tag{1.12}$$

P_a represents the reference pressure of 100 kN/m^2. Robertson and Wride (1998) and Youd et al. (2001) have proven the importance of considering the "clean-sand" equivalence SPT-N count ($(N_1)_{60cs}$) instead of $(N_1)_{60}$ and fineness content. Since the liquefaction occurrence depends on the presence of fineness content as discussed above, the SPT-N count can be converted into clean-sand equivalence SPT-N values. The $(N_1)_{60cs}$ is calculated from the recommended relationship of Youd and Noble (1997), and it is given as

$$(N_1)_{60} = \alpha + \eta(N_1)_{60} \tag{1.13}$$

where α and η are the coefficients and can be determined using following

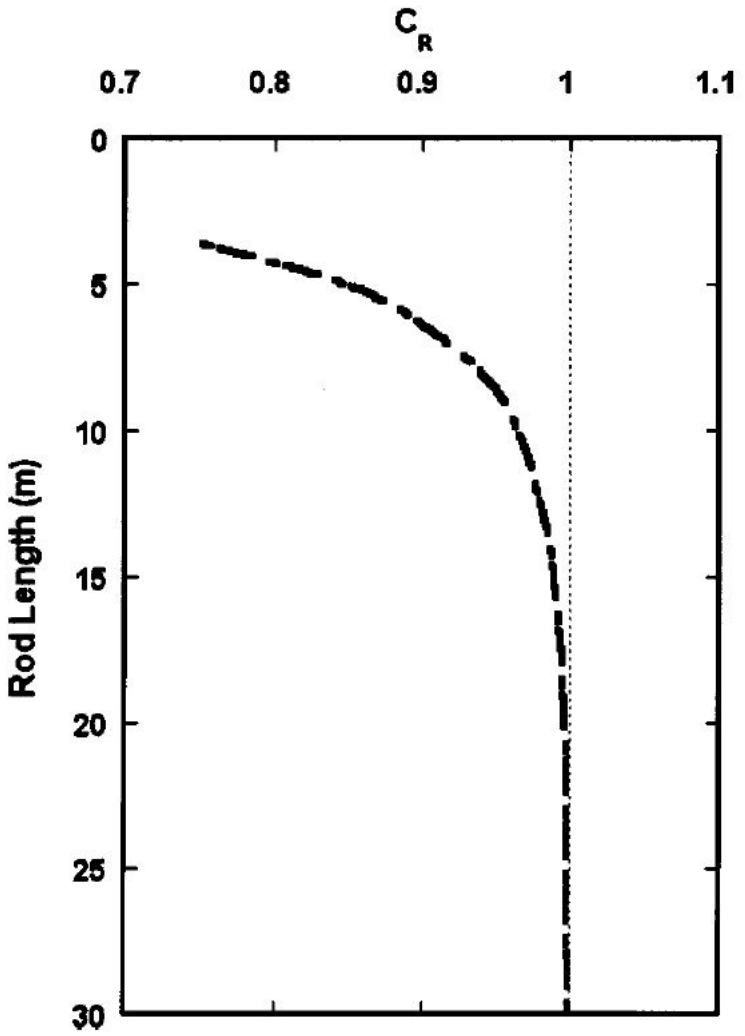

Figure 1.5: Correction for rod length C_R (Çetin et al., 2004).

equation

$$\alpha = 0 \quad \text{for} \quad FC \leq 5\%, \tag{1.14}$$

$$\alpha = exp[1.76 - \frac{190}{FC^2}] \quad \text{for} \quad 5 < FC < 35\%, \tag{1.15}$$

$$\alpha = 5.0 \quad \text{for} \quad FC \geq 35\%, \tag{1.16}$$

$$\eta = 1.0 \quad \text{for} \quad FC \leq 5\%, \tag{1.17}$$

$$\eta = [0.99 + (\frac{FC^{1.5}}{1000})] \quad \text{for} \quad 5 < FC < 35\%, \tag{1.18}$$

$$\eta = 1.2 \quad \text{for} \quad 5 < FC < 35\%. \tag{1.19}$$

The thesis focus on developing soil liquefaction potential model using cyclic stress approach using SPT based on the latest historical database.

1.2.2 Role of ANN in Evaluation of Soil Liquefaction

The Artificial Neural Network (ANN) has been used as a tool to model a cause-effect relationship in geotechnical engineering by many researchers. Functioning of the ANN model is similar to the neuron in the human brain. The neurons are trained to identify the pattern through which it can make classification among the data types. The classification of data type is possible because of the development of the interlinked relationship between the neurons. ANN provides the advantage over the traditional analysis using the statistical tools that require prior knowledge on the cause-effect relationship. From the works of Deng et al. (2005), and Deng (2006), the implicit performance function developed using ANN can be used for reliability analysis. Goh (1994) implemented the ANN technique for developing the predicting model for liquefaction using the earthquake data from 1891 to 1980. Agrawal et al. (1997) developed ANN models to investigate the susceptibility of the soil towards liquefaction based on the penetration test. Juang and Chen

(1999) developed a model to predict the occurrence of liquefaction with the help of the CPT database based on ANN technique using "C-like" programming language. The authors recommended that the Levenberg-Marquardt algorithm is highly efficient in the training of the neurons. Juang et al. (2000b) established the limit state boundary curve using the relationship developed with the help of ANN based on the SPT-database of post-performance liquefaction cases, In their model, the input parameters are normalized between the value 0 and 1 so that the input data would fit for the operation of log-sigmoid function whose limit is between 0 to 1. Samui and Sitharam (2011) investigated the soil susceptibility of the soil for liquefaction using the ANN technique but they recommended to use the tan-sigmoid function whose limit is -1 to 1.

With the help of the ANN technique, the relationship for resistance offered by the soil against soil liquefaction can be developed. ANN provides better results for the normalized data than the original data. Juang and Chen (2000) explained that the normalization of the training set to values between 0 and 1 could provide good results. The normalization procedure is as following

$$x_{norm} = \frac{(x + a)}{b} \tag{1.20}$$

where

$$a = \frac{(x_{max} - 9x_{min})}{8}$$

$$b = \frac{x_{max} - x_{min}}{0.8}$$

x is the input parameter, x_{max} and x_{min} are the maximum and minimum value of the input parameter, respectively.

Hence from the work of the above authors, it can be concluded that the ANN technique can be adopted for developing the limit state curve based on historical post-liquefaction database. On further optimization

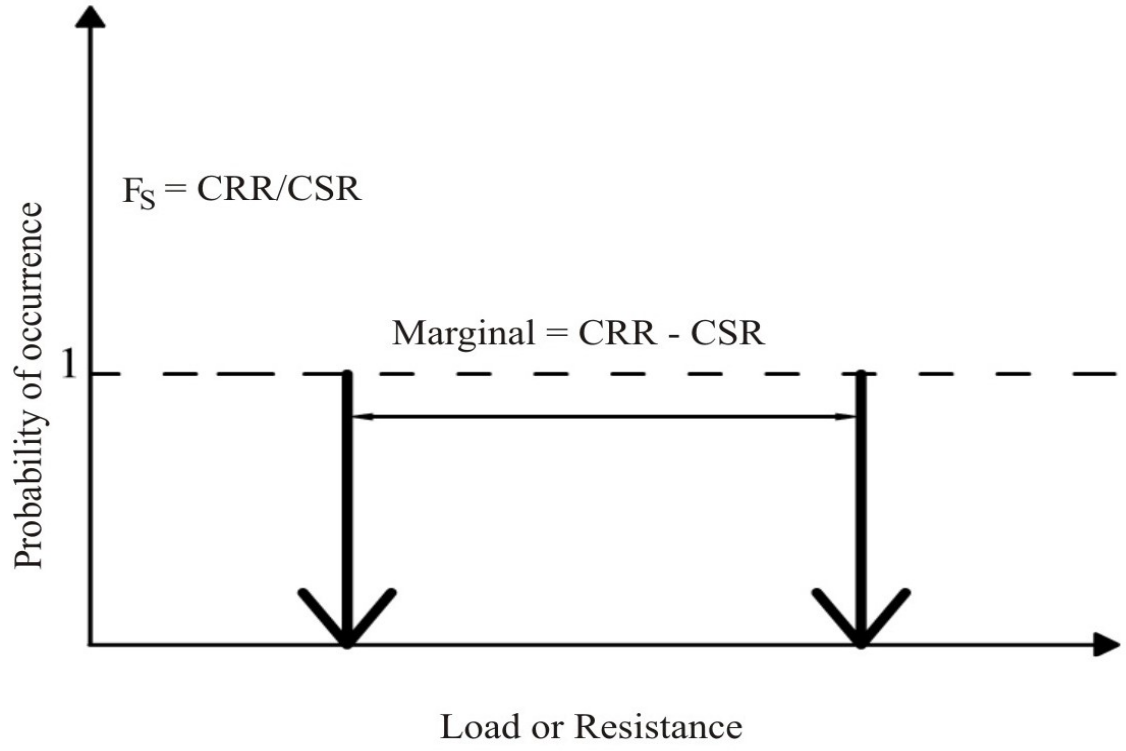

Figure 1.6: Deterministic approach for liquefaction potential evaluation

of the ANN relationship, the empirical relationship for Cyclic Resistance Ratio (CRR) can be developed.

1.2.3 Factor of Safety for Soil Liquefaction

The factor of Safety (F_s) against soil liquefaction is defined as the ratio of CRR to CSR. If $F_s \leq 1$, it refers to liquefaction state and apparently if $F_s > 1$, reflects to non-liquefaction condition. A single value for F_s is calculated based on the mean values of the CSR and CRR. This approach is known as the deterministic approach, and it is based on the assumption that there is 100% probability of occurrence of calculated CRR and CSR. Fig. 1.6 represents the idea of the deterministic approach in the evaluation of soil liquefaction.

Even though, this approach does not provide adequate

information about the behaviour of various random variables that causes liquefaction, it is still much practiced by many geo-technicians due to its simple mathematical approach with the minimum requirement of time and resources. Deterministic method for the evaluation of liquefaction potential is the "Simplified procedure" developed by Seed and Idriss (1971), which was later modified for improving the usage of in-situ test by Seed et al. (1983), Seed et al. (1985), Robertson and Campanella (1985), Robertson and Wride (1998). National Center for Earthquake Engineering Research (NCEER) workshop, 1998, has addressed reviews and recommendations for an in-situ test-based deterministic approach for determination of liquefaction potential. The factor of safety based on the idea of a deterministic approach has very less efficiency and does not truly represent the behaviour of the soil during liquefaction. The limitation of the deterministic approach is that it solely uses only the expected mean value and neglects the true nature of soil variable in the site.

1.3 Probabilistic Approach

There is an existence of the high degree of uncertainty present in the soil variables. When analyzing the behaviour of the soil strata for any engineering system, it is necessary to consider the uncertainty in every aspect. Instead of just mean values, set of all possible expected values should be considered, and the Probability Density Function (PDF) should be developed based on expected values. It is required to select the best PDF based on a certain goodness-fit test.

1.3.1 Uncertainty in Soil Parameters

It is the measure of imperfect knowledge, or probable error arises in the data collection process, modeling and analysis of engineering

system or prediction of a process. Natural uncertainties like climate, seismic, geologic, hydrologic and structural can be grouped as intrinsic variability of a system. Therefore, the performance indicators of the system can vary based on the different set of the input sequence. Uncertainty is central for the decision making and risk assessment of the system. The main question of safety or reliability in any engineering arises because of the presence of uncertainty, and so it cannot be eliminated. For limiting the uncertainty in the system, huge resources are required. This is practically not feasible and hence modeling and analyzing by considering the uncertainty is a better idea than ignoring it. Uncertainty analysis is a measure of statistical properties of the output concerning the statistical input parameters. This helps in the determination of the contribution of each input parameter to the overall uncertainty of the model output. Uncertainty in a system can be classified into two categories

- Intrinsic - results due to the presence of randomness in nature.
- Epistemic - prevails due to lack of knowledge of the system.

1.3.2 Quantification of Randomness in Soil Variables

Moments of distribution are developed from set of expectation. They explain the characteristics of the distribution. Let us consider g(x) be any function for a continuous random variable x; the expected value can be defined as

$$E[g(x)] = \int_R g(x)f(x)dx \tag{1.21}$$

where $f(x)$ represents probability density function and R is the domain for existence of continuous random variable. $E[g(x)]$ represents function for set of expected value based on the constraint function. In order to determine a number of expected values for a range of continuous random

variable, the series of moments can be estimated by evaluating following equation

$$m_i = E(x^i) = \int_R x^i f(x) dx \quad i = 0, 1, 2, ..., n \tag{1.22}$$

where i represents the order of moments and m_i is known as the i^{th} moment of the sample. The moments of the distribution can be estimated from the observed range of the random variable $(x_1, x_2, x_3, \ldots, x_n)$. The moments which are defined concerning the mean are known as central moments. Mean, and variance provides information on the location and variability (spread, dispersion) of a set of numbers, and they give information on the appearance of the distribution of the random variable. They are known as the first two statistical moments of the distribution. Variance is incorporated in the distribution as the standard deviation. Fig. 1.7 illustrates the probability distribution considering the first two statistical moments about the central moments. The third moment about the mean is called as 'skewness' that speaks about the symmetry of the density function. The fourth moment about mean is called as 'kurtosis' which explains the flatness (peakness) in the distribution. Third and fourth moments about the mean are incorporated in the distribution as the coefficient of skewness and coefficient of kurtosis, respectively. The first central moment or mean (μ) of the sample can be determined by

$$\mu = \frac{1}{n} \sum_{k=1}^{n} x_k \tag{1.23}$$

Whereas the second central moment or variance can be calculated by

$$\sigma^2 = \frac{1}{n-1} \sum_{k=1}^{n} (x_k - \mu)^2 \tag{1.24}$$

In order to acquire more information about the distribution, higher order of the central moments can be estimated using the following expression

$$c_j = \frac{1}{n} \sum_{k=1}^{n} (x_k - \mu)^j \tag{1.25}$$

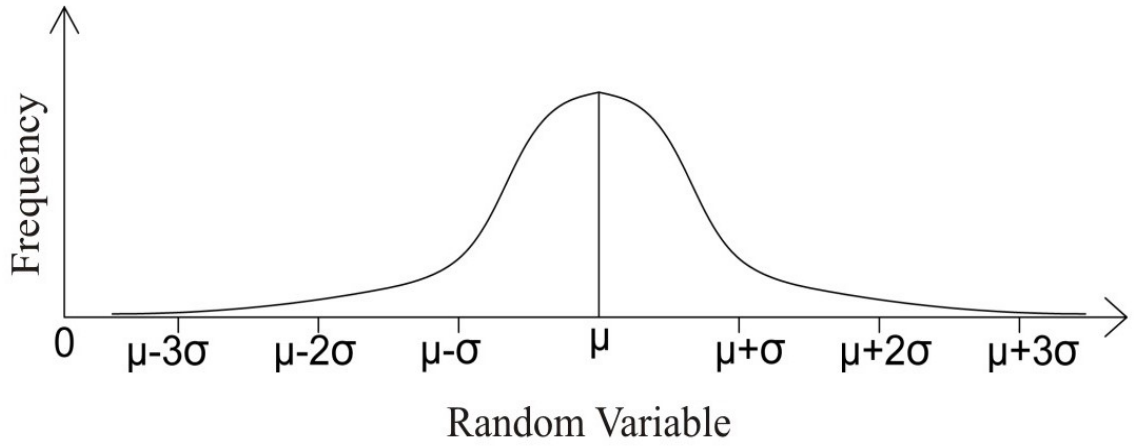

Figure 1.7: Probability distribution based on moments about the expected mean

where c_j represents the higher order of central moment whereas j is greater than 2.

The general definition for central moments for a continuous random variable x can be given as

$$c_i = E[(x-\mu)^i] = \int_R (x-\mu)^i f(x)dx \tag{1.26}$$

The coefficient of skewness can be related to the third moment and it be expressed as

$$\alpha_1 = \frac{c_3}{\sigma^3} \tag{1.27}$$

Similarly coefficient of kurtosis can written as

$$\alpha_2 = \frac{c_4}{\sigma^4} \tag{1.28}$$

The moments of the distribution can also be calculated about the origin. The mean of the distribution lies at the origin (zero). Standard normal distribution whose mean is zero, and the standard deviation is one is the best example for probability distribution based on moments at the origin. Fig. 1.8 illustrates the distribution based on the moments about the origin.

The moments about the origin for a continuous random variable x can be estimated by

$$m_i = \int_R x^i f(x) dx \tag{1.29}$$

where i represents i^{th} order. For the discrete range n of random variable x, the moments at the origin can be calculated by

$$m_j = \frac{1}{n} \sum_{k=1}^{n} x_k^j \tag{1.30}$$

The zeroth general moment is the integration of the PDF of the random

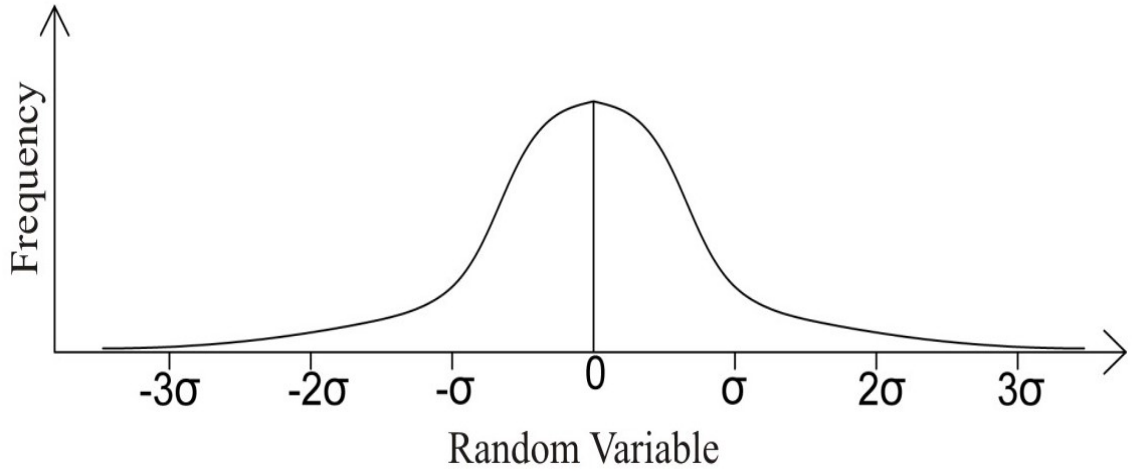

Figure 1.8: Probability distribution based on the moment about the origin

variable. Therefore, the zeroth moment is one ($m_0 = 1$). With the help of the binomial theorem, the relationship between the moments about the central and origin can be developed. It can be used for the transformation of moments and domains between the central and origin. The relationship is as following

$$E[(x-\mu)^i] = \sum_{j=0}^{i} (-1)^j \frac{i!}{j!(i-j)!} \mu^i E(x^{i-j}) \tag{1.31}$$

Therefore,

$$c_i = \sum_{j=0}^{i} (-1)^j \frac{i!}{j!(i-j)!} \mu^i m_{i-j} \tag{1.32}$$

where c_i represents central moments, m denotes moment about origin and i represents the order of moment.

The moments of a distribution can be related with the moments of its transform based on the domains from the original upper bound u and lower bound l to 0 and 1. Let the transformed variable be x', the transformed moments be c'_i, the transformed density function be denoted as $f'(x')$ and the original limit be R. The variable transformation is given by

$$x' = (x - l)/R \tag{1.33}$$

The first moment of the transformation is given by

$$c'_1 = (c_1 - l)/R \tag{1.34}$$

The density function transformation is given by

$$f'(x') = f(x)/R \tag{1.35}$$

By definition,

$$c'_i = \int_0^1 (x^i - c'_1) f'(x') dx' \tag{1.36}$$

By the substituting eq. (1.33) and eq. (1.34) in above equation, we be get

$$c'_i = c_i/R^i \tag{1.37}$$

The domain about origin λ' can be transformed to domains about the original limits λ as

$$\lambda_0 = ln\ R + \lambda'_0 - \sum_{i=1}^{m} (\frac{l}{m})^i \lambda'_i \tag{1.38}$$

$$\lambda_i = \sum_{j=i}^{m} (-1)^(i+1) \frac{j! l^{j=1}}{i!(j-i)! R^j} \lambda'_j \ i = 1, 2, ..., m \tag{1.39}$$

With the help of the moments, the PDF for any soil variable can be generated. Commonly used PDF for soil variables are normal and

lognormal distribution. Once the PDF is developed, it is highly important to check the hypothesis. This can be done using a statistical test like K-S test.

K-S test examines the relationship between the observed cumulative frequency and the CDF of the statistical distribution selected for the random variable. The test begins with sorting the values of the random variable, undrained shear strength in the present case in ascending order. Later, the maximum difference between the two cumulative distribution functions of the ordered data is estimated using the expression,

$$D_n = max|F_x(x_i) - S_n(x_i)| \tag{1.40}$$

where n stands for number of sample count of the random variable, $F_x(x_i)$ represents the CDF of the statistical distribution of the i^{th} sample of the sorted collection space x_i and the term $S_n(x_i)$ denotes the CDF of the observed ordered sample. $S_n(x_i)$ can be estimated by,

$$S_n(x_i) = \begin{cases} 0, & x < x_1 \\ \frac{m}{n}, & x_m \geq x \geq x_{m+1} \\ 1, & x \leq x_n \end{cases} \tag{1.41}$$

The significance level is related with the CDF of the random variable D_n as

$$P(D_n \geq D_n^{\alpha}) = 1 - \alpha \tag{1.42}$$

D_n^{α} values for various significance levels α can be determined using K-S test table. If the maximum difference D_n is less than or equal to the value of D_n^{α}, then the statistical distribution is accepted at that particular significance level α.

1.3.3 Principle of Maximum Entropy

One of the major issues in probabilistic design is the generation of the probability distribution from the set of information available. Conventionally, engineers would deal with a particular type of distribution for certain parameters with the assumption that the distribution would be the best fit for the engineering data.

An alternative method for determination of potential distributions comes from the method of maximum entropy. According to Jaynes principle, entropy was defined as the minimally prejudiced probability distribution is that which maximizes the entropy subject to constraints supplied by the given information(Jaynes, 1957).The entropy for continuous random variable as

$$S = -\int_R f(x) * Ln[f(x)]dx \tag{1.43}$$

where $f(x)$ stands for PDF of continuous random and R is the domain for the existence of continuous random variable. The distribution for the random variable can be generated using available engineering information. The concept of entropy can be explained mathematically by considering the Shannon principle for maximum entropy or informational entropy as

$$Maximize\, H = -\int_0^\infty f(x)Ln(f(x))dx \tag{1.44}$$

subjected to

$$G = \int_0^\infty x^i f(x) = \mu_i \quad i = 0,1,2,...,m \tag{1.45}$$

Here x^i is the moment at the origin, μ_i is the set of expectations and i stands for moment order from 0 to m. Thus, entropy is a measure of the amount of uncertainty represented by the probability distribution and is a measure of the amount of chaos or the lack of information about the soil characteristics values. To develop an appropriate probability distribution

for any random variable, the entropy of itself should be maximized. The nature of eq. (1.44) is to maximize the probability of the random variable. For particular data of a random variable, there might be many distributions suitable, but the distribution that has the highest entropy is considered to be a consistent distribution.

1.3.4 Probabilistic Approach in Soil Liquefaction

In the deterministic approach, when $F_s \geq 1$ does not completely represent the non-liquefaction condition, there are possibilities for the occurrence of liquefaction in the site. Similarly, in case of $F_s < 1$ there are possibilities for no liquefaction. This is because of not considering the variability associated with the loading CSR and resisting CRR parameter.

The idea behind the probabilistic approach can be demonstrated using Fig. 1.9. If $F_s > 1$, it resembles to be non-liquefaction condition. But on observing the same figure, the red shaded region shows that the load is greater than the resistance, and hence there are chances for the occurrence of liquefaction in the site. The statistical analysis based on the SPT-based limit state curve proposed by Seed and Idriss (1971) was utilized by Haldar and Tang (1979) to determining the probability of liquefaction (P_L). Fardis and Veneziano (1981) developed a model to determine the liquefaction potential in the sand using the idea Bayesian regression technique for 192 cyclic simple shear tests considering the uncertainties caused by the effect of sample preparation, the effect of system compliance, and stress non-uniformities. Liao et al. (1988) framed maximum likelihood estimation probabilistic regression-based models using post-liquefaction field performance database of Seed et al. (1984) for determining relationship for probability of liquefaction with respect to parameters like distance to earthquake, peak horizontal acceleration at the ground surface, normalized CSR, depth of ground water table, total

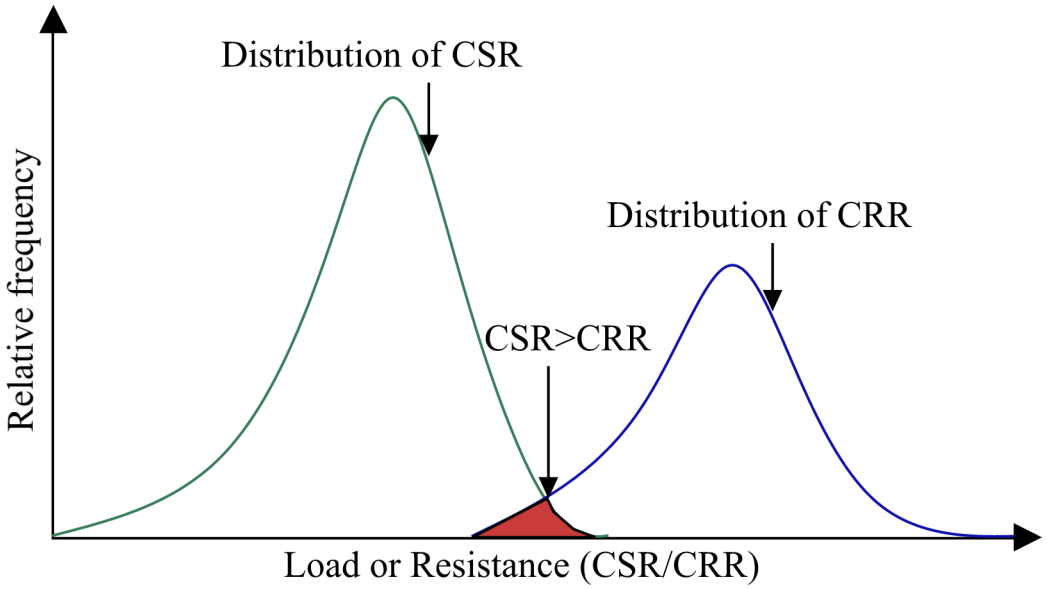

Figure 1.9: Probabilistic approach in evaluation of liquefaction potential [modified from Baecher and Christian (2005)]

vertical pressure, effective vertical pressure, corrected SPT N-count, fineness content and other soil size characteristics. Hwang and Lee (1991) developed a procedure to evaluate liquefaction potential with the help of the probability matrix and a fragility curve developed using moment magnitude by including uncertainties for the site as well as seismic parameters. The approach gives the probability of liquefaction based on significance. Youd and Noble (1997) followed up with the similar techniques of practicing the probability based logistic regression of Liao et al. (1988) with limiting the historical cases which hard to provide clarification for questionable cases. The relationship is proposed for general soil like silt and sand, but not based on the "clean" sand.

Toprak et al. (1999) also used binary-logistic regression analyses for post-liquefaction field performance data from Liao et al. (1988) to develop empirical equations for assessing P_L. Weighting factors

techniques were practiced for certain parameters before using the logistic regression. Juang et al. (2000b) used about 243 liquefaction field performance cases to develop a Bayesian mapping function that establishes a relationship between F_s and P_L. Using 141 cases out of 243, the soft-intelligence technique was utilized to develop the relationship for the deterministic method. Juang et al. (2002) suggested that the idea of implementing Bayesian mapping function approach for P_L evaluation is an appropriate technique compared to probabilistic (binary-logistic) regression-based approach. The reason behind it is that developing expression for P_L based on logistic regression approach has the least dependency on the deterministic models developed using the performance databases whereas P_L developed using Bayesian mapping function technique depends on the characteristics of considered deterministic model. Çetin et al. (2002) developed a likelihood function based on probabilistic methodology, for predicting the P_L by considering both aleatory and epistemic uncertainties. Çetin et al. (2004) used the similar idea of Toprak et al. (1999) of the probabilistic regression model for SPT database of 201 field performance data which were categorized into different classes based on the quality of data available. Boulanger and Idriss (2012) made use of the maximum likelihood function with the limit state developed by Çetin et al. (2002) along with biasing and sensitivity screening techniques for the developing liquefaction potential evaluation for probabilistic approaches. The empirical relationship is based on the performance field database of Idriss and Boulanger (2010) and Boulanger et al. (2011).

Out of the above-mentioned models, Bayesian mapping function makes more sense in developing the probabilistic relationship due to its strong dependence on the deterministic model. Thus, it provides with an effective approach for an easy transition of deterministic to probabilistic design.

1.4 Reliability Approach

The probabilistic approach includes the uncertainties of the soil parameters as a whole that is present on the site. Another limitation of the probabilistic approach is that the parametric and the modeling uncertainties are not dealt with for the estimation of P_L, and therefore, the resultant P_L leads to an erroneous prediction. Reliability approach includes the uncertainty present in the soil parameter in individual strata and analyses individual soil strata separately. Hence the system is analyzed more accurately, and results are much reliable. The reliability analysis can be done using the following method

- First Order Second Moment Reliability Method [FOSM],
- First Order Reliability Method [FORM],
- Second Order Reliability Method [SORM],
- Monte Carlo Simulation Method [MCSM].

The results of FOSM purely depends on the structure of performance function. Any changes made in the structure of performance function reflects the results of the analysis in high extend. SORM requires information on second-order derivatives of the random variable ion the performance function which increases the complexity of analysis. Jha and Suzuki (2009) made comparative studies on reliability methods for evaluation of liquefaction potential using the FOSM method, Hasofer-Lind's FORM, point estimate method and Monte Carlo simulation method. It was reported that the Monte-Carlo simulation is not commonly used for determining the probabilities of liquefaction and hence generally not preferred due to its complexities. From the works of Low and Tang (1997), Çetin (2000), Muduli and Das (2015) and

Bagheripour et al. (2012), it is understood that the FORM produces good results and hence principle ideas of FORM is implemented in present study of soil liquefaction potential.

1.4.1 Hasofer-Lind's First Order Reliability Analysis

Once the consistent distributions for random variables are identified, the system can undergo reliability analysis. In reliability analysis, both the CSR and CRR are taken to be uncertain, and the interaction between the uncertainties is analyzed. Reliability performance of a system is expressed regarding the reliability index (β), through which the probability of liquefaction can be estimated. The liquefaction state in the reliability analysis does not resemble true catastrophic failure, but it reflects expected failure. Hasofer-Lind's FORM is a stochastic approach in which random values for CSR and CSR are used to locate the minimum distance of the limit state curve from the origin. It is one of the most popular and efficient reliability analysis method (Liu and Der Kiureghian (1991), Haldar and Mahadevan (2000), Baecher and Christian (2005)). FOSM is inconsistent with the variability of the performance function relationship and does not include the performance of variance in the analysis due to which FORM method is preferred vastly. The conceptual description of FORM is presented below.

The factor of safety for soil liquefaction is given as $F_s = CRR/CSR$. If $CRR/CSR > 1$, the site is meant to be safe from liquefaction but eventually when $CRR/CSR < 1$, it is unsafe. Taking CRR as R and CSR as S, the marginal difference is given as

$$Z = R - S \tag{1.46}$$

If $Z > 0$, it indicates that liquefaction will not occur and if $Z < 0$, then it hints for the occurrence of liquefaction and hence to be unsafe. Therefore,

the performance of the boundary surface is defined at $Z = 0$. Eq. (1.46) can be also be written as

$$\mu_Z = \mu_R - \mu_S \tag{1.47}$$

where μ_R and μ_S are the mean values of resistance and load, respectively. Considering the load and the resistance to be normal variables. On treating the variables R and S to be uncertain and correlated, then the reliability index is given as,

$$\begin{aligned} \beta &= \frac{\mu_Z}{\sigma_Z} \\ &= \frac{\mu_R - \mu_S}{\sqrt{\sigma_R^2 + \sigma_S^2 - 2\rho_{RS}\sigma_R\sigma_s}} \end{aligned} \tag{1.48}$$

Here ρ_{RS} is the correlation coefficient between R and S. The term σ_R^2 and σ_s^2 are the variance of R and S, respectively that can be calculated using the corresponding standard deviation σ_R and σ_s. If the variable R and S are not having any correlation, then the β is expressed as,

$$\begin{aligned} \beta &= \frac{\mu_Z}{\sigma_Z} \\ &= \frac{\mu_R - \mu_S}{\sqrt{\sigma_R^2 + \sigma_S^2}} \end{aligned} \tag{1.49}$$

The definition of the reliability index from eqs. (1.48) and (1.49) is similar to the reliability index of FOSM. Therefore, the probability of failure (i.e., probability for occurrence of soil liquefaction, P_L) can be calculated using

$$p_f = P_L = \mathbf{\Phi}(-\beta) = 1 - \mathbf{\Phi}(\beta) \tag{1.50}$$

where $\mathbf{\Phi}$ denotes the cumulative density function of the standard normal variable. In the event, if the load and resistance are following non-normal distribution, they can be transformed to standard normal variable using the technique developed by Rackwitz and Fiessler (1978)

$$\sigma' = \frac{\phi[\Phi^{-1}F(x^*)]}{f(x^*)} \tag{1.51}$$

$$\mu' = x^* - \sigma' \Phi^{-1} F(x^*) \tag{1.52}$$

where $\mu'$and σ' means the equivalent standard mean and standard deviation, $f(x^*)$ and $F(x^*)$ represents the probability and cumulative frequency of the non-normal random variable x^*, respectively. The term ϕ denotes the cumulative density function of the non-normal random variable. According to Shinozuka (1983), the accuracy and consistency of reliability index are better with Hasofer-Lind reliability analysis for dealing with the safety of quantities. To avoid the complexity in the analysis, the variables are transformed into standard space with zero mean and unit standard deviation. The analytical procedure to calculate the standard space variable is expressed as

$$\begin{aligned} R' &= \frac{R - \mu_R}{\sigma_R} \\ S' &= \frac{S - \mu_S}{\sigma_R} \end{aligned} \tag{1.53}$$

The performance function for the uncorrelated variables can be written as

$$Z = R - Q = R'\sigma_R - S'\sigma_S + \mu_R - \mu_S \tag{1.54}$$

The origin is the point at which both R and S equal to their mean value and the distance d between the origin and the limit state curve is given as

$$d = \frac{\mu_R - \mu_S}{\sqrt{(\sigma_R^2 + \sigma_S^2)}} \tag{1.55}$$

Eqs. (1.49) and (1.55) appear to be similar, and hence the reliability index of a system can be interpreted geomerically as the shortest distance between the point defined by the expected values of the various random variable involved in the liquefaction potential evaluation and the limit state boundary curve. Fig. 1.10 represents the PDF of the performance function with linear failure criterion denoted by a dark plane, whose

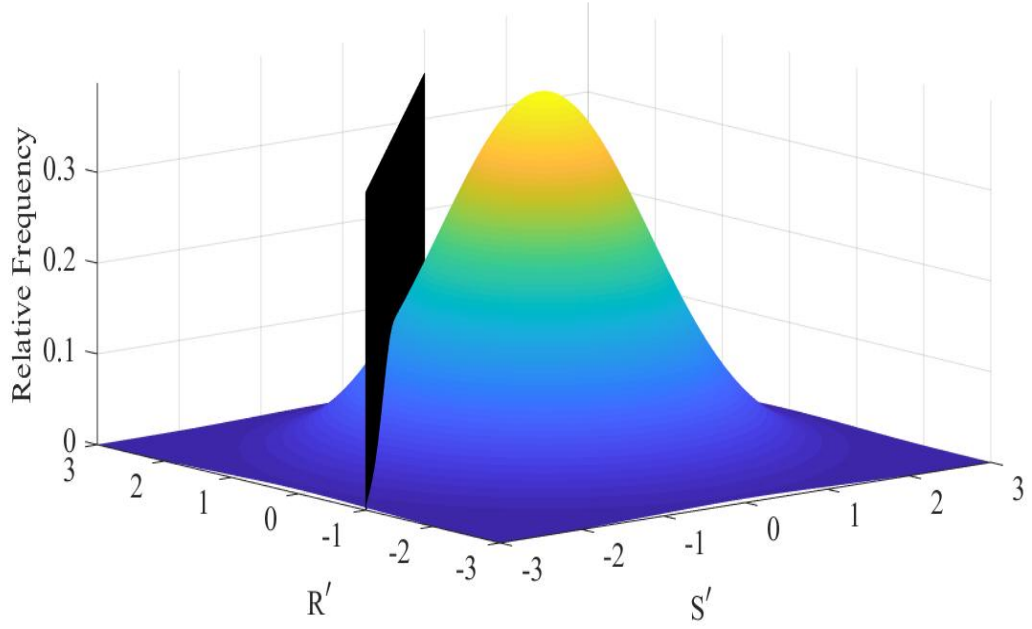

Figure 1.10: Joint PDF of the random variables with Linear failure criterion

contour map along with linear failure criterion is shown in the Fig. 1.11. Using the hypotenuses theorem and stochastic approach, the distance between the origin and the nearest point to it on limit state surface can be found. Fig. 1.12 shows the marginal distribution of the performance function that represents the safe and unsafe region which In the event of n random variable involved in the system, firstly they are reduced to standard space using the general reduction technique

$$X' = \frac{X - \mu_n}{\sigma_n} \tag{1.56}$$

where the term X' is the reduced variable in the standard space, μ_n denotes the standard normal mean of the random variable (X) and σ_n represents standard deviation of standard normal distribution of that random variable (X). Using eq. (1.56), the reduced variables can be found for all n random variables involved in the system whose performance function is $g(X)$. The minimum distance from the origin to the limit state

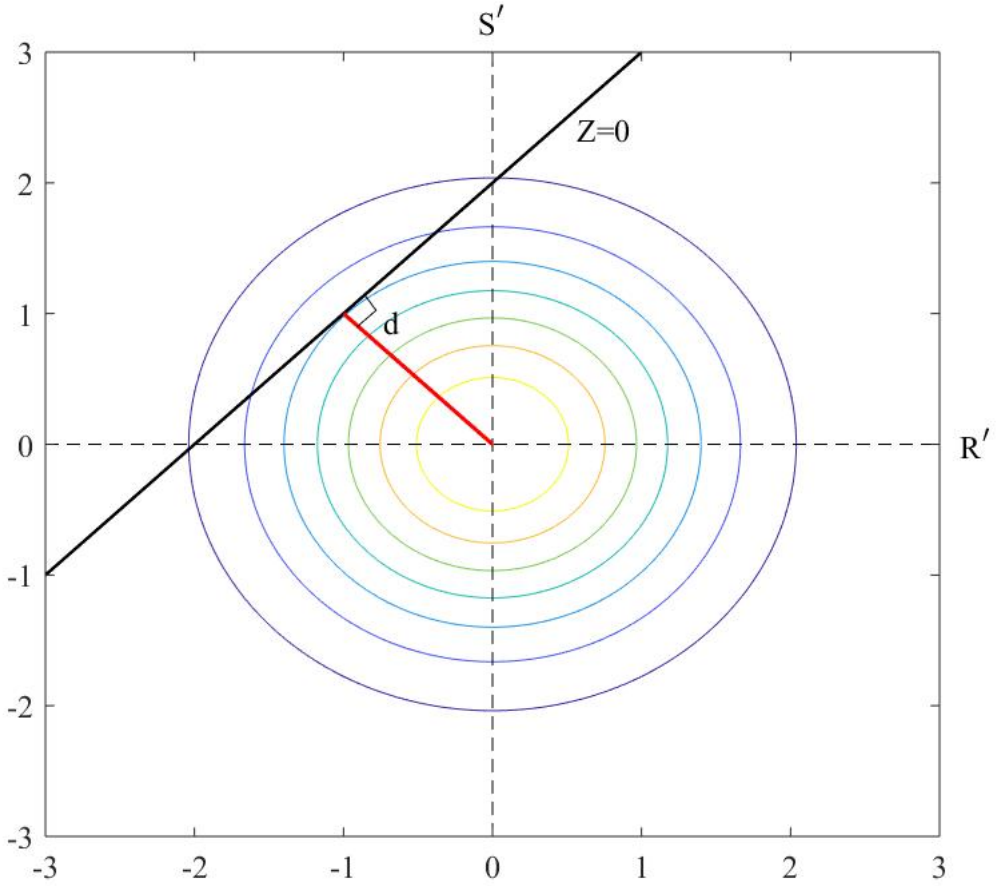

Figure 1.11: Plot of Resistance (R) & Load (S) on reduced standard space with minimum distance (d)

curve is determined using the following equation,

$$\begin{aligned} d &= min\sqrt{X_1'^2 + X_2'^2 + ... + X_n'^2} \\ &= min\sqrt{X'^T X'} \end{aligned} \tag{1.57}$$

subjected to

$$g(X) = 0 \tag{1.58}$$

According to the potential of reliability studies for Eurocodes by Low et al. (2017), if the random variables X are correlated, then the

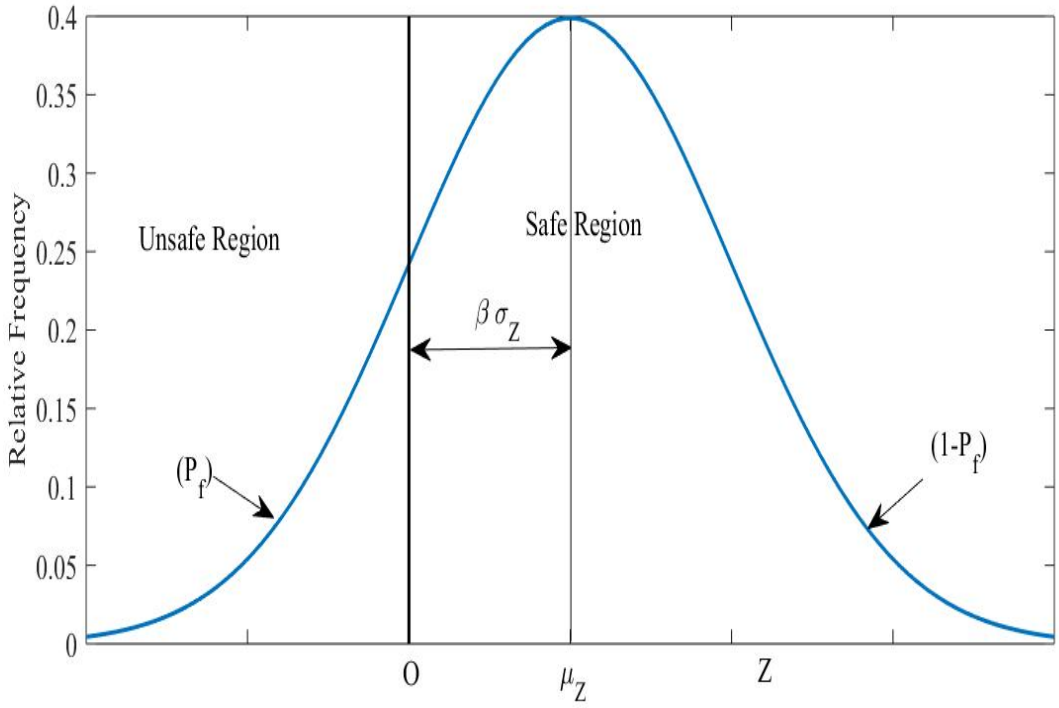

Figure 1.12: Marginal distribution of the performance function (Z)

reduced variable to the standard space should be non-correlated and this can be achieved using Cholesky decomposition technique.

$$u = L^{-1}X' \tag{1.59}$$

$$d = min\sqrt{u^T u} \tag{1.60}$$

subjected to

$$g(X) = 0 \tag{1.61}$$

where L denotes low triangle of Cholesky factors, and X represents the reduced standard normal variable in standard space. Low (2014) has explained that if the value of the performance function is negative by substituting the mean values of the random variables, the reliability index is negative of d. Similarly, if the performance function value is positive, then the reliability index is negative of d. This can also be explained well

with the help of the $R-S$ case and eq. (1.47), if the value of the μ_Z is negative, then $\beta = -d$. If the value of the μ_Z is equal to positive, then $\beta = d$. This can be mathematically explained as

$$\begin{aligned} \beta &= -d, \quad For \quad \mu_Z < 0 \\ \beta &= d, \quad For \quad \mu_Z > 0 \end{aligned} \tag{1.62}$$

1.4.2 Reliability Analysis in Soil Liquefaction

The probabilistic models include the statistical analysis of field performance post-liquefaction database. Thus, the expected mean of each input variable for every historical case is considered, through which statistical parameters for P_L distribution is estimated. The limitation of the above described probabilistic approach is that the parametric and the modeling uncertainties are not dealt with for the estimation of P_L, and the resultant P_L leads to an erroneous prediction. This problem can be overcome by performing a special approach to deal with the probabilistic approach. i.e., reliability-based probabilistic analysis of liquefaction considers the various uncertainties associated with the input variables and the model. Juang et al. (1999) implemented the idea of FORM for performing reliability analysis, considering 225 field performance post-liquefaction database based on CPT-test. An empirical relationship was framed between β and P_L with the help of Bayesian mapping function technique.

Juang et al. (2000a) performed reliability analysis using the Monte Carlo simulation technique considering 225 CPT-based liquefied and non-liquefied cases and came up with $P_L - F_s$ relationship based on Bayesian mapping function technique. But the approach failed to include modeling uncertainty. Çetin (2000) used the FORM along with the updated Bayesian mapping technique as tools for developing SPT-based

probabilistic models for evaluation of liquefaction potential. Juang et al. (2006) performed extensive sensitivity analyses for characterizing uncertainties associated with input variables in evaluating liquefaction potential of the soil for developing CRR model, later used FORM to determine the modeling uncertainty for the probabilistic model developed using the Bayesian mapping function approach. Jha and Suzuki (2009) made comparative studies on reliability methods for evaluation of liquefaction potential using FOSM, Hasofer-Lind's FORM, point estimate method and Monte Carlo simulation method. It was reported that the Monte-Carlo simulation is not commonly used for determining the probabilities of liquefaction and hence it is not preferred due to its complexities.

Using the empirical relationship for evaluation of liquefaction potential of soil developed by Youd et al. (2001), Bagheripour et al. (2012) determined FORM based reliability index and used genetic algorithm for minimization of β. Similar work was performed by Muduli and Das (2015). The CRR model was developed using 198 post-liquefaction cases based on SPT test. The research suggests that it is important for global minimizing of β rather than local minimization. Hence, for this reason, the genetic algorithm is recommended in FORM based reliability analysis. Thus using FORM, the robustness of the deterministic model can be increased, and high-efficiency results can be obtained.

1.5 Research Objective

It is important to understand that accurate and effective assessment of liquefaction potential is essential to avoid a seismic hazard in a cost-effective approach. It is necessary to take required measures for post-earthquake recovery. Soil parameters are associated with great characteristics uncertainty. The existing relationship for determining the

resistance offered by the soil in the evaluation of soil liquefaction has been developed based on the historical liquefaction cases. Using biased and expected values of the parameter can limit the effect of the uncertainties. Predominantly, it is challenging to find an alternative approach that could consider the maximum of uncertainties in an unbiased form to analyze the soil profile for engineering designing of the structures. It is significant that the approach essentially provides the probability of failure. Reliability analysis can satisfy the requirement of the above-mentioned problems. The scope of this thesis is as follows:

- To develop an empirical relationship for CRR based on the latest post-performance liquefaction historical database.
- To develop a first-order reliability method for truncated distributions.
- To develop a the probabilistic and reliability-based models using maximum entropy distributions that can analyze the occurrence of soil liquefaction in the site.
- To carry out the reliability analysis of soil liquefaction using truncated distributions developed based on censored samples.

1.6 Thesis Outline

Chapter 2: The procedure to develop truncated normal and log-normal distribution based censored samples using maximum likelihood estimator for different truncation conditions are developed.

Chapter 3: A new algorithm is proposed to carry out reliability analysis particularly when dealing with the random variable having truncated distribution.

Chapter 4: Based on the post-performance SPT historical database of soil liquefaction, a performance function of soil liquefaction is developed using neural network, regression analysis, Bayesian mapping and reliability analysis. The empirical relationship is being developed for deterministic, probabilistic and reliability based method for soil liquefaction.

Chapter 5: Reliability analysis of the soil liquefaction is performed on two liquefaction cases which involves a random variable to have truncated distribution. The truncated PDF of the random variable is developed and later used for performing reliability analysis.

Chapter 6: It summarizes the contributions of the present study and recommendations for future research work.

Chapter 2

Probability Distribution for Censored Samples

For connecting the statistical data obtained from experiments with the probability of occurrence, we need probability distributions of the sample spaces. When the data obtained from the experiment which has got a partial sampling, it is known as censored data. In this chapter, developing of truncated probability distributions for censored data is discussed.

2.1 Truncated Distributions

In engineering practice, it is not always possible to get complete information about soil variables. In such a situation, the truncated probability density function can be constructed. Truncated distribution refers to the probability distribution for a specific range, beyond which there is no interest or possibility to deal with data. Censored samples reflect the inclusion of partial data of the random variable in the experiment. Based on the availability of the censored data, truncated distributions can be developed.

2.1.1 Probability Distributions for Uncensored Samples

Normal distribution is the most commonly used to represent the continuous probability distribution of the sample space. The probability density function (PDF) of the normal distribution with mean μ and standard deviation σ is given as

$$f(x) = \frac{1}{\sqrt{2\pi\sigma^2}} exp^{\frac{-1}{2}(\frac{x-\mu}{\sigma})^2}, \quad -\infty < x < \infty \tag{2.1}$$

where μ and σ are the mean and standard deviation. The standard normal distribution can be written as

$$f(x) = \frac{1}{\sqrt{2\pi\sigma^2}} exp^{\frac{-1}{2}x^2}, \quad -\infty < x < \infty \tag{2.2}$$

In engineering problems, most of the random variable cannot have negative value due to the physical aspects. During such situations, it is appropriate to consider log-normal distribution instead of normal distribution. The PDF of the log-normal distribution can be written as

$$f(x) = \frac{1}{\zeta_x x\sqrt{2\pi}} exp\left[-\frac{lnx - \lambda_x}{\zeta_x}\right]^2, \quad 0 \le x < \infty \tag{2.3}$$

where λ_x and ζ_x are the parameters of the log-normal distribution.

2.1.2 Probability Distributions for Censored Samples

Sometimes it is not possible to investigate the complete sample space in the real field study because of physical environmental challenges and availability of resources. In such conditions, it is recommended to enforce huge efforts in collecting a large number of quality samples within the possible range. Better truncated PDF can be developed using the models of Muñoz-Cobo et al. (2017), Cohen (2016) and Lee and Lee (2002). All these model uses different estimators like maximum likelihood, methods of moments, L-moment method, etc. to determine the

statistical parameters for truncated probability distributions based on censored samples.

The PDF based on the censored sample can be lower bound truncated, upper bound truncated or doubly truncated. The PDF of the doubly truncated normal distribution is given as

$$f(x) = \frac{\frac{1}{\sigma}\phi(\frac{x-\mu}{\sigma})}{\Phi(\frac{b-\mu}{\sigma}) - \Phi(\frac{a-\mu}{\sigma})}, \quad a \le x \le b \tag{2.4}$$

where ϕ refers to the standard normal distribution and Φ denotes CDF of the normal distribution. Let us assume $\alpha = \frac{a-\mu}{\sigma}$, $\zeta = \frac{b-\mu}{\sigma}$ and $\xi = \frac{x-\mu}{\sigma}$. Then PDF of the truncated distribution can be written as

$$f(x) = \frac{\phi(\xi)}{\sigma Z}, \quad a \le x \le b \tag{2.5}$$

where $Z = \Phi(\zeta) - \Phi(\alpha)$. In case, the sample space has single truncated point i.e, lower truncated point then $Z = 1 - \Phi(\alpha)$. Similarly, for upper truncated point, $Z = \Phi(\zeta)$, PDF of the doubly truncated log-normal distribution can be written as

$$f(x) = \frac{\frac{1}{\zeta_x}\phi(\frac{lnx-\lambda_x}{\zeta_x})}{\Phi(\frac{lnb-\lambda_x}{\zeta_x}) - \Phi(\frac{lna-\lambda_x}{\zeta_x})}, \quad a \le x \le b \tag{2.6}$$

where ϕ refers to the standard normal distribution and Φ denotes CDF of the standard normal distribution. Let us assume $\alpha_1 = \frac{lna-\lambda_x}{\sigma}$, $\zeta_1 = \frac{lnb-\lambda_x}{\zeta_x}$ and $\xi_1 = \frac{lnx-\lambda_x}{\zeta_x}$. Then PDF of the truncated distribution can be written as

$$f(x) = \frac{\phi(\xi_1)}{\zeta_x Z_1}, \quad a \le x \le b \tag{2.7}$$

where $Z_1 = \Phi(\zeta_1) - \Phi(\alpha_1)$. In case, the sample space has single truncated point i.e, lower truncated point then $Z_1 = 1 - \Phi(\alpha_1)$. Similarly, for upper truncated point, $Z_1 = \Phi(\zeta_1)$.

2.1.3 Estimation of Parameters

For developing the truncated PDF from censored samples, it is required to estimate the statistical parameters of the distribution.

Different estimators can be judged by their properties, such as unbiasedness, mean square error (MSE), consistency and asymptotic distribution. The bias of an estimator is the difference between this estimator's expected value and the true value of the parameter being estimated. Thus, bias of an estimator W of a parameter θ is defined by

$$Bias_\theta(W) = E_\theta(W-\theta) = E_\theta(W) - \theta \tag{2.8}$$

where $E(.)$ denotes expected value over the continuous distribution $f(x|\theta)$ and is defined by,

$$E(x) = \int_{-\infty}^{\infty} xf(x)dx \tag{2.9}$$

MSE is the function of θ defined by $E_\theta(W-\theta)^2$. MSE measures the average squared difference between the estimator W and the parameter θ. When its value goes to zero, it will be better.

Maximum likelihood estimation (MLE) is the most popular method to derive estimators. This technique is based on the idea to find the values of the distribution parameter that maximizes the likelihood function form θ from the density function. MLE is one of the effective estimators, since it is based on the total analytic maximization procedure.

Consider $X_1, X_2, \ldots, X_n$ are independent and identically distributed sample from a population with pdf $f(x|\theta_1, \ldots, \theta_k)$. The likelihood function is a function of the parameters of a statistical model given data and defined by (Cohen, 2016)

$$L(\theta|x) = L(\theta_1, \ldots, \theta_k | X_1, \ldots, X_n) = \prod_{i=1}^{n} f(X_i|\theta_1, \ldots, \theta_k) \tag{2.10}$$

Note that θ will be the function's variable and consider the observed values $X_1, \ldots, X_n$ to be fixed "parameters" of this function. Practically, it is easier to use the log-likelihood which is defined as

$$lnL(\theta|x) = L(\theta_1, \ldots, \theta_k | X_1, \ldots, X_n) = \prod_{i=1}^{n} lnf(X_i|\theta_1, \ldots, \theta_k) \tag{2.11}$$

Let us estimate the parameters of the truncated normal distribution using the MLE. The likelihood for the truncated normal distribution is given as

$$L(\mu,\sigma^2)=\prod_{i=1}^{n} f(X_i)=(z)^{-n}\left(\sqrt{2\pi\sigma^2}\right)exp\left[\frac{-\sum_{i=1}^{n}(X_i-\mu)^2}{2\sigma^2}\right] \tag{2.12}$$

The log-likelihood of the above function can be written as

$$l=lnL(\mu,\sigma^2)=-nln(z)-nln(\sqrt{2\pi\sigma^2})-\frac{\sum_{i=1}^{n}(X_i-\mu)^2}{2\sigma^2} \tag{2.13}$$

Considering the doubly truncated normal distribution case, the probability function can be written as,

$$\Psi(\mu,\sigma)=\int_a^b \frac{1}{\sqrt{2\pi\sigma^2}}exp\left[\frac{-(X-\mu)}{2\sigma^2}\right]dX \tag{2.14}$$

$$\Psi_\mu(\mu,\sigma)=\frac{\partial\Psi}{\partial\mu}=\int_a^b exp\left[\frac{-(X-\mu)}{2\sigma^2}\right]\frac{X-\mu}{\sigma^3\sqrt{2\pi}}dX \tag{2.15}$$

$$\Psi_\sigma(\mu,\sigma)=\frac{\partial\Psi}{\partial\sigma}=\int_a^b exp\left[\frac{-(X-\mu)}{2\sigma^2}\right]\left[\frac{(X-\mu)^2}{\sigma^4\sqrt{2\pi}}-\frac{1}{\sigma^2\sqrt{2\pi}}\right]dX \tag{2.16}$$

Therefore, the gradient vector of the log-likelihood function with respect to the parameter μ and σ can be given as

$$G=\begin{bmatrix}\frac{\partial l}{\partial\mu}\\ \frac{\partial l}{\partial\sigma}\end{bmatrix}=\begin{bmatrix}-n\frac{\Psi_\mu}{\Psi}-\frac{1}{\sigma^2}(n\mu-\sum_{i=1}^{n}X_i)\\ -n\frac{\Psi_\sigma}{\Psi}-\frac{n}{\sigma}+(\frac{\sum_{i=1}^{n}(X_i-\mu)^2}{\sigma^3})\end{bmatrix} \tag{2.17}$$

The solution for the system of equations can be obtained using Newton Raphson's method. The procedure for singly truncated normal distribution would be the same; only the limits of the sample space will vary.

The likelihood for truncated log-normal distribution is given as

$$L(\lambda_x,\zeta_x^2)=\prod_{i=1}^{n} f(X_i)=(z_1)^{-n}\left(\sqrt{2\pi^2\zeta_x^2}\right)exp\left[\frac{-\sum_{i=1}^{n}(ln(X_i-a)-\lambda_x)^2}{2\zeta_x^2}\right] \tag{2.18}$$

The log-likelihood function of eq. (2.18) can be written as

$$l = lnL(\lambda_x, \zeta_x^2) = -nln(z_1) - nln(\sqrt{2\pi\zeta_x^2}) - \frac{\sum_{i=1}^{n}(ln(X_i - a) - \lambda_x)^2}{2\zeta_x^2} \quad (2.19)$$

Considering $Y_i = X_i - a$. Eq. (2.3) for doubly truncated distribution can be written as

$$f(x) = \frac{1}{\zeta_x x\sqrt{2\pi}} exp\left[-\frac{Y - \lambda_x}{\zeta_x}\right]^2, \quad a < Y < b \quad (2.20)$$

The above equation can be written as a function of Ψ,

$$\Psi(\lambda_x, \zeta_x) = \int_a^b \frac{1}{\sqrt{2\pi\zeta_x^2}} exp\left[\frac{-(Y - \lambda_x)}{2\zeta_x^2}\right] dY \quad (2.21)$$

$$\Psi_{\lambda x}(\lambda_x, \zeta_x) = \frac{\partial\Psi}{\partial\lambda_x} = \int_a^b exp\left[\frac{-(Y - \lambda_x)}{2\zeta_x^2}\right] \frac{Y - \lambda_x}{\zeta_x^3\sqrt{2\pi}} dY \quad (2.22)$$

$$\Psi_{\zeta x}(\lambda_x, \zeta_x) = \frac{\partial\Psi}{\partial\zeta_x} = \int_a^b exp\left[\frac{-(Y - \lambda_x)}{2\zeta_x^2}\right] \left[\frac{(Y - \lambda_x)^2}{\zeta_x^4\sqrt{2\pi}} - \frac{1}{\zeta_x^2\sqrt{2\pi}}\right] dY \quad (2.23)$$

Hence, the gradient vector of the log-likelihood function can be obtained as

$$G = \begin{bmatrix} \frac{\partial l}{\partial\lambda_x} \\ \frac{\partial l}{\partial\zeta_x} \end{bmatrix} = \begin{bmatrix} -n\frac{\Psi_{\lambda x}}{\Psi} - \frac{1}{\zeta_x^2}(n\lambda_x - \sum_{i=1}^{n} Y_i) \\ -n\frac{\Psi_{\zeta x}}{\Psi} - \frac{n}{\zeta_x} + (\frac{\sum_{i=1}^{n}(Y_i - \lambda_x)^2}{\zeta_x^3}) \end{bmatrix} \quad (2.24)$$

The solution for the system of equations can be obtained using Newton Raphson's method. Once the statistical parameter λ_x and ζ_X are calculated, they can be substituted into eq. (2.6) to construct the truncated log-normal distribution.

2.2 Comparative Studies of Truncated Distributions based on Censored Samples

With the help of MLE technique explained in the previous section, the parameters of the truncated distribution for different condition can be calculated. Normal and log-normal truncated distributions are developed

for the undrained shear strength (s_u) of the soil present on the bank of Nipigon river, Nipigon, Ontario, Canada collected using vane shear test. The data is presented in Table 2.1.

Table 2.1: s_u of the soil in kN/m^2 present at the bank of Nipigon river, calculated using vane shear test by Singh (2018).

55	35	47	39	38	56	57	52	69	68	52	35	102	42
35	42	40	40	62	60	70	72	35	44	59	42	100	32
72	85	70	47	75	82	69	72	68	40	42	71	55	

Let us develop the truncated normal and log-normal distributions for different condition like doubly truncated, lower truncated and upper bound truncated distribution based on the data present in Table 2.1 and check for the best fit among the two distribution types for each case. K-S test for good fitness investigation with 1% significance is carried out on the undrained shear strength data presented in Table 2.1 whose true mean and standard deviation of the is $56.8kN/m^2$ and $17.9kN/m^2$, respectively.

2.2.1 Methodology

Since, there are only 41 entries of s_u in Table 2.1, the entries of the sample space can be increased by generating random numbers which represents the same true mean and standard deviation. Table 2.2 shows the different size of the sample that is generated and the one with least MSE value is chosen. The sample size of 5000 has got the least error of 0.0006 and hence, it is selected to generate samples. Initially, the truncation point is fixed and the sample space is reduced. Therefore, censored sample space is obtained. The truncated normal mean and standard deviation is calculated by equating eq. (2.17) to zero and solving it using Newton Raphson technique. Similarly, for truncated log-normal mean and standard deviation is determined solving eq. (2.24).

Table 2.2: Undrained shear strength of different sample size generated on true mean and standard deviation

Sample Size	**Mean**	**Standard deviation**	**MSE**
500	56.4096	18.5770	0.2949
1000	56.8353	18.1288	0.0266
5000	57.1493	17.9762	0.0706
10000	56.8334	18.0021	0.0061
50000	**56.7473**	**17.9194**	**0.0006**
100000	56.8158	17.9236	0.0008

2.2.2 Results and Discussions

- In the case of Lower bound truncated probability distribution, the lower bound truncation point is fixed at $32kN/m^2$. The normal and log-normal truncated distributions are shown in Figs. 2.1 and 2.2, respectively, and the K-S investigation for the best-fit is shown in Tables 2.3 and 2.4, respectively. From K-S test table, $D_n^{0.01} = 0.25$ and it is found that both distributions pass the test.

- In the case of the doubly truncated probability distribution, the lower bound is fixed at $32kN/m^2$ and the upper bound is maintained at $102kN/m^2$. The normal and log-normal truncated distributions are shown in Figs. 2.3 and 2.4, respectively and the K-S investigation for the best-fit are shown in Tables 2.5 and 2.6, respectively. From K-S test table, $D_n^{0.01} = 0.25$ and it is found that the truncated log-normal distribution passes the test but the truncated normal distribution fails.

- To develop upper truncated normal distribution, the truncation point is fixed as $102kN/m^2$. The normal and log-normal truncated distributions are shown in Figs. 2.5 and 2.6, respectively and the K-S investigation for the best-fit are shown in Tables 2.7 and 2.8, respectively. From K-S test table, $D_n^{0.01} = 0.25$ and the maximum

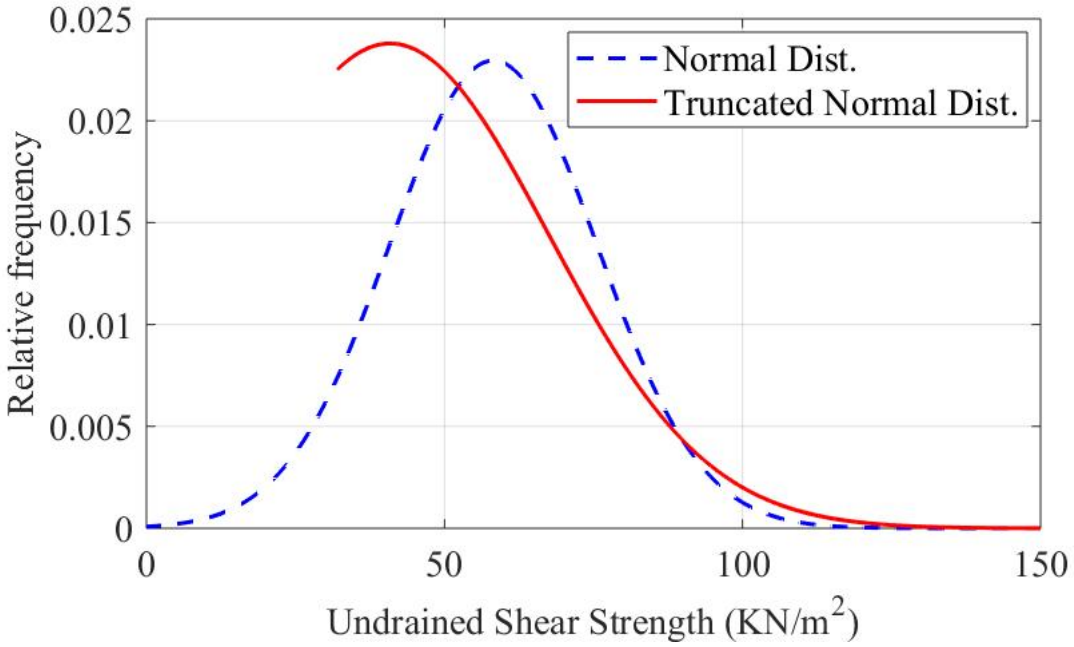

Figure 2.1: Lower bound truncated normal distribution of censored sample

values lies to be 0.239 for both distributions. It is found that both distributions pass the test.

The statistical parameters μ and σ of truncated normal distribution for all the three different conditions are estimated by solving eq. (2.17). Table 2.9 shows the estimated values of μ and σ for different truncated normal distributions. Truncated normal distributions are constructed by using the estimated values of μ and σ in eq. (2.4) and they are shown in Figs. 2.2, 2.4 and 2.6. Similarly, the statistical parameters λ_x and ζ_x of truncated log-normal distribution for all the three different conditions are estimated by solving Eq. (2.24) and they are presented in Table 2.10. Using these estimated statistical values, truncated log-normal distributions are constructed and shown in Figs. 2.2, 2.4 and 2.6.

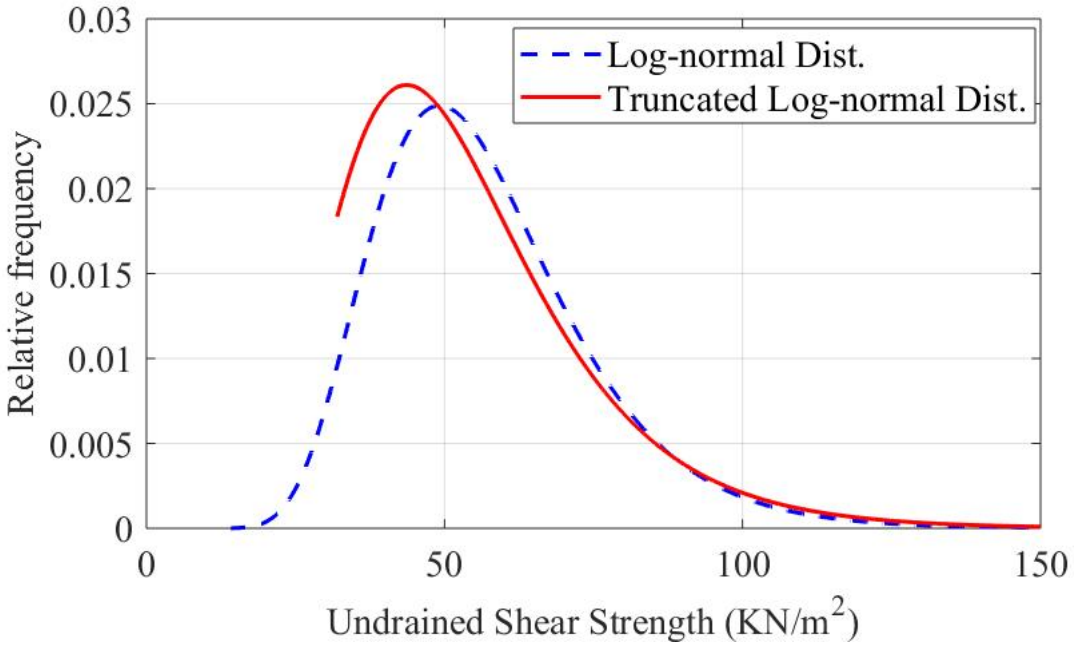

Figure 2.2: Lower bound truncated log-normal distribution of censored sample

Table 2.3: K-S test for lower truncated normal distribution of s_u

m	s_u	$S_n = m/n$	Fe	$D_n = max\|F_x(x_i) - S_n(x_i)\|$
1	32	0.02	0.00	0.024
2	35	0.05	0.07	0.020
3	35	0.07	0.07	0.005
4	35	0.10	0.07	0.029
5	35	0.12	0.07	0.053
6	38	0.15	0.14	0.007
7	39	0.17	0.16	0.008
8	40	0.20	0.19	0.009
9	40	0.22	0.19	0.033
10	40	0.24	0.19	0.057

Continued on next page

Table 2.3 – continued from previous page

m	s_u	$S_n = m/n$	Fe	$D_n = max\|F_x(x_i) - S_n(x_i)\|$
11	42	0.27	0.23	0.034
12	42	0.29	0.23	0.059
13	42	0.32	0.23	0.083
14	**42**	**0.34**	**0.23**	**0.239**
15	44	0.37	0.28	0.084
16	47	0.39	0.35	0.039
17	47	0.41	0.35	0.063
18	52	0.44	0.46	0.025
19	52	0.46	0.46	0.001
20	55	0.49	0.53	0.040
21	55	0.51	0.53	0.016
22	56	0.54	0.55	0.012
23	57	0.56	0.57	0.008
24	59	0.59	0.61	0.022
25	60	0.61	0.63	0.016
26	62	0.63	0.66	0.027
27	68	0.66	0.76	0.098
28	68	0.68	0.76	0.073
29	69	0.71	0.77	0.063
30	69	0.73	0.77	0.038
31	70	0.76	0.78	0.027
32	70	0.78	0.78	0.003
33	71	0.80	0.80	0.009
34	72	0.83	0.81	0.021
35	72	0.85	0.81	0.045
36	72	0.88	0.81	0.070
37	75	0.90	0.84	0.060

Continued on next page

Table 2.3 – continued from previous page

m	s_u	$S_n = m/n$	Fe	$D_n = max\|F_x(x_i) - S_n(x_i)\|$
38	82	0.93	0.90	0.023
39	85	0.95	0.92	0.028
40	100	0.98	0.98	0.004
41	102	1.00	0.98	0.017

Table 2.4: K-S test for lower truncated log-normal distribution of s_u

m	s_u	$S_n = m/n$	Fe	$D_n = max\|F_x(x_i) - S_n(x_i)\|$
1	32	0.02	0.00	0.024
2	35	0.05	0.12	0.066
3	35	0.07	0.12	0.042
4	35	0.10	0.12	0.018
5	35	0.12	0.12	0.007
6	38	0.15	0.22	0.076
7	39	0.17	0.26	0.086
8	40	0.20	0.29	0.094
9	40	0.22	0.29	0.069
10	40	0.24	0.29	0.045
11	42	0.27	0.35	0.083
12	42	0.29	0.35	0.058
13	42	0.32	0.35	0.034
14	**42**	**0.34**	**0.35**	**0.239**
15	44	0.37	0.41	0.043
16	47	0.39	0.49	0.097
17	47	0.41	0.49	0.073

Continued on next page

Table 2.4 – continued from previous page

m	s_u	$S_n = m/n$	Fe	$D_n = max\|F_x(x_i) - S_n(x_i)\|$
18	52	0.44	0.60	0.159
19	52	0.46	0.60	0.135
20	55	0.49	0.65	0.166
21	55	0.51	0.65	0.141
22	56	0.54	0.67	0.134
23	57	0.56	0.69	0.125
24	59	0.59	0.72	0.131
25	60	0.61	0.73	0.120
26	62	0.63	0.76	0.121
27	68	0.66	0.82	0.160
28	68	0.68	0.82	0.136
29	69	0.71	0.83	0.120
30	69	0.73	0.83	0.096
31	70	0.76	0.84	0.080
32	70	0.78	0.84	0.056
33	71	0.80	0.84	0.039
34	72	0.83	0.85	0.022
35	72	0.85	0.85	0.002
36	72	0.88	0.85	0.027
37	75	0.90	0.87	0.030
38	82	0.93	0.91	0.017
39	85	0.95	0.92	0.029
40	100	0.98	0.96	0.014
41	102	1.00	0.97	0.035

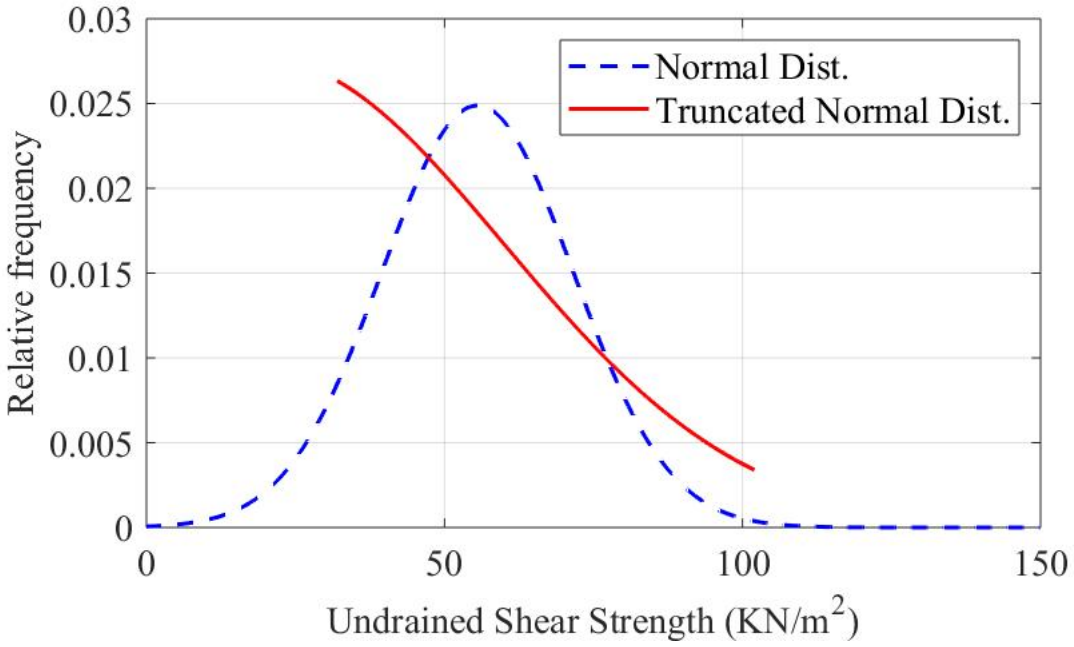

Figure 2.3: Doubly truncated normal distribution of censored sample

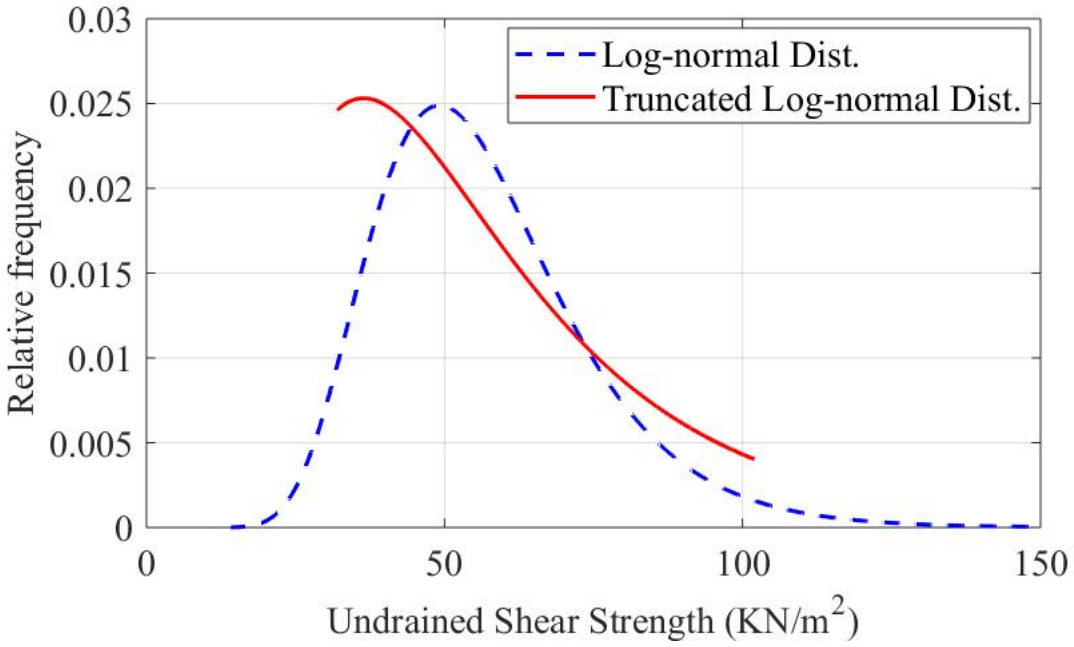

Figure 2.4: Doubly truncated log-normal distribution of censored sample

Table 2.5: K-S test for doubly truncated normal distribution of s_u

m	s_u	$S_n = m/n$	Fe	$D_n = max\|F_x(x_i) - S_n(x_i)\|$
1	32	0.02	0.00	0.024
2	35	0.05	0.03	0.020
3	35	0.07	0.03	0.044
4	35	0.10	0.03	0.069
5	35	0.12	0.03	0.093
6	38	0.15	0.06	0.090
7	39	0.17	0.07	0.105
8	40	0.20	0.07	0.120
9	40	0.22	0.07	0.145
10	40	0.24	0.07	0.169
11	42	0.27	0.09	0.176
12	42	0.29	0.09	0.200
13	42	0.32	0.09	0.225
14	42	0.34	0.09	0.239
15	44	0.37	0.11	0.256
16	47	0.39	0.13	0.256
17	47	0.41	0.13	0.280
18	52	0.44	0.17	0.266
19	52	0.46	0.17	0.291
20	55	0.49	0.19	0.294
21	55	0.51	0.19	0.318
22	56	0.54	0.20	0.336
23	57	0.56	0.21	0.353
24	59	0.59	0.22	0.365
25	60	0.61	0.23	0.383
26	62	0.63	0.24	0.395

Continued on next page

Table 2.5 – continued from previous page

m	s_u	$S_n = m/n$	Fe	$D_n = max\|F_x(x_i) - S_n(x_i)\|$
27	68	0.66	0.27	0.387
28	68	0.68	0.27	0.412
29	69	0.71	0.28	0.431
30	69	0.73	0.28	0.456
31	70	0.76	0.28	0.475
32	70	0.78	0.28	0.500
33	71	0.80	0.29	0.520
34	72	0.83	0.29	0.540
35	72	0.85	0.29	0.564
36	72	0.88	0.29	0.588
37	75	0.90	0.30	0.600
38	82	0.93	0.33	0.600
39	85	0.95	0.34	0.616
40	100	0.98	0.37	0.611
41	**102**	**1.00**	**0.37**	**0.632**

Table 2.6: K-S test for doubly truncated log-normal distribution of s_u

m	s_u	$S_n = m/n$	Fe	$D_n = max\|F_x(x_i) - S_n(x_i)\|$
1	32	0.02	0.00	0.024
2	35	0.05	0.07	0.026
3	35	0.07	0.07	0.002
4	35	0.10	0.07	0.023
5	35	0.12	0.07	0.047
6	38	0.15	0.15	0.004

Continued on next page

Table 2.6 – continued from previous page

m	s_u	$S_n = m/n$	Fe	$D_n = max\|F_x(x_i) - S_n(x_i)\|$
7	39	0.17	0.18	0.005
8	40	0.20	0.20	0.006
9	40	0.22	0.20	0.019
10	40	0.24	0.20	0.043
11	42	0.27	0.25	0.018
12	42	0.29	0.25	0.042
13	42	0.32	0.25	0.067
14	**42**	**0.34**	**0.25**	**0.239**
15	44	0.37	0.30	0.067
16	47	0.39	0.37	0.022
17	47	0.41	0.37	0.046
18	52	0.44	0.48	0.037
19	52	0.46	0.48	0.012
20	55	0.49	0.53	0.046
21	55	0.51	0.53	0.022
22	56	0.54	0.55	0.016
23	57	0.56	0.57	0.010
24	59	0.59	0.61	, 0.020
25	60	0.61	0.62	0.013
26	62	0.63	0.65	0.020
27	68	0.66	0.74	0.081
28	68	0.68	0.74	0.056
29	69	0.71	0.75	0.045
30	69	0.73	0.75	0.020
31	70	0.76	0.76	0.008
32	70	0.78	0.76	0.016
33	71	0.80	0.78	0.029

Continued on next page

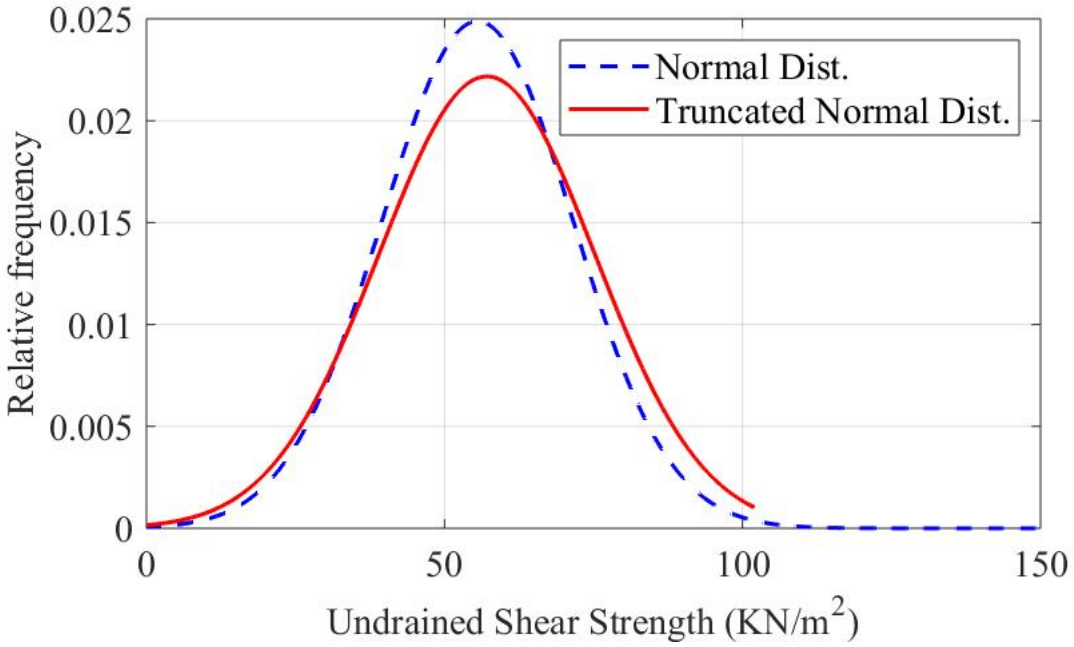

Figure 2.5: Upper bound truncated normal distribution of censored sample

Table 2.6 – continued from previous page

m	s_u	$S_n = m/n$	Fe	$D_n = max\|F_x(x_i) - S_n(x_i)\|$
34	72	0.83	0.79	0.042
35	72	0.85	0.79	0.066
36	72	0.88	0.79	0.091
37	75	0.90	0.82	0.083
38	82	0.93	0.88	0.043
39	85	0.95	0.91	0.045
40	100	0.98	0.99	0.016
41	102	1.00	1.00	0.000

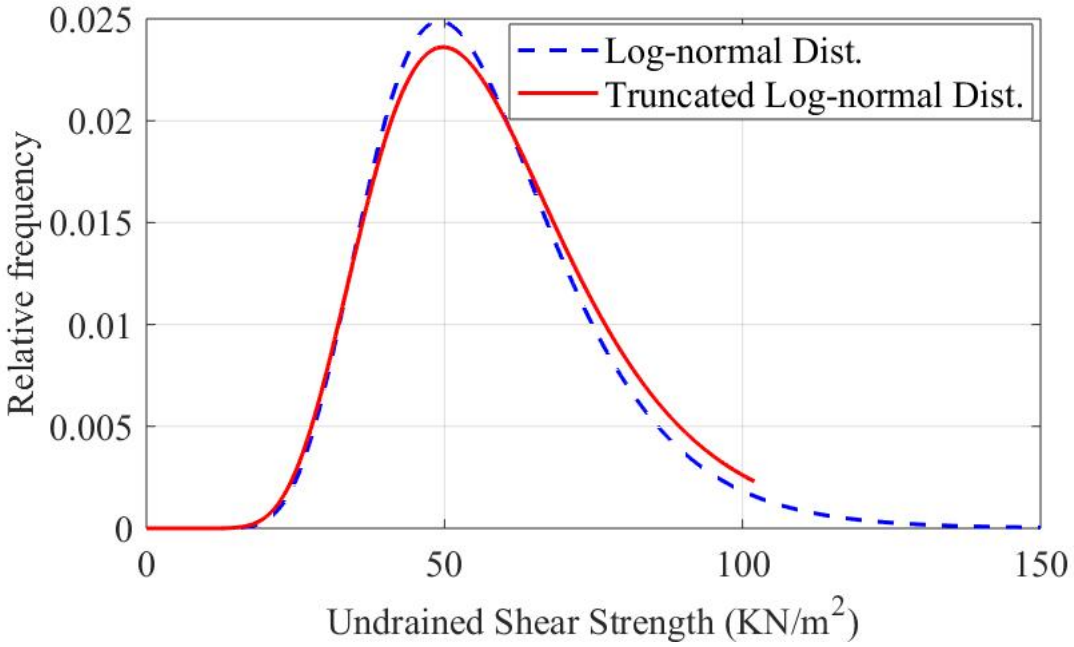

Figure 2.6: Upper bound truncated log-normal distribution of censored sample

Table 2.7: K-S test for Upper truncated normal distribution of s_u

m	s_u	$S_n = m/n$	Fe	$D_n = max\|F_x(x_i) - S_n(x_i)\|$
1	32	0.02	0.08	0.058
2	35	0.05	0.11	0.062
3	35	0.07	0.11	0.038
4	35	0.10	0.11	0.013
5	35	0.12	0.11	0.011
6	38	0.15	0.15	0.001
7	39	0.17	0.16	0.012
8	40	0.20	0.17	0.022
9	40	0.22	0.17	0.047
10	40	0.24	0.17	0.071

Continued on next page

Table 2.7 – continued from previous page

m	s_u	$S_n = m/n$	Fe	$D_n = max\|F_x(x_i) - S_n(x_i)\|$
11	42	0.27	0.20	0.066
12	42	0.29	0.20	0.090
13	42	0.32	0.20	0.115
14	**42**	**0.34**	**0.20**	**0.239**
15	44	0.37	0.24	0.131
16	47	0.39	0.29	0.101
17	47	0.41	0.29	0.125
18	52	0.44	0.39	0.049
19	52	0.46	0.39	0.073
20	55	0.49	0.46	0.032
21	55	0.51	0.46	0.057
22	56	0.54	0.48	0.059
23	57	0.56	0.50	0.061
24	59	0.59	0.54	0.041
25	60	0.61	0.57	0.044
26	62	0.63	0.61	0.025
27	68	0.66	0.73	0.072
28	68	0.68	0.73	0.047
29	69	0.71	0.75	0.041
30	69	0.73	0.75	0.017
31	70	0.76	0.77	0.010
32	70	0.78	0.77	0.015
33	71	0.80	0.78	0.022
34	72	0.83	0.80	0.030
35	72	0.85	0.80	0.055
36	72	0.88	0.80	0.079
37	75	0.90	0.84	0.059

Continued on next page

Table 2.7 – continued from previous page

m	s_u	$S_n = m/n$	Fe	$D_n = max\|F_x(x_i) - S_n(x_i)\|$
38	82	0.93	0.92	0.006
39	85	0.95	0.94	0.008
40	100	0.98	1.00	0.021
41	102	1.00	1.00	0.001

Table 2.8: K-S test for Upper truncated log-normal distribution of s_u

m	s_u	$S_n = m/n$	Fe	$D_n = max\|F_x(x_i) - S_n(x_i)\|$
1	32	0.02	0.05	0.026
2	35	0.05	0.09	0.036
3	35	0.07	0.09	0.012
4	35	0.10	0.09	0.013
5	35	0.12	0.09	0.037
6	38	0.15	0.13	0.015
7	39	0.17	0.15	0.022
8	40	0.20	0.17	0.028
9	40	0.22	0.17	0.053
10	40	0.24	0.17	0.077
11	42	0.27	0.21	0.062
12	42	0.29	0.21	0.086
13	42	0.32	0.21	0.110
14	**42**	**0.34**	**0.21**	**0.239**
15	44	0.37	0.25	0.116
16	47	0.39	0.32	0.072
17	47	0.41	0.32	0.097

Continued on next page

Table 2.8 – continued from previous page

m	s_u	$S_n = m/n$	Fe	$D_n = max\|F_x(x_i) - S_n(x_i)\|$
18	52	0.44	0.44	0.004
19	52	0.46	0.44	0.028
20	55	0.49	0.50	0.017
21	55	0.51	0.50	0.008
22	56	0.54	0.53	0.010
23	57	0.56	0.55	0.012
24	59	0.59	0.59	0.006
25	60	0.61	0.61	0.002
26	62	0.63	0.65	0.017
27	68	0.66	0.75	0.095
28	68	0.68	0.75	0.071
29	69	0.71	0.77	0.061
30	69	0.73	0.77	0.037
31	70	0.76	0.78	0.026
32	70	0.78	0.78	0.002
33	71	0.80	0.80	0.009
34	72	0.83	0.81	0.020
35	72	0.85	0.81	0.044
36	72	0.88	0.81	0.069
37	75	0.90	0.84	0.058
38	82	0.93	0.91	0.017
39	85	0.95	0.93	0.020
40	100	0.98	1.00	0.019
41	102	1.00	1.00	0.000

Table 2.9: Statistical parameters of the truncated normal distribution calculated using MLE

Truncated Distribution Type	μ (kN/m^2)	σ (kN/m^2)
Lower bound trun. normal	40.8749	26.5877
Doubly trun. normal	19.7879	40.1499
Upper bound trun. normal	57.1179	18.1112

Table 2.10: Statistical parameters of the truncated log-normal distribution calculated using MLE

Truncated Distribution Type	λ_x (kN/m^2)	ζ_x (kN/m^2)
Lower bound trun. log-normal	3.9119	0.3691
Doubly trun. log-normal	3.8831	0.5374
Upper bound trun. log-normal	4.0179	0.3326

2.3 Summary

In this chapter, the procedure for developing truncated normal and log-normal distribution using information available from censored samples has been explained. MLE method has been used for determining the parameters of PDF based on censored samples for different truncation conditions. On generating the truncated PDF, a comparative study is made to judge the best-fit distribution for censored data of sample space.

Chapter 3

Reliability Analysis using Truncated Distributions

The minimum distance between the origin and the limit state boundary, i.e., the reliability index β should be globally minimum when performing reliability analysis on an engineering system. This chapter presents a new algorithm to search for the global minimum distance between the origin and the limit state curve using the interior point method.

3.1 Global Search Technique

According to Liu and Der Kiureghian (1991), the distance between the origin and the point on the limit state function should be globally minimum because the minimization optimization in the reliability depends on the initial guess. There might be several local minimum distances between the origin and the limit state boundary surface. With different initial guess, the value of β can vary. This distance does not reflect the actual reliability index. It is essential in Hasofer-Lind's reliability analysis to locate the very nearest and globally minimum distance of the origin to the limit state boundary. The global search process of the minimum distance is very crucial in reliability

analysis, and hence it should be highly accurate for large tolerance level.

A new algorithm is incorporated in this thesis by using *global search-fmincon* function available in MATLAB programming. The function uses the interior point method to perform minimum optimization. The function *fmincon* can optimize a non-linear equation that is subjected to a set of constraints. The solution obtained using *fmincon* is going to be the local minimum distance. The result of this function depends highly on the initial guess which was provided to start iteration. It identifies the minimum value which is near to the start point for the search algorithm. Neither-less judging the result as the local nor global minimum, and the function throws the value of β. The results obtained by these functions are meant to be less accurate.

In the global search algorithm, the function will undergo multiple directions in search of minimum distance. It is similar to multi-start *fmincon*. From the set of local minimum identified by the *fmincon* function, the one which is least of all the values is returned by the *global-search* function. The function takes the initial guesses as the center point and starts to search for the minimum value in one direction. Once the function locates a minimum value, the search is carried out in another direction. The function will search in all possible directions until it finds the minimum value ending up in Not-A-Number (NAN) which means infinity or obtains the maximum tolerance level. The advantage of this algorithm is that the search time is less, the function calculates the first-order derivatives by itself which is the part of the interior point method, and the search distance is globally minimum. This algorithm provides the advantage of performing reliability analysis for any complicated performance function for which first-order derivatives are difficult to obtain.

3.2 FORM for Truncated Distribution

In the reliability analysis of an engineering model that consists of the truncated distribution, there will be a set of limitation for the flow of search design points beyond the truncated point. Hence, this also forms a constraint in the reliability analysis besides performance function $Z = 0$ in eq. (1.54). In the $Z = R - S$ system, if the random variable S has a truncated distribution, the optimization for search of the design points is not supposed to be carried out beyond the truncated point of S. Therefore, the model will have two constraints, i.e. $Z = 0$ and S should be greater or less than the truncated point depending on the truncation condition. Inspired by the idea of Melchers et al. (2003), the following algorithm is proposed. The conceptual ideas of the interior point method is being well explained by Wächter and Biegler (2006). The algorithm of reliability optimization is explained below.

Let us consider the system for reliability analysis consisting of normal independent random variable $X_1, X_2, \ldots, X_n$ involved in the performance function $g(X)$, and X' represents the reduced space variable which can be calculated using the procedure explained in eq. (1.53). Consider $p(X)$ as a function of eq. (1.57) used for determining the minimum distance between the origin and limit state curve which reflects β. The term X is lower bound truncated at a.

$$\begin{aligned} p(X) = d &= min\sqrt{X_1'^2 + X_2'^2 + \cdots + X_n'^2} \\ &= min\sqrt{X'^T X'} \end{aligned} \tag{3.1}$$

subjected to

$$\begin{aligned} g(X) &= 0 \\ X &\geq a \end{aligned} \tag{3.2}$$

Step 1: Transformation of the problem statement to standard form.

$$p(X) = min\sqrt{X'^{T}X'} \tag{3.3}$$

subjected to

$$\begin{aligned} c(X) &= 0 \\ S &\geq a \end{aligned} \tag{3.4}$$

where

$$c(X) = \begin{cases} g(X) = 0 \\ X - a - S = 0 \end{cases} \tag{3.5}$$

where S is the stack variable which functions to set the inequality constraint equation to zero. $c(X)$ is the function that includes both equality and inequality constraints.

Step 2: Use the barrier function for the inequality constraints, i.e., $X \geq a$ by including the parameter ν.

$$X \in R^n,\ p(X) - \nu ln \sum_{i=1}^{n}(X) = 0 \tag{3.6}$$

subjected to

$$c(X) = 0 \tag{3.7}$$

Step 3: Apply Karush-KuHn-Tucker (KKT) conditions (Wächter and Biegler, 2006) for the barrier problem with respect to $X = 0$.

$$\begin{aligned} \Delta p(X) + \lambda \Delta c(X) - \nu \sum_{i=1}^{n} \frac{1}{X_i} &= 0 \\ c(X) &= 0 \end{aligned} \tag{3.8}$$

where λ is the coefficient for equality constraint.

Step 4: Define $z_i = \frac{v}{X_i}$. Since a new term z_i is included, the modified version of KKT condition can be wriiten as

$$\begin{aligned} \Delta p(X) + \lambda \Delta c(X) - z = 0 \\ c(X) = 0 \\ (Xz - v)e = 0 \end{aligned} \tag{3.9}$$

where e is a singular matrix.

Step 5: Establish the modified set of KKT condition using Newton Raphson's method for search direction concerning to X.

$$\begin{bmatrix} w & \Delta c(X_k) & -I \\ \Delta c(X_k)^T & 0 & 0 \\ z_k & 0 & X_k \end{bmatrix} \begin{bmatrix} d_k^X \\ d_k^\lambda \\ d_k^z \end{bmatrix} = - \begin{bmatrix} \Delta p(X_k) + \lambda \Delta c(X_k) - z_k \\ c(X_k) \\ X_k z_k e - v_j e \end{bmatrix} \tag{3.10}$$

where $w = \Delta_{XX}^2 L(X, \lambda, z) = \Delta_{XX}^2 (p(X_k) + \lambda c(X_k)^T - z)$, z_k and X_k have diagonal matrix structure. The term k represents iteration count and v_j represents the fixed value of barrier function.

Step 6: Make initial guess of X_k and λ_k. Fixed the value of v_j. Rearrange the Newton Raphson's into symmetric linear system.

$$\begin{bmatrix} w + E & \Delta c(X) \\ \Delta c(X)^T & 0 \end{bmatrix} \begin{bmatrix} dX \\ d\lambda \end{bmatrix} = - \begin{bmatrix} \Delta p(X) + \lambda \Delta c(X) \\ c(x) \end{bmatrix} \tag{3.11}$$

where

$$E = X^{-1} * z \tag{3.12}$$

$$dz = vX^{-1}e - z - \sum dX \tag{3.13}$$

Solve the system of equations by the iterative procedure of $K + 1$ equations in Newton Raphson's technique until KKT conditions and

tolerance level are satisfied. Revise the initial guess so that the complete model is analyzed.

$$\begin{aligned} x_{k+1} &= x_k + \alpha_x * d_k^x \\ \lambda_{k+1} &= \lambda_k + \alpha_\lambda * d_k^\lambda \end{aligned} \tag{3.14}$$

The value of α ranges from 0 and 1. Once the required X values satisfying the above-mentioned criteria are determined, they are substituted in the function $p(X)$ to determine β. The generalized idea of the proposed algorithm is shown in Fig. 3.1.

Example 1: Consider the limit state function shown in eq. (3.15). The random variable x_1 is truncated at lower bound value of 9. The mean and standard deviation of the random variable x_1 is 10.29 and 0.794, respectively. Random variable x_2 is normally distributed with mean of 12.0 and standard deviation equal to 1.5. This problem is extracted from Melchers et al. (2003).

$$z = 5x_1 + 3x_1x_2 - 240 \tag{3.15}$$

Based on the proposed algorithm, a sample iteration procedure is shown below. The problem statement for truncated based FORM can be written as

$$p(x) = min\sqrt{\left[\frac{x_i - \mu_i}{\sigma_i}\right] * \left[\frac{x_i - \mu_i}{\sigma_i}\right]^T}\ ,\ i = 1,2 \tag{3.16}$$

subjected to

$$\begin{aligned} g(x) &= 5x_1 + 3x_1x_2 - 240 \\ x_1 &\geq 9 \end{aligned} \tag{3.17}$$

Step 1: Converting the problem statement into standard form.

$$p(x) = min\sqrt{\left[\frac{x_i - \mu_i}{\sigma_i}\right] * \left[\frac{x_i - \mu_i}{\sigma_i}\right]^T}\ ,\ i = 1,2 \tag{3.18}$$

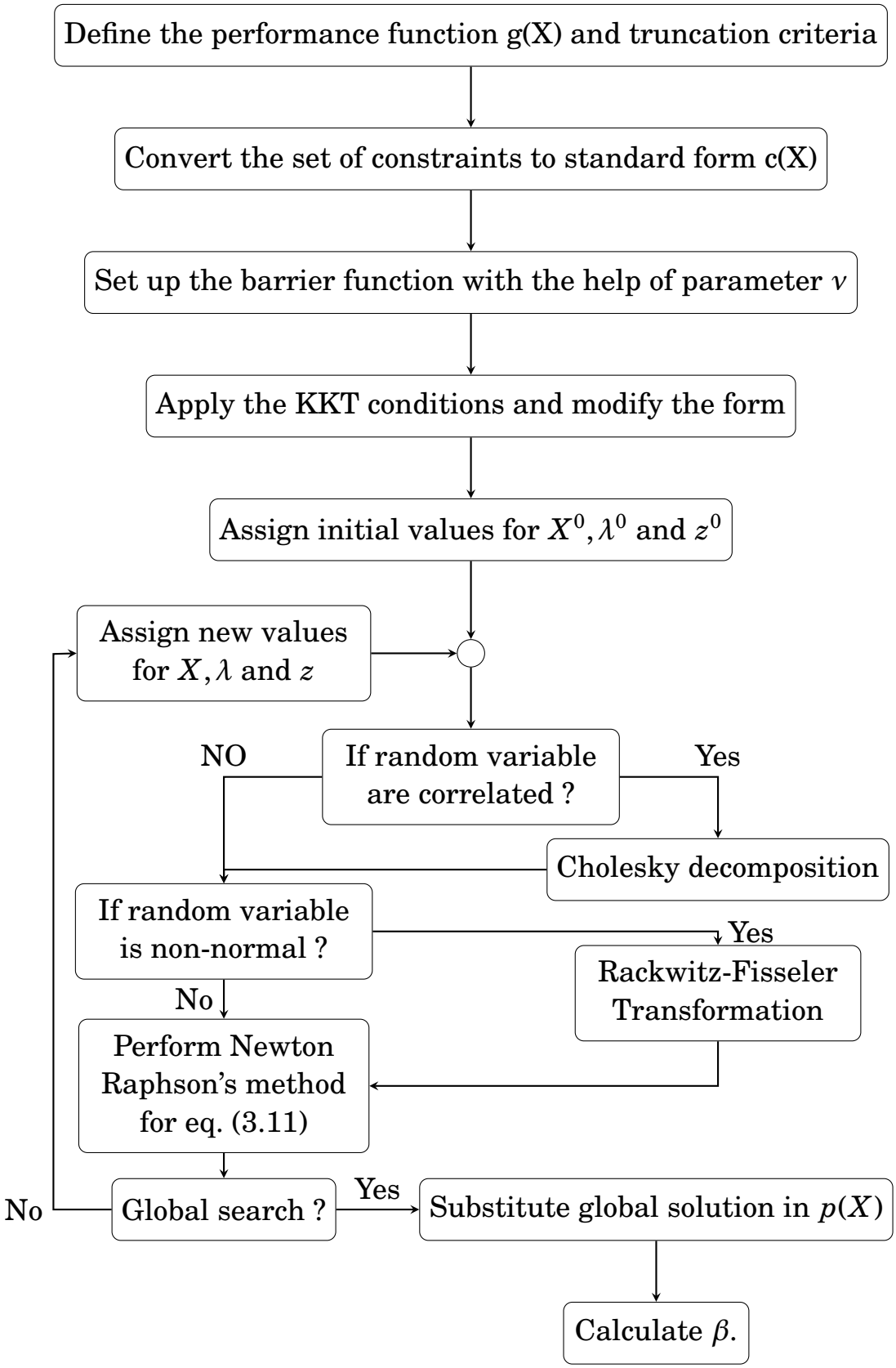

Figure 3.1: Algorithm for FORM based on truncated distribution

subjected to

$$\begin{aligned} c(x) &= 0 \\ S &\geq 0 \end{aligned} \tag{3.19}$$

where

$$c(x) = \begin{cases} 5x_1 + 3x_1x_2 - 240 \\ x_1 - 9 - S \end{cases} \tag{3.20}$$

The function $p(x)$ can be written as

$$\begin{aligned} p(x) &= \sqrt{\left[\frac{x_i - \mu_i}{\sigma_i}\right] * \left[\frac{x_i - \mu_i}{\sigma_i}\right]^T}, \; i = 1,2 \\ &= \sqrt{\left[\frac{x_i - \mu_i}{\sigma_i}\right]^2} \\ &= \sum_{i=1}^{2} \frac{x_i - \mu_i}{\sigma_i} \end{aligned} \tag{3.21}$$

Step 2: Setting up the barrier function ν for inequality constraint.

$$p(x) - \nu \sum_{i=1}^{2} ln x_i = 0 \tag{3.22}$$

subjected to

$$c(x) = 0 \tag{3.23}$$

Step 3: Applying KKT conditions for above problem statement with equating to zeros.

$$\begin{aligned} \Delta p(x) + \lambda \Delta(x) - \nu \sum_{i=1}^{2} \frac{1}{x_i} &= 0 \\ c(x) &= 0 \end{aligned} \tag{3.24}$$

Step 4: Defining the z matrix and the modified version of KKT condition can be written as

$$\begin{aligned} \Delta p(x) + \lambda \Delta(x) - z &= 0 \\ c(x) &= 0 \\ xze - \nu e &= 0 \end{aligned} \tag{3.25}$$

where e is singular matrix and z is diagonal matrix which can be written as

$$z = \begin{bmatrix} z_1 & 0 \\ 0 & z_2 \end{bmatrix}$$

z_1 & z_2 are equal to $\frac{v}{x_1}$ and $\frac{v}{x_2}$, respectively.

Step 5: Establishing the modified set of KKT condition feasible to Newton Raphson's method.

$$\Delta_x c(x) = \begin{bmatrix} 5+3x_2 & -1 \\ 3x_1 & 0 \end{bmatrix}$$

$$\Delta_x p(x) = \begin{bmatrix} \frac{1}{\sigma_1} \\ \frac{1}{\sigma_2} \end{bmatrix}$$

For constructing the hessian matrix w,

$$w = \Delta^2_{xx} L(x, \lambda, z) = \Delta^2_{xx}(p(x) + \lambda_1 c_1(x)^T + \lambda_2 c_2(x)^T - z) \tag{3.26}$$

By taking the second order partial derivatives, we get

$$\Delta^2_{xx} p(x) = 0 \ ,$$

$$\Delta^2_{xx} c_1(x) = \begin{bmatrix} 0 & 3 \\ 3 & 0 \end{bmatrix}$$

$$\Delta^2_{xx} c_2(x) = 0$$

Therefore,

$$\begin{aligned} w &= \lambda_1 * \Delta^2_{xx} c_1(x) \\ &= \lambda_1 * \begin{bmatrix} 0 & 3 \\ 3 & 0 \end{bmatrix} \end{aligned} \tag{3.27}$$

$$\begin{bmatrix} w & \Delta c_1(x_k) & \Delta c_2(x_k) & -I \\ \Delta c_1(x_k)^T & \Delta c_2(x_k)^T & 0 & 0 \\ z & 0 & 0 & x_k \end{bmatrix} \begin{bmatrix} d_k^{x1} \\ d_k^{x2} \\ d_k^{\lambda 1} \\ d_k^{\lambda 2} \\ d_k^{z1} \\ d_k^{z2} \end{bmatrix} = \\ - \begin{bmatrix} \Delta p(x_k) + \lambda_{1k} \Delta c_1(x_k)^T + \lambda_{2k} \Delta c_2(x_k)^T - z_k \\ c(x_k) \\ x_k z_k e - \nu e \end{bmatrix} \tag{3.28}$$

Step 6: Transforming the system of equation into symmetrically linear. The value of barrier function is fixed as $\nu_j = 1$ and alpha values in eq. 3.14 is taken as 1. Let the initial guesses for $x_{1k} = 10.29$, $x_{2K} = 12.0$, $\lambda_{1K} = 0$, $\lambda_{2K} = 0$.

From eq. (3.20),

$$\begin{aligned} S &= 10.29 - 9 \\ &= 1.29 \end{aligned} \tag{3.29}$$

From eq. (3.12),

$$\begin{aligned} E &= \begin{bmatrix} 0.0972 & 0 \\ 0 & 0.0833 \end{bmatrix} * \begin{bmatrix} \frac{1}{10.29} & 0 \\ 0 & \frac{1}{12} \end{bmatrix} \\ &= \begin{bmatrix} 0.0094 & 0 \\ 0 & 0.0069 \end{bmatrix} \end{aligned} \tag{3.30}$$

Therefore, the linear system of eq. (3.28) can be written as

$$\begin{bmatrix} 0.0094 & 0 & 41 & 1 \\ 0 & 0.0069 & 30.87 & 0 \\ 41 & 30.87 & 0 & 0 \\ 1 & 0 & 0 & 0 \end{bmatrix} * \begin{bmatrix} d_k^{x_1} \\ d_k^{x_2} \\ d_k^{\lambda_1} \\ d_k^{\lambda_2} \end{bmatrix} = \begin{bmatrix} 1.26 \\ 0.67 \\ -240 \\ 9 \end{bmatrix} \tag{3.31}$$

The above equation is in the form of $AX = B$. Therefore, $X = A^{-1}B$.

$$\begin{bmatrix} d_k^{x_1} \\ d_k^{x_2} \\ d_k^{\lambda_1} \\ d_k^{\lambda_2} \end{bmatrix} = \begin{bmatrix} 9.0000 \\ -19.7279 \\ 0.0261 \\ 0.1047 \end{bmatrix} \tag{3.32}$$

The new iterative values using eq. (3.14) are found to be $x_1 = 19.29$, $x_2 = -7.73$, $\lambda_1 = 0.0261$ and $\lambda_2 = 0.1047$. Therefore, the iterative procedure carries for different values of v_j till the KKT conditions are satisfied.

On performing the truncated based FORM using MATLAB, β is found to be 3.5756 and probability of failure was $1.7470 * 10^{-4}$. This solution matches approximately with the results of Melchers et al. (2003) ($\beta = 3.61$, the probability of failure = $1.55 * 10^{-4}$). The analysis is carried out using MATLAB programming, and the sample output is presented in appendix A.

3.3 Truncated based Reliability Analysis of Bearing Capacity of Strip Footing

The probability of failure of a shallow strip footing is being investigated whose width is 1.2m, and the surcharge load on the footing is 18 kPa. The load at the base of the footing is 200 KN/m, and the unit weight of the soil is about 20 KN/m^2. The cohesion and the frictional angle are considered to be a normal random variable whose mean and standard deviation are 20,5 KN/m^2 and 15,2°, respectively. It was found that the correlation coefficient between the variables is -0.5.

Let's determine the probability of failure with a condition that the designing of the footing is done based on the inference that the upper bound of the cohesion is limited at $30KN/m^2$ and the upper bound truncated point of the frictional angle is 18°. The performance function of

the model is shown in eq. (3.33). The problem statement is taken from Low (2014).

$$PerFn = q_u - q \tag{3.33}$$

where

$$\begin{aligned} q_u &= cN_c + p_0 N_q + \frac{B}{2}\gamma N_\gamma \\ N_q &= e^{\pi tan\phi} tan^2(45 + \frac{\phi}{2}) \\ N_c &= (N_q - 1)cot\phi \\ N_\gamma &= 2(N_q - 1)tan\phi \end{aligned} \tag{3.34}$$

c is the cohesion, ϕ denotes frictional angle, p_0 is the surcharge load, and γ is the unit weight of the soil. The estimated truncated normal distribution statistical parameters using MLE for cohesion and frictional angle is (19.8,4.95)KN/m^2 and (14.9,1.97)°, respectively. The truncated normal probability distribution of cohesion and the frictional angle is shown in Figs. 3.2 and 3.3, respectively. The probability of failure is found to be 0.8884, corresponding to β=-1.2182.

3.3.1 Truncated based Reliability Analysis of Bearing Capacity of Strip Footing at Nipigon

The reliability analysis can be performed on truncated log-normal distribution developed based on censored samples. Let us consider the log-normal probability distribution of undrained shear strength which is being illustrated in chapter 2 (Figs. 2.2, 2.4, & 2.6). Eq. (3.33) is used as performance function. The depth of the footing is taken as 1.2m, and the load at the base of the footing is taken as 200 KN/m. Since the soil is clay, the parameter ϕ becomes zero. The density of the soil is considered as a random variable which follows log-normal distribution, and the statistical parameter is taken as (19,3.8) (Singh, 2018). By making the limitation for the flow of design point as explained in section 3.2. β and

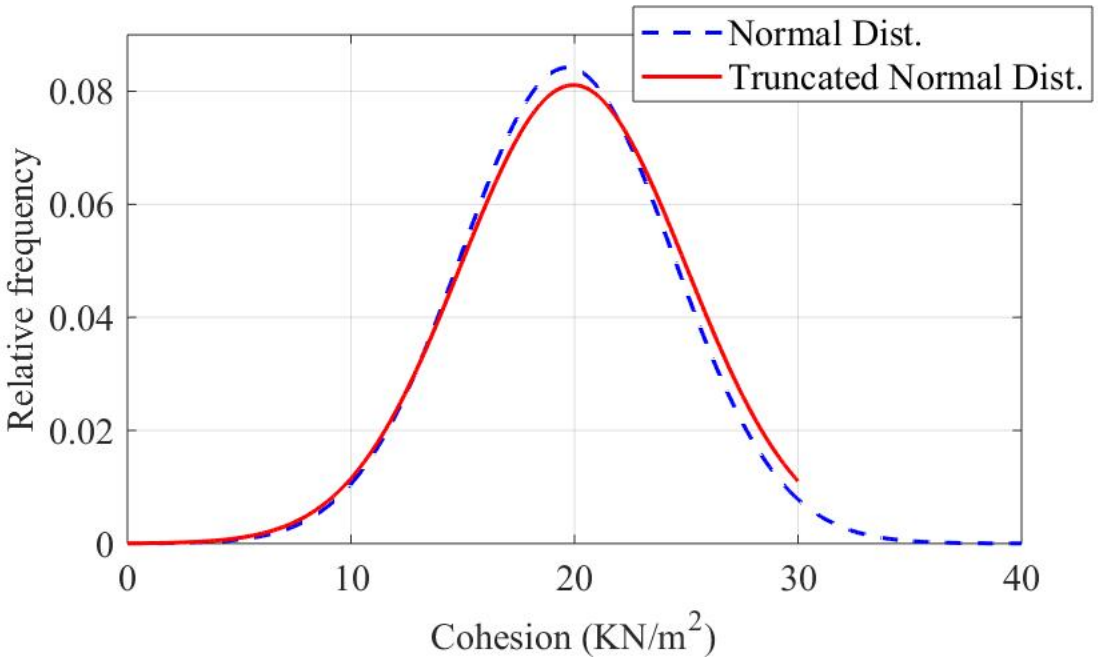

Figure 3.2: Upper bound truncated normal probability distribution of cohesion

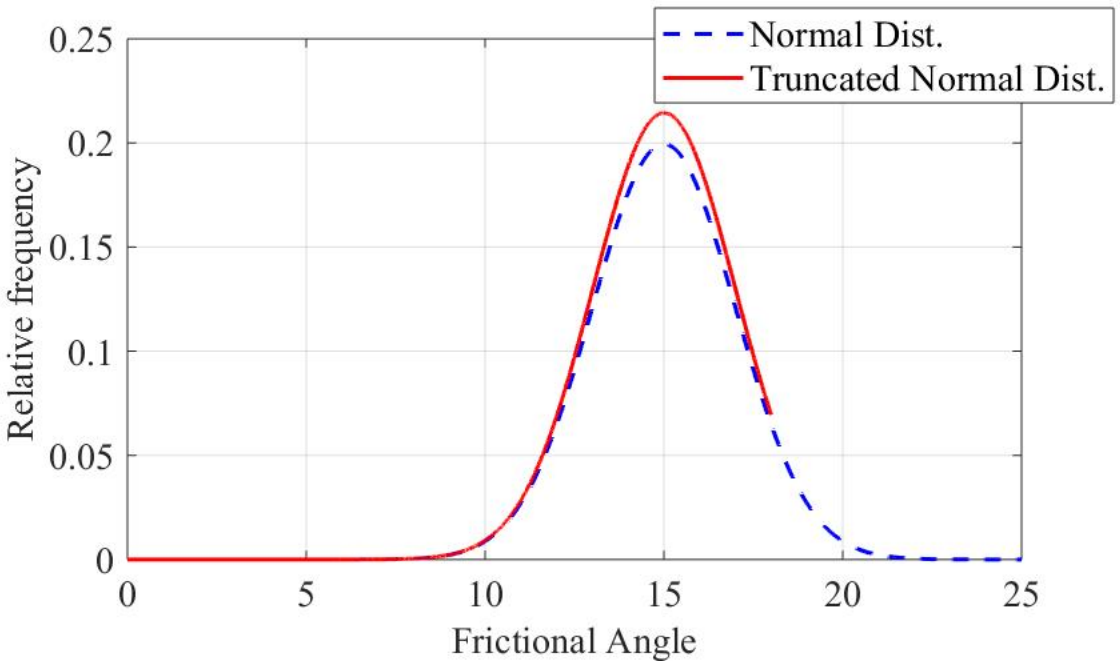

Figure 3.3: Upper bound truncated normal probability distribution of frictional angle

the probability of failure for the strip footing are determined for various truncation conditions and shown in Table 3.1.

Table 3.1: Reliability analysis of strip footing based on censored samples

Truncated Distribution Condition	β	Probability of Failure
Doubly truncated	1.5029	0.0664
Lower bound truncated	1.2692	0.1022
Upper bound truncated	1.4064	1.4064

3.4 Summary

In current chapter, determining the Hasofer-Lind's reliability index using interior point method available in *fmincon* function has been discussed. The proposed algorithm produced acceptable results. Later, truncated based FORM for soil bearing capacity of strip footing of two different problem statements are carried out. From the results obtained, it is concluded that the proposed algorithm can be used to determine the probability of failure using FORM based on truncated distributions.

Chapter 4

Soil Liquefaction Potential

Triggering of soil liquefaction arises due to the increase in the pore-pressure which is a function of the ground motion induced by the earthquake. In-situ test makes it feasible to determine the soil liquefaction resistance offered by the soil. An empirical relationship can be developed using artificial intelligence and regression analysis based on historical post-liquefaction cases. This chapter presents the procedure to evaluate the liquefaction potential of the soil using deterministic, probabilistic and reliability approach.

4.1 Methodolgy

For evaluating the liquefaction potential of soil strata, it is important to investigate the relationship between the Cyclic Stress Ratio (CSR) and Cyclic Resistance Ratio (CRR) from past historical cases. With this aspect about 213 post-liquefaction cases from Çetin et al. (2004) and Çetin et al. (2016) are taken. The database is presented in Table B.1. The table complies of 117 liquefied cases and 96 non-liquefied cases. The details include the mean and standard deviation of the soil, site and seismic parameters. For the analysis of the soil liquefaction potential, parameters of seismic, soil and site like total pressure and effective

pressure at the critical depth, horizontal peak ground acceleration, stress reduction factor, SPT-N value, fineness content of the soil and magnitude of the earthquake must be considered. The significance of these parameters has been already discussed in the chapter 1. For the reliability analysis of soil liquefaction potential, the coefficient of correlations are taken from the Juang et al. (2008).

In the present study, the prediction for the occurrence of soil liquefaction is being done using Liquefaction Index (LI) function which is developed using ANN. LI is a function that is framed using liquefaction parameters which separates the liquefaction cases from non-liquefaction cases. With the help of LI function and the search algorithm, critical CSR values are determined. The neural network model for LI function is developed based on the guidelines provided by Beale et al. (2012). On the other hand, the clean-sand equivalent SPT-N count $(N_1)_{60cs}$ is determined using eqs. 1.13-1.19. The boundary curve reflecting the "limit state curve" is determined using regression analysis between the critical cyclic stress ratio (CRR) and $(N_1)_{60cs}$. Using the limit state curve, liquefaction potential is evaluated for 213 cases, and the maximum entropy distribution is developed for both liquefaction and non-liquefaction cases. The Bayesian function is used for developing the probability of liquefaction (P_L).

For quantifying the uncertainty present and including them in the model, reliability-based analysis associated with the Bayesian function approach is used. The Bayesian theory of conditional probability is used to relate factor of safety (F_s) with P_L. Hasofer-Lind FORM is used to carry out a reliability-based analysis of liquefaction potential. The model which uses the global search option involved with $fmincon$ function with interior point method available in MATLAB programming is used for determining the global minimum distance or reliability index in the reduced space of Hasofer-Lind's ellipsoid. Sensitivity analysis is

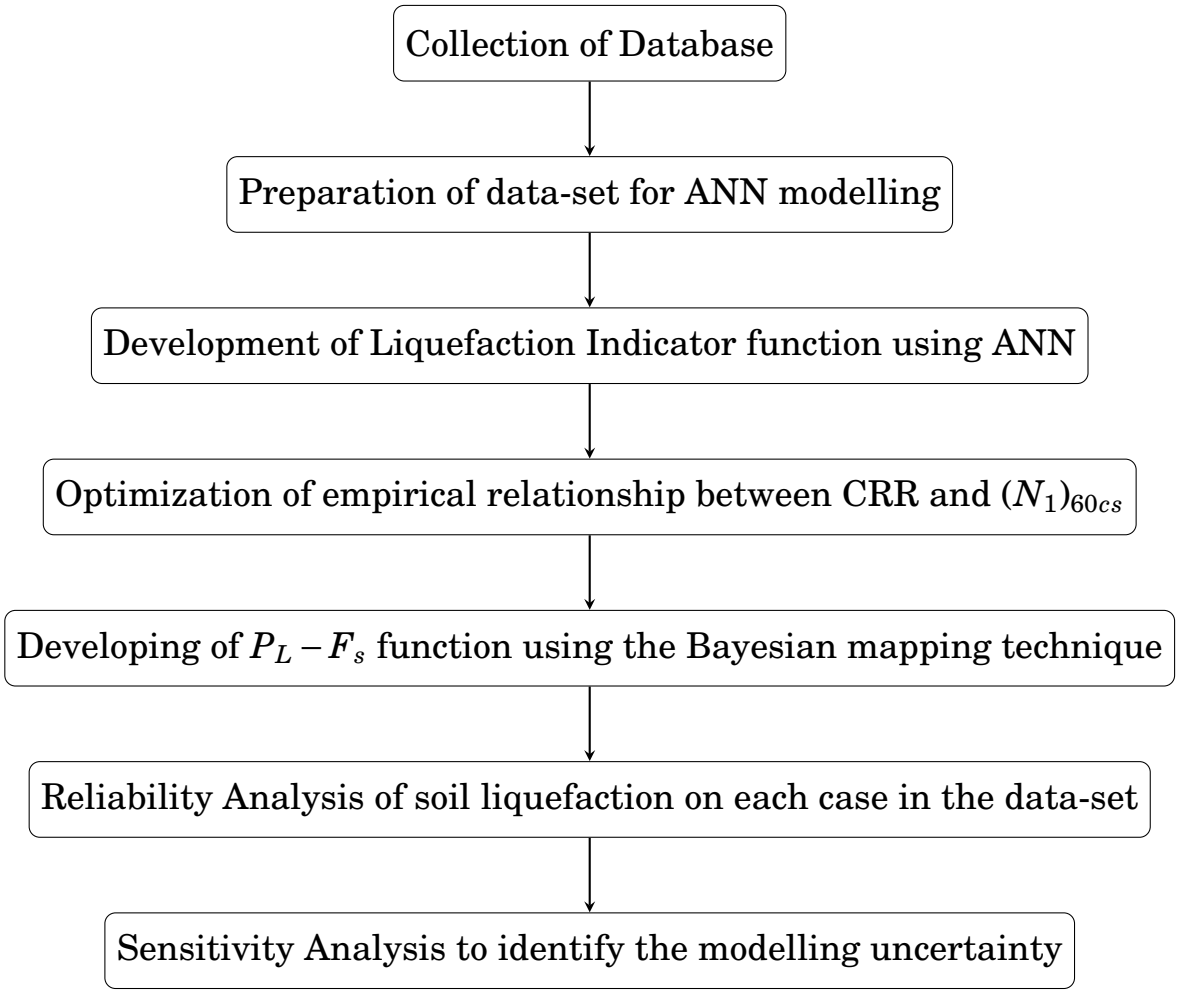

Figure 4.1: Flowchart of the proposed research for developing relationships to estimate the liquefaction potential

performed for determining the modeling uncertainty. MATLAB programs are developed for the neural network model, the maximum entropy probability distribution and reliability-based analysis. Rackwitz and Fiessler (1978) method is used for the transformation of the maximum entropy variables to the equivalent standard normal variables. Fig. 4.1 describes the sequential stages of research for developing soil liquefaction potential relationships.

4.2 Developing Relationship Between CRR and SPT-N

The preliminary step in framing the limit state curve is to separate the liquefaction cases and non-liquefaction cases. The LI can predict, the occurrence of liquefaction in the site. LI function can be developed with the help of ANN by representing one as liquefied case and zero as the non-liquefied case. Liquefaction indicator is expressed as

$$LI = f(CSR, (N_1)_{60}, FCI, \sigma'_v) \tag{4.1}$$

where LI stands for Liquefaction index, CSR is the cyclic stress ratio that can be calculated using eq. 1.9 developed by Idriss and Boulanger (2006), $(N_1)_{60}$ stands for the corrected SPT-N count, FCI denotes the Fines Content Indicator, σ'_v stands for effective pressure at the critical depth. The value of FCI is obtained based on the fineness content of the soil, and presented in Table 4.1. FCI is classified into three categories, i.e., $FC \leq 5, 5 < FC < 35, FC \geq 35$, where FC stands for fineness content.

Triggering of the soil liquefaction is associated with the fineness content of the soil, and hence based on the fineness content; adjustments are made to SPT-N values. FCI is used for the transformation of the corrected SPT-N values to clean sand equivalent SPT-N values. Therefore, $(N_1)_{60}$ and FCI are the important parameters in calculating of soil resistance to liquefaction (CRR).

Table 4.1: Fines content indicator Juang et al. (2000b)

Fineness content FC (%)	**Fines content indicator, FCI**
FC ≤ 5	1
5 < FC < 35	2
FC ≥ 35	3

LI function has a high rate of non-linearity with the associated parameters, and hence it is a complicated task to determine the exact

relationship. By using appropriate ANN functions and number of neurons, the effective model for LI function can be developed. Hence, an ANN model for LI function is created using a three-layer feedforward back-propagation network with four neurons in the hidden layer and one neuron in the output layer. The number of neurons in the hidden layer is decided based on the trial and error technique. The transformation function for each neuron in both the layers is taken as Log-sigmoid. The function has the limit from 0 to 1, which suits best for our case as 0 denotes non-liquefaction and 1 indicates as liquefaction case. The feed forward back-propagation neural network view for liquefaction indicator function is shown in Fig. 4.2 and the skeleton diagram is demonstrated in Fig. 4.3. Initially the inputs have equal weighs. By gradually reducing the root mean square of prediction errors during network training to an acceptable level, the weights and biases are determined.

The mathematical expression of the described feed forward back-propagation neural network can be written as

$$LI = f_T\left\{B_0 + \sum_{k=1}^{n}\left[W_k f_T\left(B_{Hk} + \sum_{i=1}^{m} W_{ik} P_i\right)\right]\right\} \tag{4.2}$$

where B_0 is the bias for the output layer which contains one neuron in it; W_k is the weight of the connection between neuron k of the hidden layer and the single output layer neuron; B_{Hk} is the bias at neuron k of the hidden layer ($k = 1, n$); W_{ik} is the weight of the connection between input variable ($i = 1, m$) and neuron k of the hidden layer; P_i is the input parameter. For LI function, the number of inputs are 4 as per eq. 4.1.

The definition of the log-sigmoid transformation function is given as

$$f_T(x) = \frac{1}{(1 + e^{-x})} \tag{4.3}$$

The neurons have to be trained first using a set of data to identify the type of case and to have better functionality. This is similar to the human

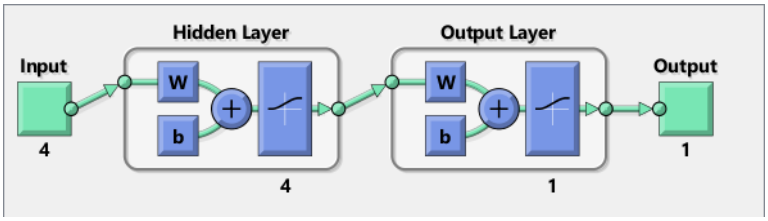

Figure 4.2: Neural Network for LI function

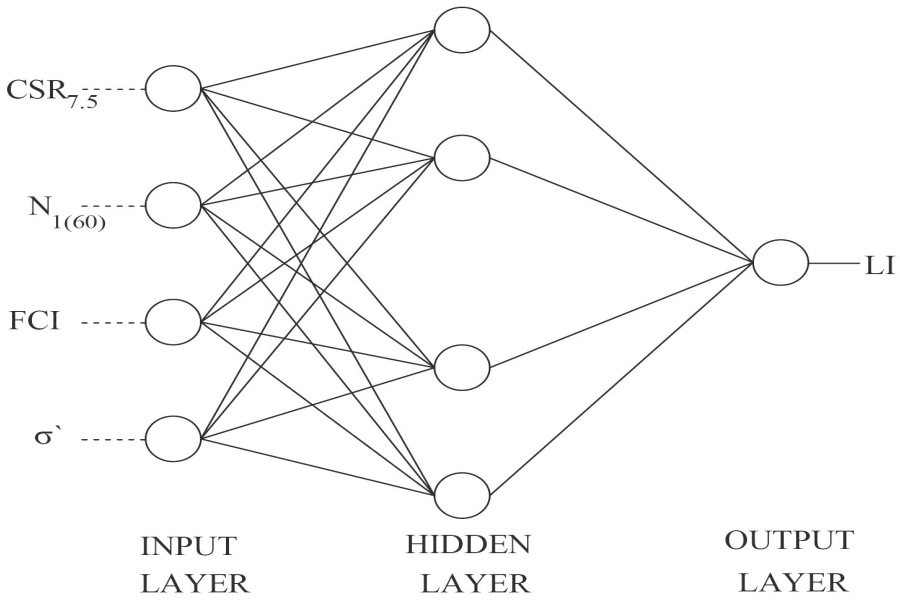

Figure 4.3: Skeleton diagram of the neural network

brain. The learning of the neurons is later examined by using testing data. The neurons are trained until the goals are being achieved. Levenberg-Marquardt back-propagation is used as the training function since it provides high computational efficiency (Juang and Chen, 1999).

A total of 163 cases are used for the training of ANN model, and the rest of the 50 cases are used for the validation of the model. The training set consits of 95 liquefaction cases and 68 non-liquefaction cases. The testing set has 34 number of liquefaction cases and 16 number of non-liquefaction cases. The input parameters $CSR, (N_1)_{60}, FCI$ and σ'_v are

normalized to value between 0 and 1. It is clear that the output set or the targets describe liquefaction or non-liquefaction which is represented by 0 and 1, hence normalization is not required for these targets. Normalization of the data is done using eq. 1.20. With the help of generalization ideas, the issue of over-fitting or over-training of neurons that arises in the neural network can be avoided. With generalization, the efficiency of predicting the liquefaction condition improves. The ideology of taking multiple numbers of neural networks as a tool of generalization is utilized for modeling.

Once the training of multiple networks is over, based on the mean square root (mse) value, the coefficient of determination (R^2) and accurate prediction of the soil liquefaction condition, the best network is selected. Ten number of neural networks were used for generalization and the 3^{rd} network was found to satisfy above-mentioned criteria and hence it is considered to be the best model. The output of the MATLAB programming for the neural network modeling is shown in appendix C. The training state of a network is shown in Fig. 4.4 and the training performance of the best model is shown in Fig. 4.5.

The accuracy of the neural network model is calculated based on the success rate. The success rate is explained by Juang and Chen (2000), which is one of the appropriate approaches for measuring the efficiency of the trained model. The success rate of the selected best model is defined as the accurate prediction of the occurrence of liquefaction or not. In order words, the prediction is awarded to be successful for the case CRR>CSR provided that non-liquefaction was observed at the site. This success can be even related to liquefaction in the same way, i.e., the prediction is successful for CRR<CSR and liquefaction was experienced in the site. The success rate of the best model was 93.89%. The correlation of determination (R^2) for the training set, validation set, and complete data

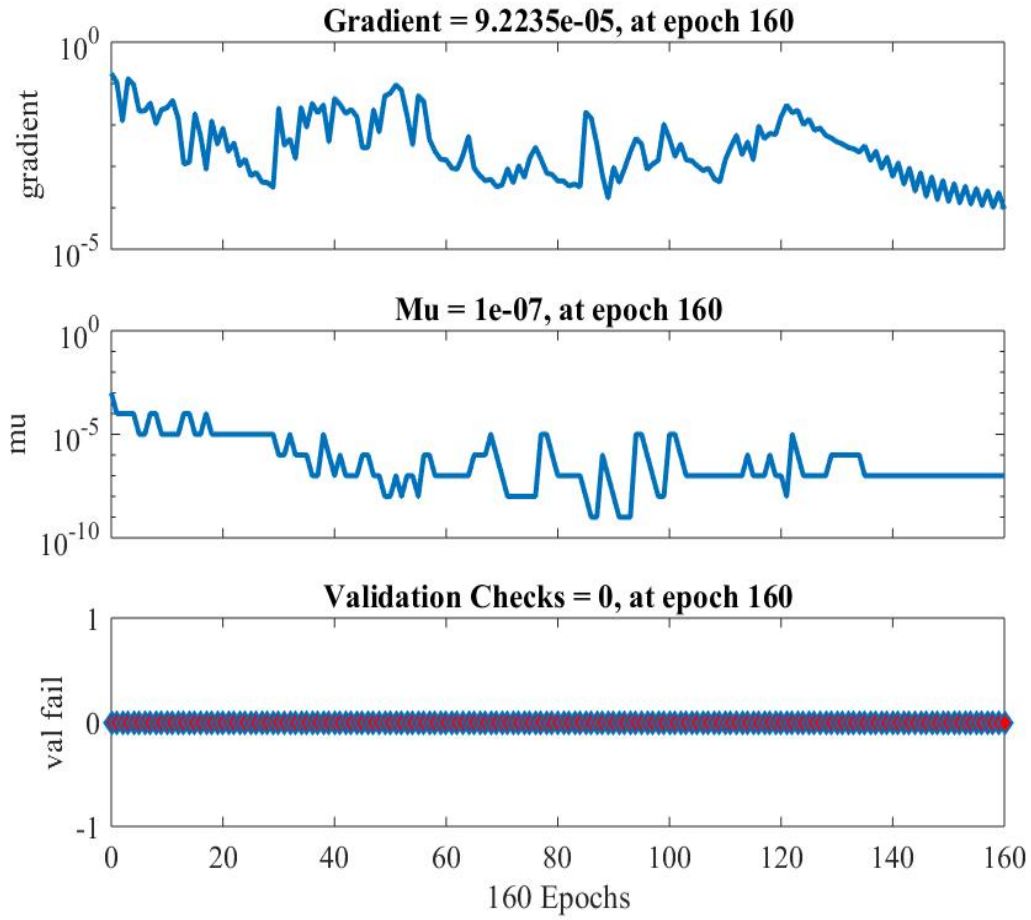

Figure 4.4: Training state of neural network model

was found to be 0.95,0.71 and 0.89, respectively, and they are shown in Figs. 4.6, 4.7 and 4.8. The details about the weight and bias of the best model are presented in Table 4.2.

Using the developed best ANN model for LI function, the unknown points that form boundary curve should be identified. For this purpose, the searching algorithm for the unknown points developed by Juang et al. (2000b) is used and the critical CSR value is calculated. The searching algorithm for the critical CSR is shown in Fig. 4.9. Liquefied and non-liquefied cases in the database can be represented as a point in the limit state surface. The optimization procedure in the searching

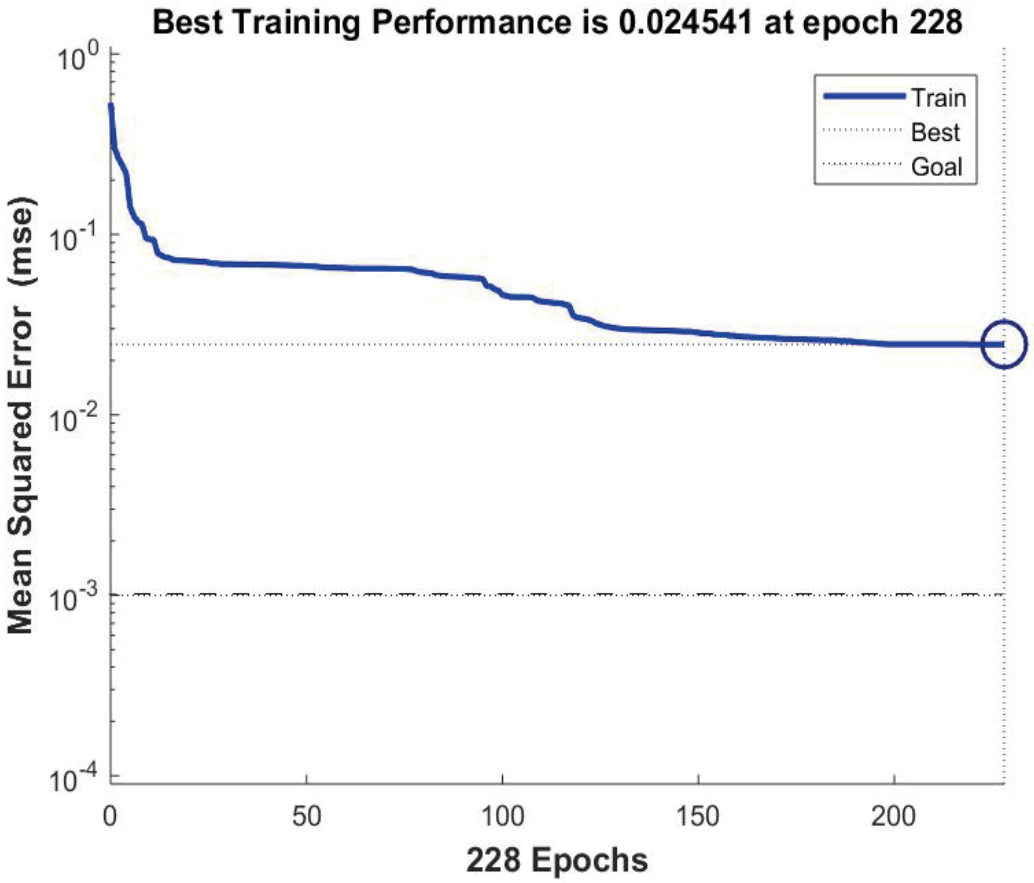

Figure 4.5: Training performance of ANN model

Table 4.2: Details about the weighs and bias of best model

Hidden	Weight					Bias	
neuron	W_{ik}				W_k	B_k	B_0
(k)	Input 1	Input 2	Input 3	Input 4	Output	Hidden layer	Output layer
k=1	-2.02	-0.75	21.93	0.97	-2553.43	-8.41	-1625
k=2	188.25	52.67	64.85	54.02	419.16	-88.67	
k=3	44.36	-7.08	-33.14	8.87	1962.74	1.03	
K=4	-89.14	18.71	112.41	-20.78	1237.46	-12.88	

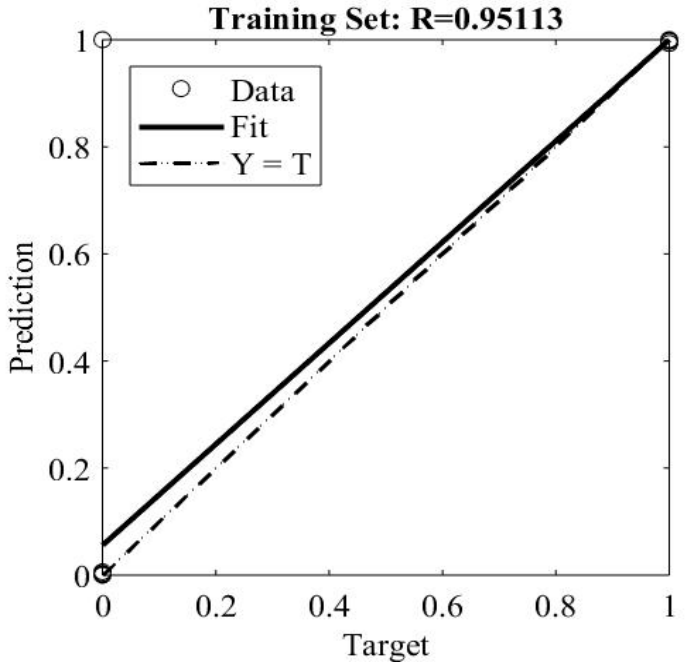

Figure 4.6: Comparison of target and ANN model prediction for training set

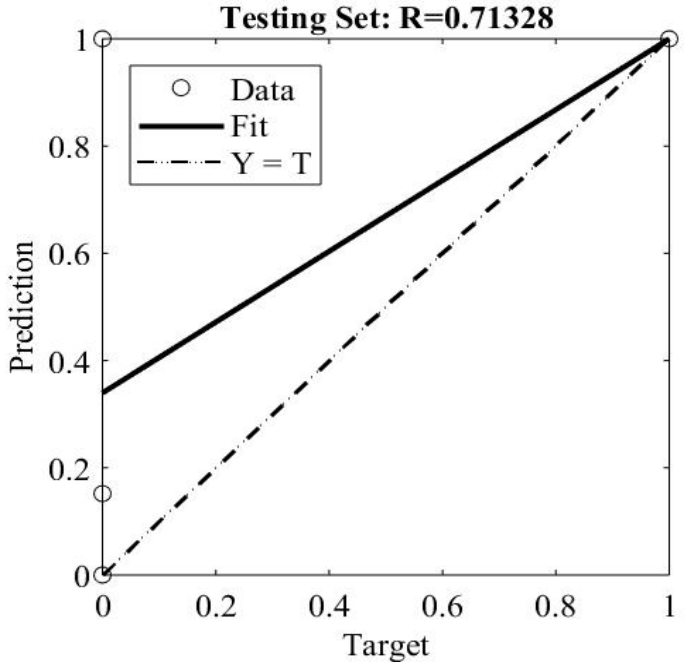

Figure 4.7: Comparison of target and ANN model prediction for testing set

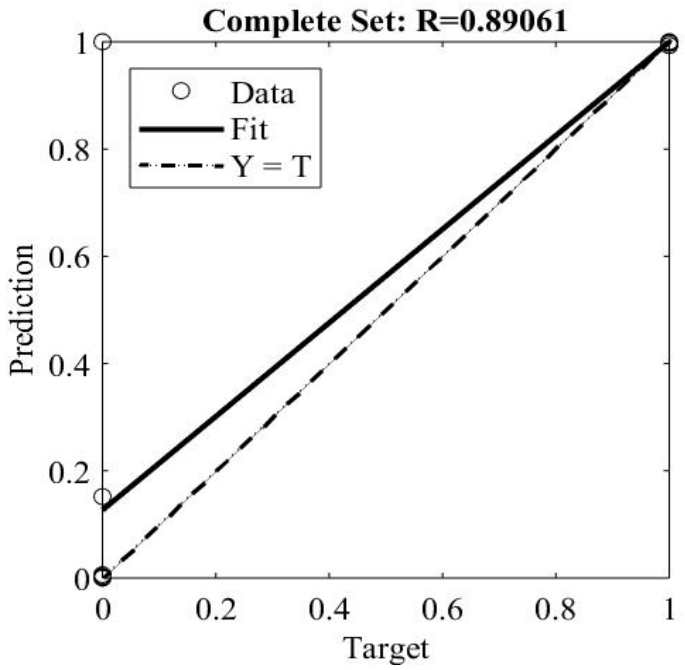

Figure 4.8: Comparison of target and ANN model prediction for complete data-set

algorithm can be well understood by using the flowchart shown in Fig. 4.10. The liquefied cases can be located above the limit state curve, and the non-liquefied case can be located below the limit state curve. This can be explained by using performance function $CRR - CSR$.

When the $CRR - CSR$ is equal to zero, the point lies on the limit state boundary. If $CRR - CSR > 1$, liquefaction will not occur, and the point lies below the limit state boundary. When $CRR - CSR < 1$, liquefaction occurs, and the point lies above the boundary. The blue square in Fig. 4.9 represents the non-liquefied case whereas the red circle represents the liquefied case. The liquefied case follows path A and the non-liquefied case follows path B. When dealing with the red circle that lies above the limit state curve (liquefied case), the cyclic stress induced by the earthquake is reduced following path A, and it is then evaluated in the LI function obtained from the best ANN model (Eq. 4.2).

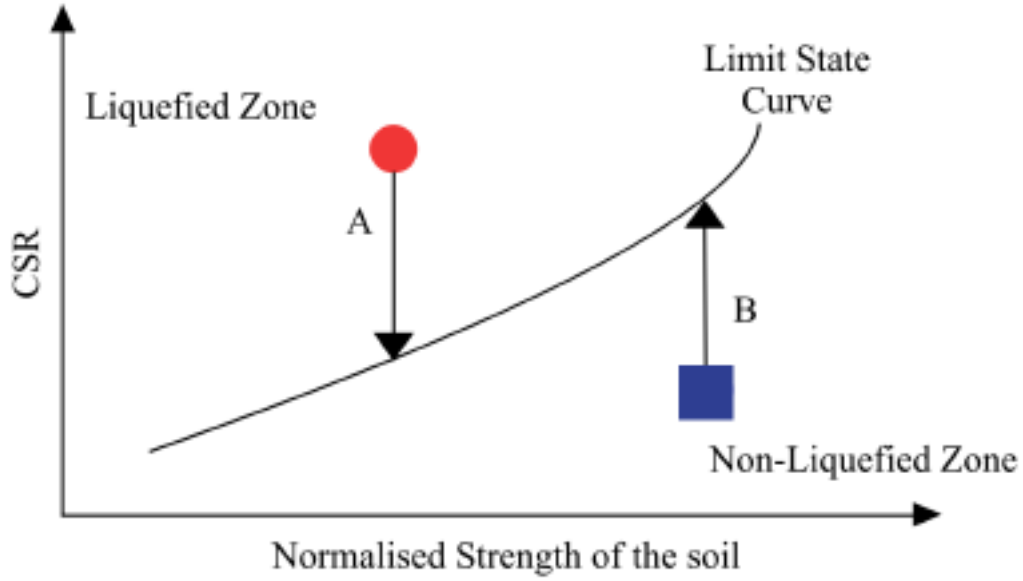

Figure 4.9: Searching for points on the limit state boundary, modified from Juang et al. (2000b)

This process of continuity in the decrease of CSR value carries out till the red circle falls on the limit state curve, i.e., the value of the LI changes from 1 to 0 and thus liquefaction condition changes from liquefaction to non-liquefaction. Similar procedure was carried out for the non-liquefaction state. The blue square follows the path along B, and the cyclic stress induced by the earthquake is increased by a small value, and each time the values are evaluated in the ANN-based developed LI function (eq. 4.2). By doing so, the blue square follows path B, and once it reaches the limit state boundary, the process of increasing the CSR value comes to an end. The value of LI changes from 0 to 1 and therefore, the liquefaction condition eventually changes from non-liquefied to liquefied state. The updated CSR values are the critical cyclic stress (critical CSR or CRR) values for the particular soil condition. The optimization of the CSR values based on the above concept is carried out using a code developed, with the help of MATLAB programming.

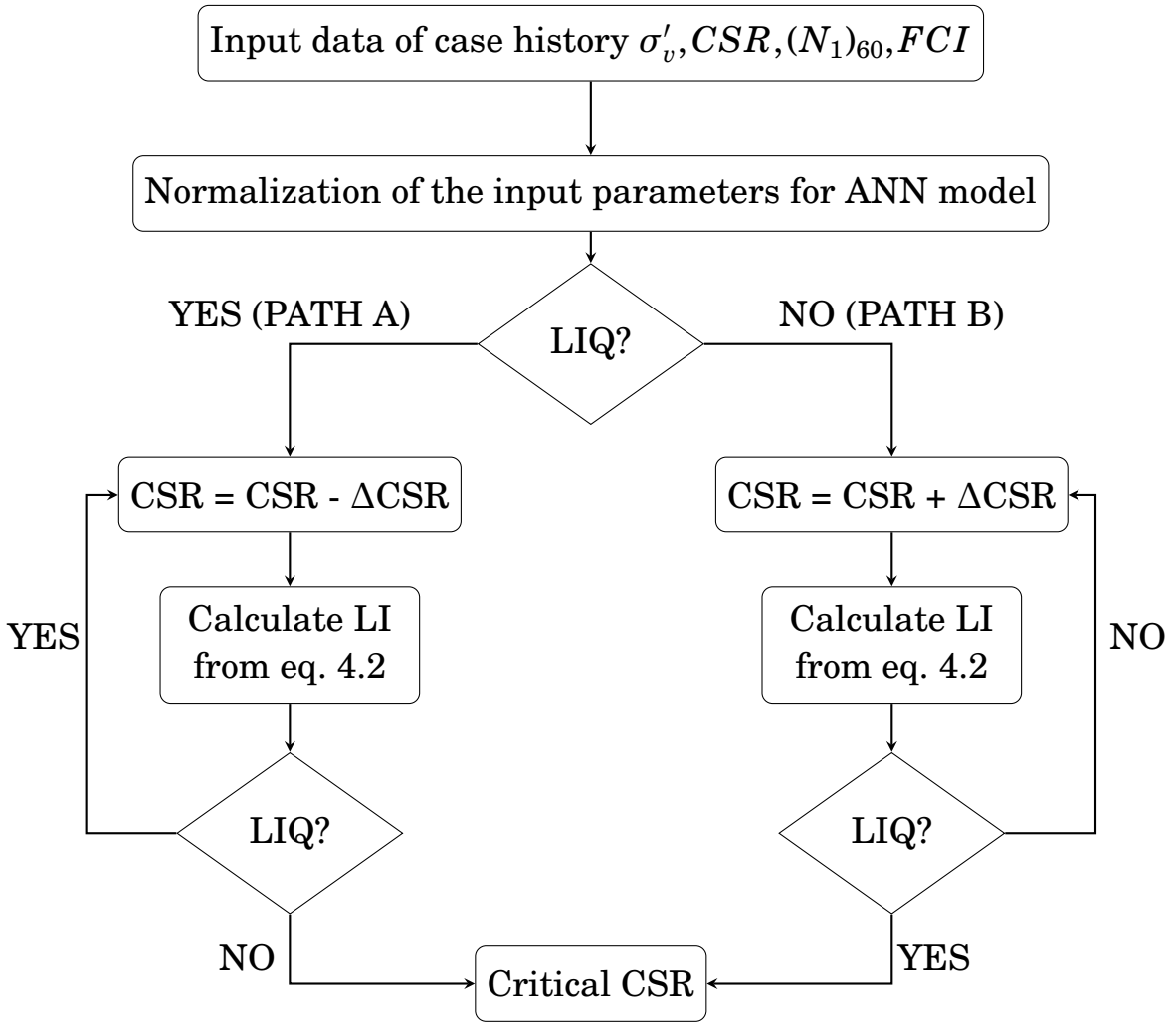

Figure 4.10: Searching algorithm for critical CSR, modified from Juang et al. (2000b)

Sometimes for a few cases, the optimization of the CSR values may not be successful. This is well explained by Seed et al. (1984) and Juang et al. (2000b). The critical CSR for such cases requires searching beyond the upper and lower bound limit beyond the range of the database. Using the search algorithm, a total of 187 data points have been identified. These data points of critical CSR define the limit state surface. Critical CSR is referred as CRR and it is a function of three parameters, $(N_1)_{60}$,

FCI and σ'_v. It can be mathematically represented as

$$CRR = f((N_1)_{60}, FCI, \sigma'_v) \tag{4.4}$$

Based on eq. (4.4), the limit state equation can be established. The relationship among the above parameters is highly non-linear. The clean sand equivalent SPT-N count ($(N_1)_{60cs}$) can be calculated using eq. (1.13). With the help of non-linear regression analysis, the relationship between the critical CSR and $(N_1)_{60cs}$ is determined. The best fit of the regression model is found for reduced 187 data points, and shown in the Fig 4.11. The best fit curve defines the limit state boundary for the liquefaction potential. The empirical equation from regression analysis is

$$CRR_{7.5} = \left[\frac{(N_1)_{60cs}}{82.3}\right]^2 + \left[\frac{(N_1)_{60cs}}{973.7}\right] + \left[\frac{1}{11.4}\right] \tag{4.5}$$

Empirical relationship of $CRR_{7.5}$ found using regression analysis

Based on the above equation, potential of strong liquefaction resistance offered by the soil can be determined. Observing Fig.4.11, it can be commented that the relationship will have good performance for $(N_1)_{60cs} \leq 35$. Beyond this, the curve is defined with fewer points, and it is hard to accurately predict the $CRR_{7.5}$ using the obtained relationship. Therefore, the application of eq. (4.5) is limited to 35, and beyond this point, the effectiveness of prediction would be less. $(N_1)_{60cs} \geq 35$ sense for inter-medium soil type and hence there are less chance for soil liquefaction to occur. Eq. (4.5) covers almost all the soil that can undergo liquefaction. F_s against the soil liquefaction is defined as the ratio of $CRR_{7.5}$ to CSR. It is important to know that the probability of liquefaction occurrence can be calculated using F_s. The relationship between the probability of liquefaction and factor of safety can be developed using the Bayesian mapping function technique. Initially, F_s is calculated for all the post-liquefaction cases. Using the calculated values of F_s for both liquefaction

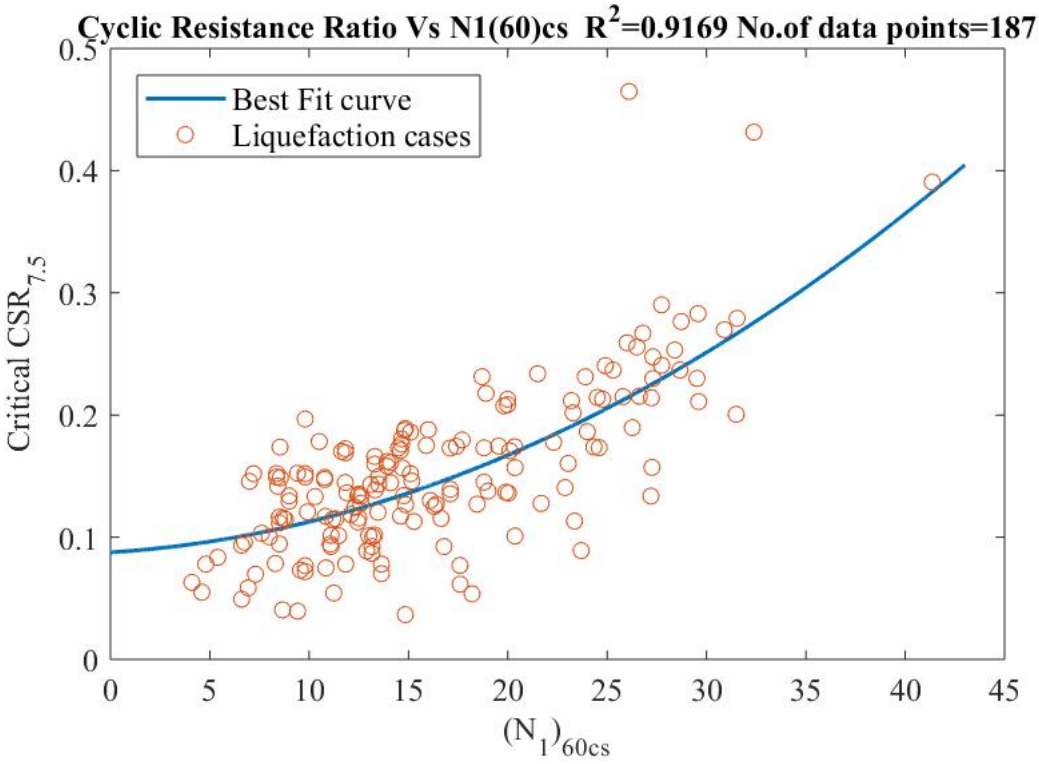

Figure 4.11: Relationship between $(N_1)_{60cs}$ and critical $CSR_{7.5}$

and non-liquefaction cases, the histogram was plotted individually. From the histogram, probabilities for liquefaction or non-liquefaction can be determined.

The maximum entropy distribution of different orders are developed for both the liquefaction categories. Using the calculated values of F_s and Bayesian mapping function, the conditional probability of liquefaction for the soil can be evaluated. According to Juang et al. (1999), the probability of liquefaction based on the condition of F_s can be written as

$$P(\frac{L}{F_s}) = \frac{P(\frac{F_s}{L})P(L)}{P(\frac{F_s}{L})P(L) + P(\frac{F_s}{NL})P(NL)} \tag{4.6}$$

where $P(\frac{L}{F_s})$ represents the probability of liquefaction for a particular F_s. The term $P(\frac{F_s}{L})$ is the probability distribution for liquefaction occurring at

F_s. Similarly, $P(\frac{F_s}{NL})$ is the probability distribution for non-liquefaction at F_s. The terms $P(L)$ and $P(NL)$ represents prior probabilities of liquefaction and non-liquefaction, respectively.

Eq. (4.6) can be further reduced by considering the term $P(\frac{L}{F_s})$ and $P(\frac{F_s}{NL})$

$$P(\frac{F_s}{L}) = \int_{F_s}^{F_s+\Delta F_s} f_L(x)dx \tag{4.7}$$

$$P(\frac{F_s}{NL}) = \int_{F_s}^{F_s+\Delta F_s} f_N L(x)dx \tag{4.8}$$

where $f_L(x)$ and $f_{NL}(x)$ are the relative frequencies of F_s and can be obtained from the PDF of liquefaction and non-liquefaction cases, respectively. The change in the F_s is very less, $\Delta F_s \rightarrow 0$. Therefore, eq. (4.6) can be rewritten as

$$P(\frac{L}{F_s}) = \frac{f_L(F_s)P(L)}{f_L(F_s)P(L) + f_{NL}(F_s)P(NL)} \tag{4.9}$$

Juang et al. (1999) has approximated the above equation with the help of the maximum entropy principle. The entropy for liquefaction and non-liquefaction is identical. Based on the concept explained on entropy in chapter 1, it is clear that $P(L) = P(NL)$.

$$P_L = \frac{f_L(F_s)}{f_L(F_s) + f_{NL}(F_s)} \tag{4.10}$$

The 3^{rd} order maximum entropy distribution was found to be the best fit for liquefied cases as shown in Fig. 4.12. Whereas, the 5^{th} order maximum entropy distribution fits best for the non-liquefaction cases as represented in Fig. 4.13. Now, the PDF for the liquefied and non-liquefied cases is available. By using the Bayesian mapping technique eq. (4.10), the function for $P_L - F_s$ is developed. The approximation of best fit for all the liquefaction cases in $P_L - F_s$ is done using logistic regression and shown in Fig. 4.14. The mapping equation is given as

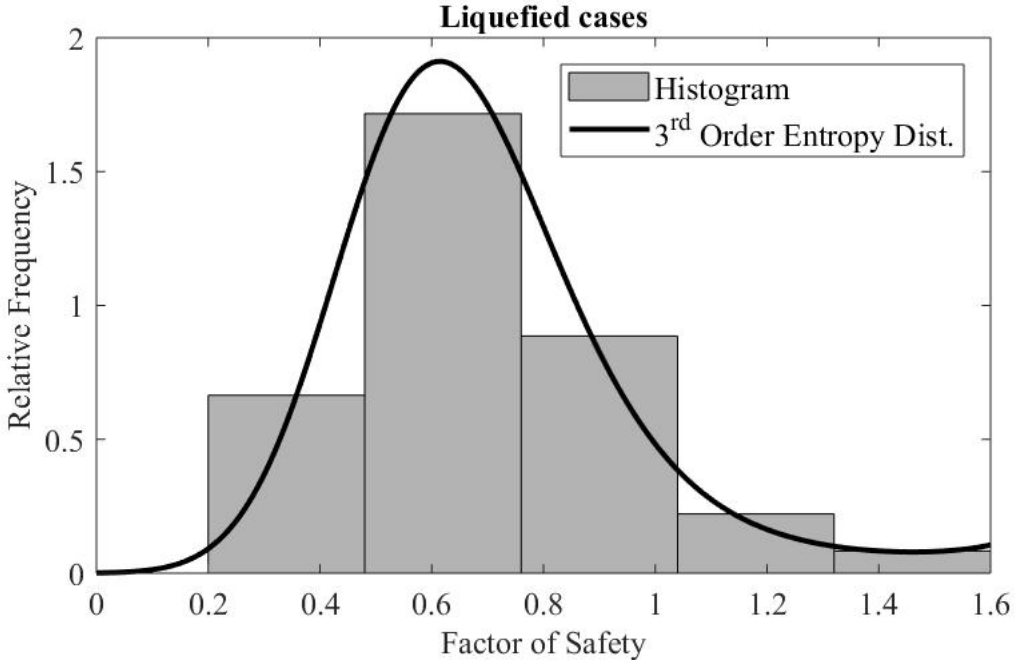

Figure 4.12: Probability distribution along with histogram for liquefied cases

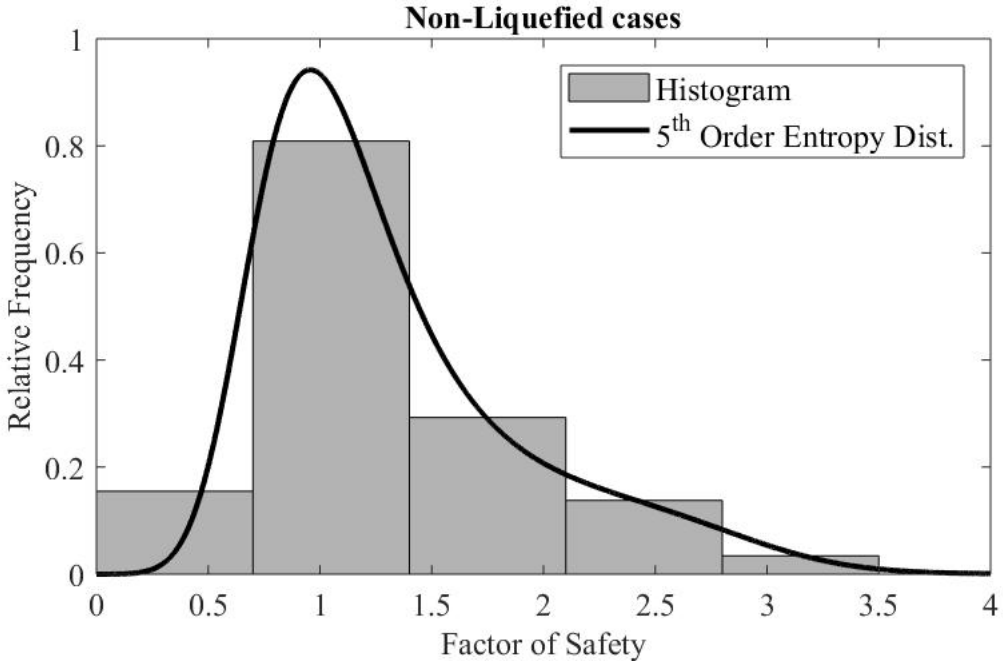

Figure 4.13: Probability distribution along with histogram for non-liquefied cases

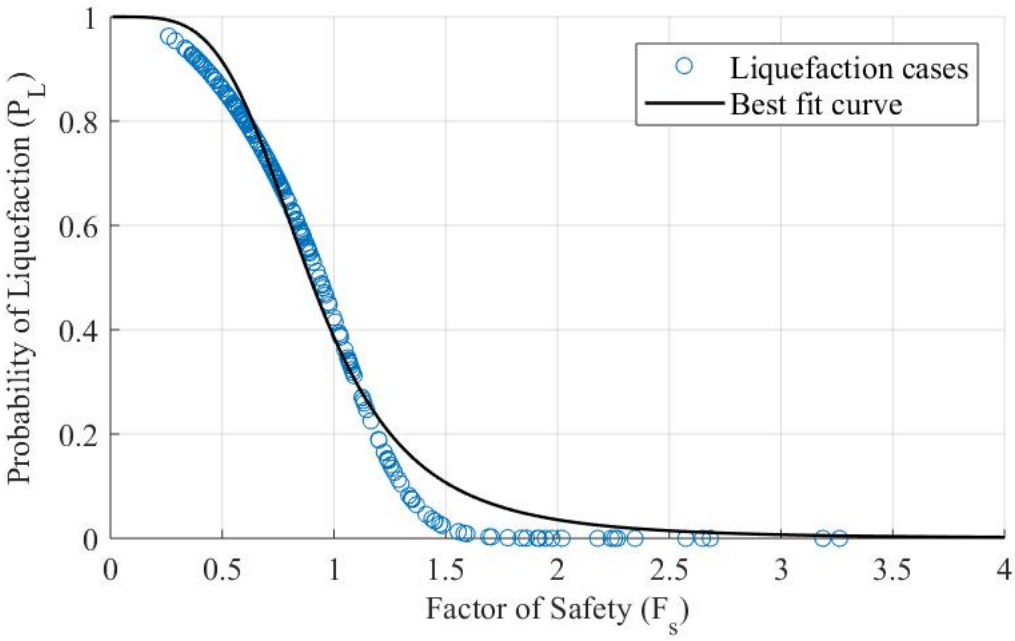

Figure 4.14: $P_L - F_s$ along with the best fit mapping function

$$P_L = \frac{1}{1+(\frac{F_s}{A})^B} \tag{4.11}$$

where A and B are the coefficients and were found to be 0.8922 and 4.085, respectively with a coefficient of correlation 0.98. On observing Fig.4.14, it can be noticed that at $F_s = 1$, the probability of liquefaction is 0.377. Apparently, when $F_s = 1$, P_L should be equal to 0.5. This rule is not following in our case. Hence, it is due to the existence of modeling uncertainty in the developed limit state empirical relationship. The problem can be overcome by identifying the model uncertainty in the system.

4.3 Investigating the Model Uncertainty using Reliability Analysis

Often the limit state curve needs to be biased so that it can separate the liquefaction cases from non-liquefaction cases. The term bias

refers to the constant that is included in the model so that $F_s = 1$ and $P_L = 0.5$. The revised equation can be written as

$$g(Z) = c * CRR - CSR \tag{4.12}$$

where c represents the modeling uncertainty of the developed model.

The position of c can also be located with CSR or can be two constants positioned CRR and CSR. Juang et al. (2006) conducted sensitivity analysis and found that the results obtained with different positioning of the constant will not have variation. The model uncertainty can be identified by dealing with the parametric uncertainty in the model. There are six parameters in the model which makes a large impact on the performance of the model. The uncertainty in the performance function is written as

$$\begin{aligned} g(Z) &= c * CRR - CSR \\ &= f(c, (N_1)_{60}, FC\sigma_v, \sigma'_v, a_{max}, M) \end{aligned} \tag{4.13}$$

Concerning on the second part of the above equation, there are seven uncertainties in the model. The first uncertainty c is the model uncertainty whose mean μ_c and COV (ratio of standard deviation to mean) have to be identified. The next six terms represent the uncertainties associated with the individual parameters of soil liquefaction that mainly govern the performance of the limit state function. With the inspiration of work by Juang et al. (2008), $(N_1)_{60}, FC, \sigma_v, \sigma'_v, a_{max}, M$ are taken as random variables. $(N_1)_{60}$ and FC are used for the calculation of the CRR. MSF is the function of M, and K_σ is function of σ'_v, $CSR_{7.5}$ additionally requires σ_v, a_{max} and rd. Stress reduction factor is the function of depth and hence in our case, the critical depth is taken to be constant. Even though, uncertainties do exists in the depth, due to lack of information, it is considered as constants.

Table 4.3: Coefficient of correlation among the random variables from Juang et al. (2008)

Random Variables	$(N_1)_{60}$	FC	σ_v	σ'_v	a_{max}	M
$(N_1)_{60}$	1	0	0.3	0.3	0	0
FC	0	1	0	0	0	0
σ_v	0.3	0	1	0.9	0	0
σ'_v	0.3	0	0.9	1	0	0
a_{max}	0	0	0	0	1	0.9
M	0	0	0	0	0.9	1

To perform reliability analysis on the liquefaction cases, it is required to know the mean and COV of the random variables. From the mean and standard deviation for all the random variables except that M is presented in appendix A. Moss (2003) has approximated the relation to estimate the standard deviation for M based on the liquefaction earthquake year, which includes most of the earthquake year present in the data-set considered in the present study. Hence the relation can be used to determine the standard deviation of the earthquake's magnitude.

$$\sigma_M = 0.5 - 0.45log(M) \tag{4.14}$$

It is essential to check the correlation between the random variables considered for reliability analysis. Juang et al. (2008) have determined the correlation between the random variables using sensitivity analysis, which deliberately indicates the presence of correlation between the random input variables.

The coefficient of correlation between the random variables is shown in Table 4.3. According to Phoon and Kulhawy (2005), there would be a weak correlation between the model uncertainty c and the input random variable and hence the correlation of the model uncertainty with other input variables can be considered as 0. The value of reliability index

for the post-performance liquefaction cases is obtained using the *global search fmincon* algorithm as described in chapter 3 and lets represent this reliability index as β_1.

The PDF of reliability index for the liquefied and non-liquefied cases along with the histograms is shown in Figs. 4.15 and 4.16, respectively. The reliability index β_1 has the model uncertainty of μ_c as 1 and COV as 0. Using the Bayesian mapping function technique, the relationship between the $P_L - \beta$ can be estimated and showed in Fig. 4.17. The Bayesian mapping function for $P_L - \beta$ can be expressed as

$$(P_L) = \frac{f_L(\beta)}{f_L(\beta) + f_{NL}(\beta)} \tag{4.15}$$

where $f_L(\beta)$ and $f_{NL}(\beta)$ denotes the relative frequency of liquefied and non-liquefied cases which can be obtained from Figs. 4.15 and 4.16, respectively.

On observing Fig. 4.17, it can be seen at $\beta = 0$, the probability of the liquefaction is 0.49. But based on the standard normal distribution, the probability of a random variable at 0 is 0.5. Hence the obtained relationship $P_L - \beta$ needs to be biased. The biasing procedure similar to Juang et al. (2006) is implemented. By varying the values of μ_c and COV of c, the model uncertainty can be identified. The P_L for corresponding β, obtained from the first order reliability method (FORM) method is taken as the standard for biasing the $P_L - \beta$ relationship developed using eq. (4.15).

As mentioned above at $\beta = 0$, the probability of liquefaction P_L should be equal to 0. But this criteria is found not to be satisfied from Fig. 4.17. The curve should be biased so that the issue of conservatism can be removed. This is done by sensitivity analysis in which the μ_c and its COV are changed for each trail of reliability analysis on 186 liquefaction cases. The values for μ_c is varied from 0.1-1.15 with an increment of 0.05.

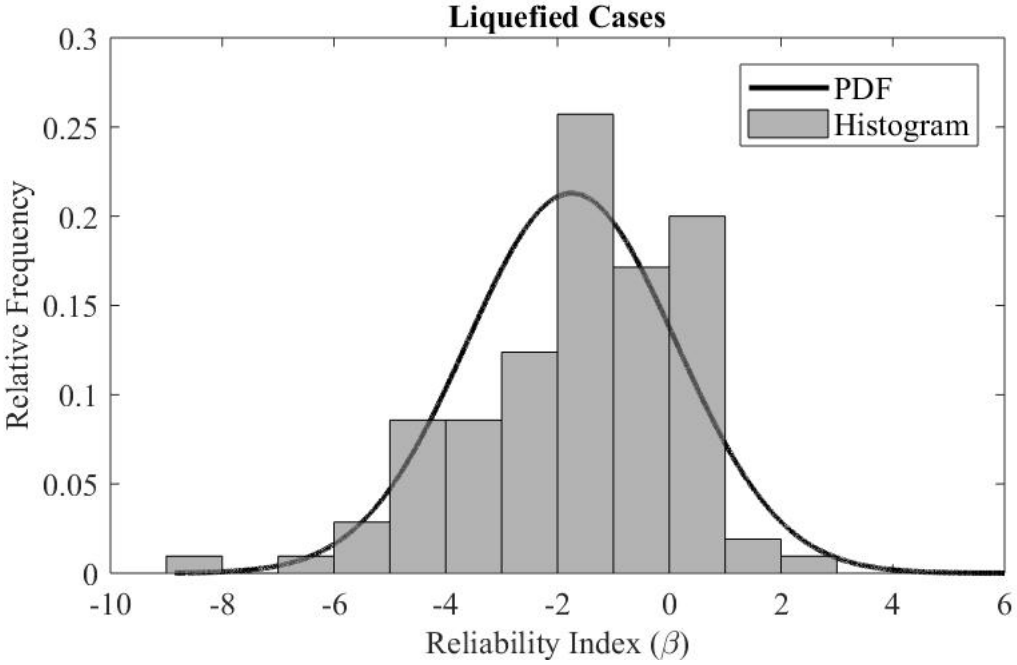

Figure 4.15: β for liquefied cases

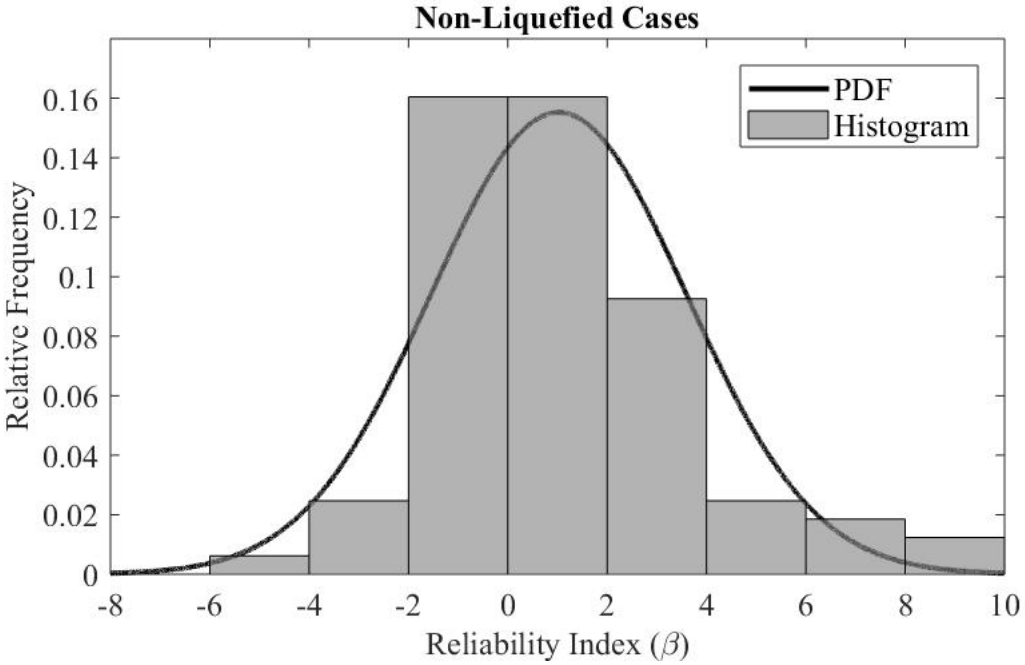

Figure 4.16: β for non-liquefied cases

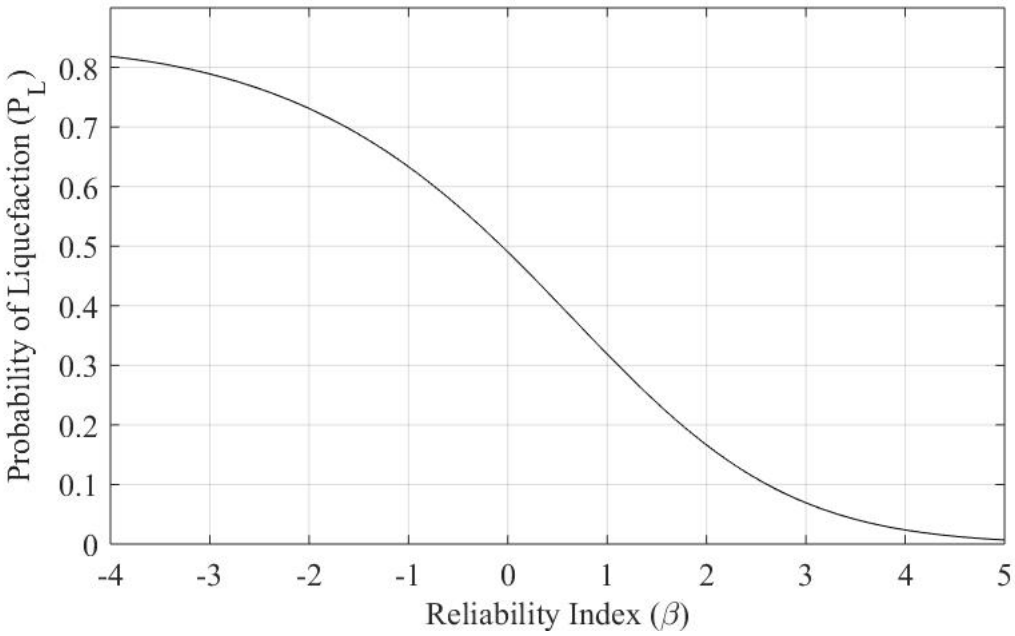

Figure 4.17: Relationship between the $P_L - \beta$ for liquefaction cases

The present results are compared with the results of reliability index β_1. The value of μ_c which has the least error (RMSE) is selected for the model. Initially, the value of μ_c is considered as 1 and three values of COV (0,0.1 & 0.2) have been taken.

The reliability analysis is carried out on 186 cases followed by Bayesian mapping technique, and the result is shown in Fig. 4.18. It can be seen that the curve with COV=0.1 and COV=0, is near to desired target point, i.e., $P_L = 0.5$ at $\beta = 0$. The values of P_L recorded for the same curves at $\beta = 0$ are 0.47 and 0.49, respectively. But the RMSE value of curves with COV=0.1 and COV=0 was found to be 0.12 and 0.14, respectively. Next, the mean of the model uncertainty is changed from 1 to 1.15 with an increment of 0.05 with maintaining COV=0.1.

The $P_L - \beta$ mapping function for this condition is shown in Fig.4.19. It can be seen that for the curve, μ_c=1.05 and μ_c=1.1 are near to

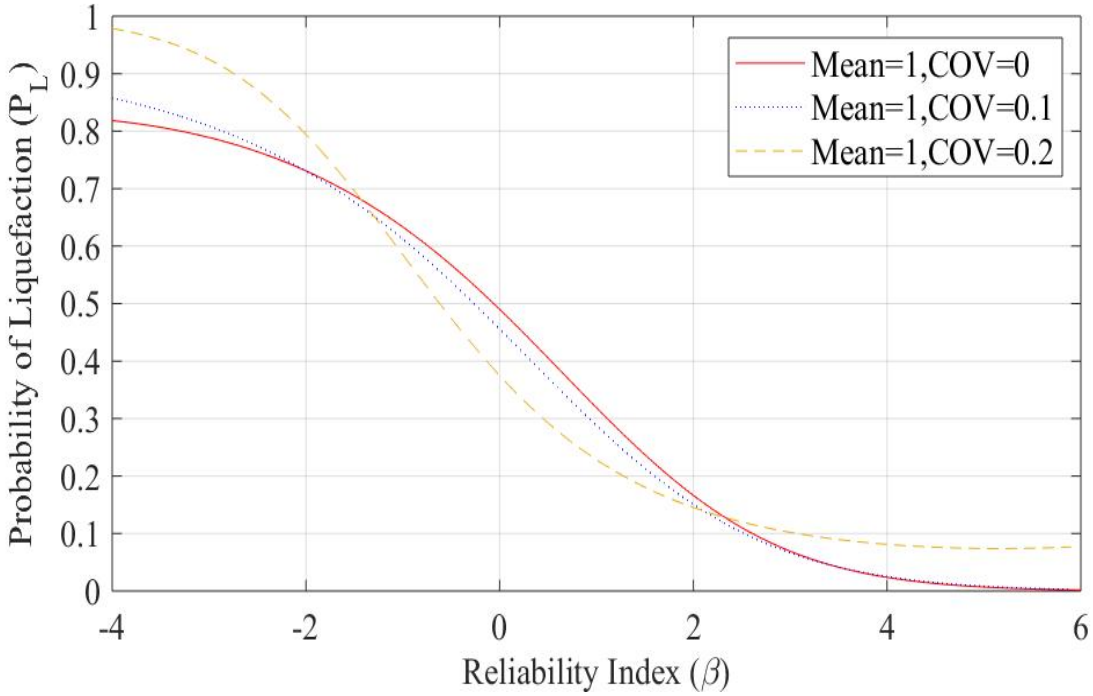

Figure 4.18: $P_L - \beta$ mapping functions using $\mu_c = 1$ and varying COV

the target point. $P_L = 0.498$ at $\beta = 0$ was found for the curve with μ_c=1.05 and COV=0.1. Similarly, it was found for the curve with μ_c=1.1 and COV=0.1, $P_L = 0.5004$ at $\beta = 0$. The RMSE value of curve μ_c=1.1 and COV=0.1 from Fig. 4.19 when compared with reliability index β_1 was found to be 0.07 whereas the RMSE value of curve μ_c=1.05 and COV=0.1 was found to be 0.11. Therefore, the curve with μ_c=1.1 and COV=0.1 is chosen.

4.4 Case study 1: 1978 Miyagiken-oki Earthquake at Ishinomakai-2

Liquefaction potential of the soil is investigated to determine P_L. The soil and seismic parameters at the critical depth are as following, $(N_1)_{60} = 3.7$, $FC = 10\%$, $\sigma_v = 58.8kPa$, $\sigma'_v = 36.9kPa$, $a_{max} = 0.2g$, $M_w = 7.4$ and the standard deviation of these parameters are 0.7, 2%, 12.8

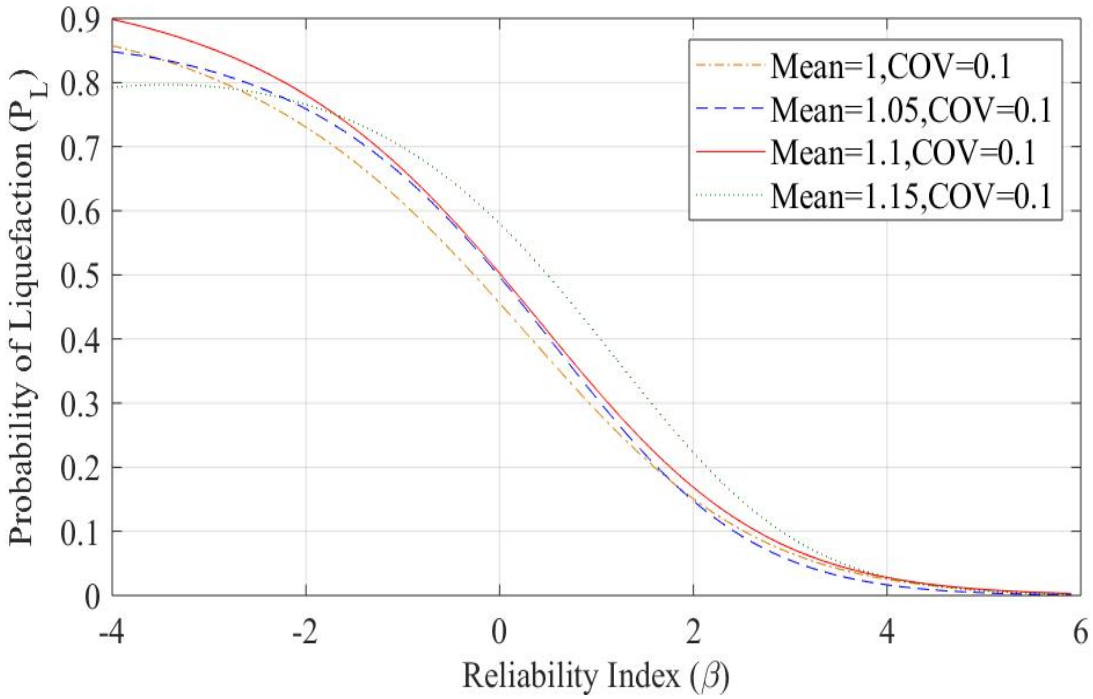

Figure 4.19: $P_L - \beta$ mapping functions using COV = 0.1 and varying μ_c

kPa, 5.9 kPa,0.2 and 0.74, respectively. The stress reduction factor at the critical depth is 0.9. In FORM analysis, eq. 1.60 is optimized, eq. 4.13 acts as constraint. The mean and COV of model uncertainty is taken as 1.1 and 0.1, respectively. The probability of liquefaction was found to be 0.8947 which is almost equivalent to the value of 0.91 from the findings of Juang et al. (2008). Therefore, this conforms that there are good number of chances for soil liquefaction occurrence at the site.

4.5 Case study 2: 1977 Argentina Earthquake at San Juan B-5

From the records of Çetin et al. (2004), non-liquefaction was observed at the site. The mean values of the soil and the site parameters are as following: $(N_1)_{60}$ = 15.2, FC = 3%, σ_v = 45.6kPa, σ'_v = 38.1kPa, a_{max} = 0.2g, M_w = 7.4 and the standard deviation of the parameters are 0.4, 0.1%, 4.9 kPa, 3.24 kPa, 0.015 and 0.74, respectively. Eq. 4.13 acts as

constraint in FORM analysis. The mean and COV of model uncertainty is taken as 1.1 and 0.1, respectively. On performing the FORM analysis, the probability of liquefaction was found as 0.49 which is in tally with P_L = 0.49 of Muduli and Das (2015). There is a good consistency in the results, the CRR empirical relationship and the value of modeling uncertainty is acceptable. Therefore, the performance function is developed and it can be further used for the carrying out reliability analysis of truncated distribution.

4.6 Summary

A three-layer ANN model has been developed using the post-performance liquefaction data-set. This model predicts the occurrence of liquefaction or not, in the site. With the help of the developed model, the limit state boundary points is determined. The search algorithm includes the procedure to increase the CSR value for non-liquefaction condition and decrease the value of CSR for liquefaction condition. From the search algorithm, the critical CSR values are determined. The data points are used along with the 'clean' sand equivalent SPT-N count to establish a relationship for limit state boundary curve.

Using the Bayesian mapping techniques, $F_s - P_L$ is plotted, and the relationship is approximated by regression analysis. It was found the limit state equation had model uncertainty present in it. By performing FORM and sensitivity analysis, model uncertainty is determined. Next, soil liquefaction potential evaluation was carried out on two different cases which have completely different properties. The results are in acceptable range with the models developed by other researchers. This confirms the consistency in the results obtained from the model developed in the present study. Hence, the entropy distribution along with the global search *fmincon* based FORM can be used for evaluation of liquefaction potential.

Chapter 5

Evaluation of Soil Liquefaction using Truncated Distribution

In this chapter, evaluation of soil liquefaction potential is carried out by considering a random variable having truncated distribution. Two case studies are made, i.e., liquefied condition and non-liquefaction condition. In the present study, the truncation is done for PDF of SPT-N variable since it reflects resistance offered by the soil.

5.1 Case study 1: 1978 Miyagiken-oki Earthquake at Ishinomakai-2

Liquefaction potential of the soil is investigated to determine probability of liquefaction (P_L). The soil and seismic parameters at the critical depth are as following, $(N_1)_{60}$ = 3.7, FC = 10%, σ_v = 58.8kPa, σ'_v = 36.3kPa, a_{max} = 0.2g, M_w = 7.4 and the standard deviation of the parameters are 0.7, 2%, 12.8 kPa, 5.9 kPa,0.02g and 0.7, respectively. The stress reduction factor at the critical depth is 0.9. The mean of model uncertainty is 1.1 and its COV is 0.1. Eq. (4.12) is taken as the performance function. $(N_1)_{60}$ is taken as a log-normal truncated variable with at the lower bound at 3, the statistical parameters estimation using MLE are

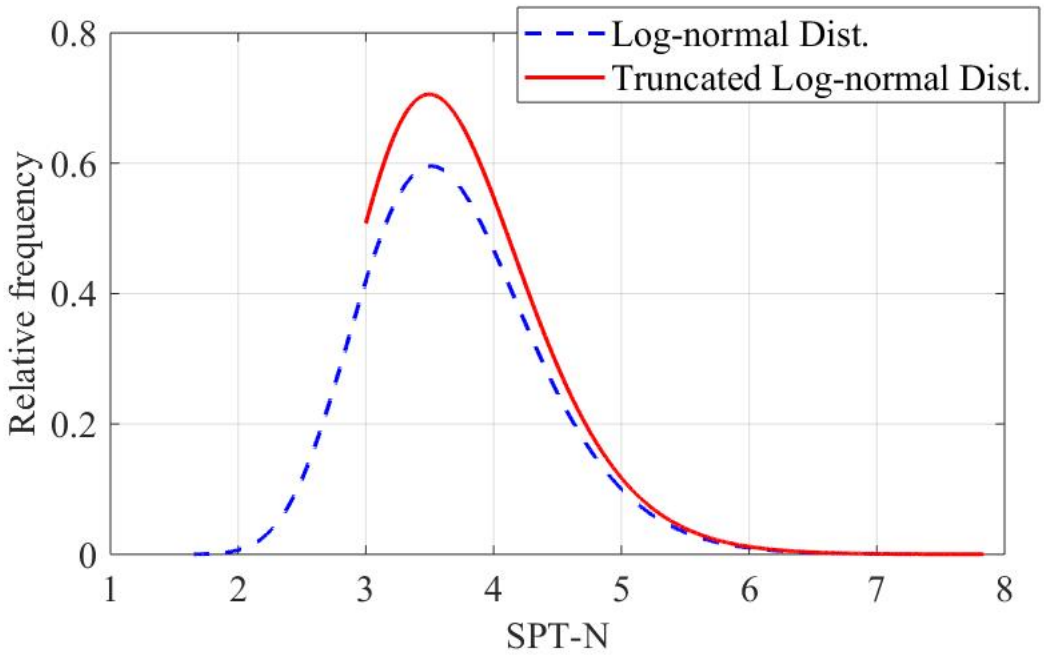

Figure 5.1: Lower bound truncated log-normal distribution of SPT-N value

(1.29,0.19). The truncated PDF is shown in Fig. 5.1. Eq. 4.13 acts as constraint in the FORM analysis. FORM analysis is carried out as per the procedure explained in section 3.2. Therefore, on performing reliability analysis, $\beta = -1.66$ & $P_L = 0.98$.

5.2 Case study 2: 1977 Argentina Earthquake at San Juan B-5

From the records of Çetin et al. (2004), non-liquefaction was observed at the site. The mean values of the soil and the site parameters are as following: $(N_1)_{60}$ = 15.2, FC = 3%, σ_v = 45.6kPa, σ'_v = 38.1kPa, a_{max} = 0.2g, M_w = 7.4 and the standard deviation of these parameters are 0.4, 0.1%, 4.9 kPa, 3.24 kPa, 0.015g and 0.7, respectively. The model uncertainty is 1.1 and the corresponding COV is 0.1. The performance function can be written using eq. (4.12). $(N_1)_{60}$ is taken as a truncated upper bound normal variable with the cut off point at 18. The upper bound truncated normal distribution of SPT-N for present case is shown in Fig.

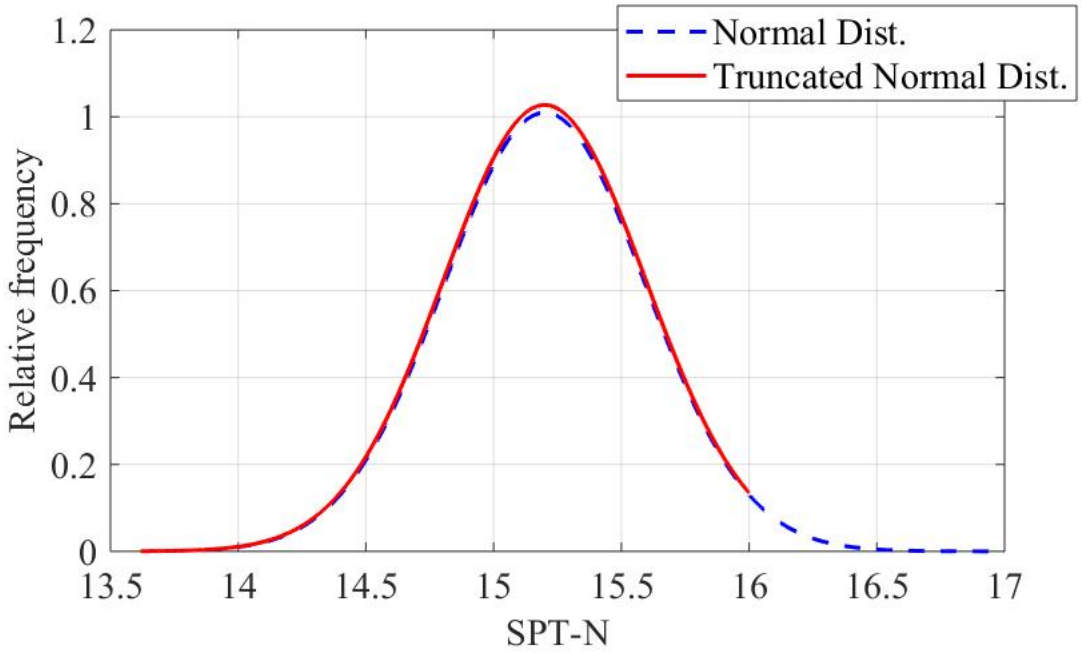

Figure 5.2: Upper bound truncated normal distribution of SPT-N value

5.2 and the statistical parameters calculated using MLE are (15.20,0.4). Eq. 4.13 acts as constraint in FORM analysis. FORM analysis is carried out as per the procedure explained in section 3.2. Therefore, on performing reliability analysis, it was found that $P_L = 0.022$.

5.3 Summary

In this chapter, reliability analysis of the soil liquefaction is carried out using the truncated normal and log-normal distributions. Using the truncated normal and log-normal distributions, the reliability analysis of the soil liquefaction based on censored samples is carried out. The proposed approach takes an advantage of varying the limiting conditions of the soil variables to study the performance of the soil strata towards soil liquefaction.

Chapter 6

Conclusions

The study focuses on evaluating liquefaction potential of the soil based on the post-performance SPT test data-set which can be later used for performing reliability analysis based on censored samples. Novel methods have been developed for investigating soil liquefaction potential. The contribution and findings of the thesis are summarized as follows.

6.1 Contribution

The soil whose fineness content greater than 7% is likely to susceptible to soil liquefaction irrespective of soil type. The novel models developed in this thesis provides significance for in-situ determination of liquefaction potential of soil. The contributions are as following,

6.1.1 Developing Truncated Distribution based on Censored Samples

There is a great extent of uncertainty present in soils and site characteristics. Accurate representation and effective use of the random variables are very crucial in investigation and designing of structures. The normal and log-normal distributions are widely used in the

engineering practice for representing the statistical variation of the random variable. For censored samples, the statistical parameters of truncated normal and log-normal distribution are obtained using MLE technique. The parameters of the distribution vary depending upon the truncation conditions. Based on the determined parameters and truncation conditions, various truncated probability distributions are plotted.

6.1.2 Hasofer-Lind's FORM Using Global Optimum Function for Truncated Distributions

Evaluation of soil liquefaction of soils must consider all the uncertainties in soil strata. Hasofer-Lind's FORM is a stochastic based approach in which the probability of failure can be determined conveniently. β is the minimum distance between the origin of the joint PDF of random variable involved in the system and the limit state boundary curve. The distance should be globally minimum, and this can be achieved with the help of *fmincon* function that uses interior point technique and on the whole, defined along with the global search option. When dealing with the truncated distributions, there is limitation in the flow of iteration points. The proposed algorithm allows to define the range for search of design points. The function makes multiple direction searches for the minimum distance. It also gives the advantage of calculating the gradient function by the program and hence it is not required to know information about the partial derivatives of the random variables involved in the system. Therefore, any complex engineering structures can be potentially analyzed.

6.1.3 Limit State Performance Function for Soil Liquefaction Potential Evaluation

About 213 post-performance liquefaction data-set based on the SPT-test is collected from Çetin et al. (2004) and Çetin et al. (2016). A three-layer ANN model was built with 4 neurons in the hidden layer. About 163 cases are used for training of the ANN model, and the rest of 50 cases have been used for validation of the ANN. The success rate was about 93.89%. The developed ANN model helps in the prediction of the liquefaction condition at the site. With the help of the developed model and search algorithm described by Juang et al. (2000b), the CRR was determined. On processing the CRR values for both liquefaction condition and equivalent 'clean' sand corrected normalized SPT-N count $(N_1)_{60cs}$ for regression analysis, the limit state curve is developed. The developed empirical relationship needed to be biased and hence for this reason techniques like reliability analysis and Bayesian mapping were used. It is recommended to make use of the reliability model instead of the deterministic and probabilistic model because it effectually involves the modeling uncertainty and therefore, good results have been obtained.

6.1.4 Reliability Analysis of Soil Liquefaction using Truncated Distributions

Using the developed limit state curve and determined modeling uncertainty, the performance of the soil strata under various limiting conditions was evaluated. The reliability analysis was carried out for any bound conditions. Two case studies have been conducted for different soil conditions. Reliability analysis of soil liquefaction using truncated distributions has been carried out, and the probability of failure and reliability index have been successfully obtained.

6.2 Recommendations for Further Research

- The soil liquefaction hazard analysis efforts can be extended to develop a probabilistic model for estimation of liquefaction-induced ground deformation.
- The similar innovative ideas can be used in the development of soil liquefaction potential relationship for CPT and shear wave velocity (V_s) based on in-situ approaches.
- A comparative studies can be carried out between the global search using *fmincon* with interior point method and genetic algorithm, to check the efficiency.
- The SORM can be used for reliability analysis of soil liquefaction potential to achieve more accuracy in finding β and P_L.

Bibliography

Agrawal, G., Chameau, J.-L. A., and Bourdeau, P. L. (1997). Assessing the liquefaction susceptibility at a site based on information from penetration testing. In *Artificial neural networks for civil engineers: fundamentals and applications*, pages 185–214. ASCE.

Andrews, D. C. and Martin, G. R. (2000). Criteria for liquefaction of silty soils. In *Proc., 12th World Conf. on Earthquake Engineering*. NZ Soc. for EQ Engrg. Upper Hutt, New Zealand.

Baecher, G. B. and Christian, J. T. (2005). *Reliability and Statistics in Geotechnical Engineering*. John Wiley & Sons.

Bagheripour, M., Shooshpasha, I., and Afzalirad, M. (2012). A genetic algorithm approach for assessing soil liquefaction potential based on reliability method. *Journal of Earth System Science*, 121(1):45–62.

Beale, M. H., Hagan, M. T., and Demuth, H. B. (2012). Neural network toolbox users guide. In *R2012a, The MathWorks, Inc., 3 Apple Hill Drive Natick, MA 01760-2098„ www. mathworks. com*. Citeseer.

Boulanger, R. and Idriss, I. (2006). Liquefaction susceptibility criteria for silts and clay. *Journal of Geotechnical and Geoenvironmental Engineering*, 132(11):1413–1426.

Boulanger, R. W. and Idriss, I. (2012). Probabilistic standard penetration test–based liquefaction–triggering procedure. *Journal of Geotechnical and Geoenvironmental Engineering*, 138(10):1185–1195.

Boulanger, R. W., Wilson, D. W., and Idriss, I. (2011). Examination and re-evalaution of SPT-based liquefaction triggering case histories. *Journal of Geotechnical and Geoenvironmental Engineering*, 138(8):898–909.

Çetin, K. Ö. (2000). *Reliability-Based Assessment of Seismic Soil Liquefaction Initiation Hazard*. University of California, Berkeley.

Çetin, K. Ö., Der Kiureghian, A., and Seed, R. B. (2002). Probabilistic models for the initiation of seismic soil liquefaction. *Structural Safety*, 24(1):67–82.

Çetin, K. Ö., Seed, R. B., Der Kiureghian, A., Tokimatsu, K., Harder Jr, L. F., Kayen, R. E., and Moss, R. E. (2004). Standard penetration test-based probabilistic and deterministic assessment of seismic soil liquefaction potential. *Journal of Geotechnical and Geoenvironmental Engineering*, 130(12):1314–1340.

Çetin, K. Ö., Seed, R. B., Kayen, R. E., Moss, R. E., Bilge, H. T., Ilgac, M., and Chowdhury, K. (2016). Summary of SPT based field case history data of cetin (2016) database. Technical report, Middle East Technical University.

Chu, D. B., Stewart, J. P., Lee, S., Tsai, J.-S., Lin, P., Chu, B., Seed, R. B., Hsu, S., Yu, M., and Wang, M. C. (2004). Documentation of soil conditions at liquefaction and non-liquefaction sites from 1999 chi–chi (taiwan) earthquake. *Soil Dynamics and Earthquake Engineering*, 24(9-10):647–657.

Cohen, A. C. (2016). *Truncated and censored samples: theory and applications*. CRC press.

Deng, J. (2006). Structural reliability analysis for implicit performance function using radial basis function network. *International Journal of Solids and Structures*, 43(11-12):3255–3291.

Deng, J., Gu, D., Li, X., and Yue, Z. Q. (2005). Structural reliability analysis for implicit performance functions using artificial neural network. *Structural Safety*, 27(1):25–48.

Fardis, M. N. and Veneziano, D. (1981). Statistical analysis of sand liquefaction. *Journal of Geotechnical and Geoenvironmental Engineering*, 107(ASCE 16604 Proceeding).

Goh, A. T. (1994). Seismic liquefaction potential assessed by neural networks. *Journal of Geotechnical engineering*, 120(9):1467–1480.

Guha-Sapir, D., Hoyois, P., Wallemacq, P., and Below, R. (2016). Annual Disaster Statistical Review 2016: The Numbers and Trends. *Brussels: CRED*.

Haldar, A. and Mahadevan, S. (2000). *Probability, Reliability, and Statistical Methods in Engineering Design*. John Wiley.

Haldar, A. and Tang, W. H. (1979). Probabilistic evaluation of liquefaction potential. ASCE J Geotech Eng Div.

Hwang, H. and Lee, C. S. (1991). Parametric study of site response analysis. *Soil Dynamics and Earthquake Engineering*, 10(6):282–290.

Idriss, I. and Boulanger, R. (2006). Semi-empirical procedures for evaluating liquefaction potential during earthquakes. *Soil Dynamics and Earthquake Engineering*, 26(2-4):115–130.

Idriss, I. and Boulanger, R. W. (2010). SPT-based liquefaction triggering procedures. *Rep. UCD/CGM-10*, 2:4–13.

Jaynes, E. (1957). Information Theory and Statistical Mechanics. *Physics Reviews*, 106:620.

Jha, S. K. and Suzuki, K. (2009). Reliability analysis of soil liquefaction based on standard penetration test. *Computers and Geotechnics*, 36(4):589–596.

Juang, C. H., Chen, C., Rosowsky, D., and Tang, W. (2000a). CPT-based liquefaction analysis, part 2: Reliability for design. *Geotechnique*, 50(5):593–599.

Juang, C. H. and Chen, C. J. (1999). CPT-based liquefaction evaluation using artificial neural networks. *Computer-Aided Civil and Infrastructure Engineering*, 14(3):221–229.

Juang, C. H. and Chen, C. J. (2000). A rational method for development of limit state for liquefaction evaluation based on shear wave velocity measurements. *International Journal for Numerical and Analytical Methods in Geomechanics*, 24(1):1–27.

Juang, C. H., Chen, C. J., Jiang, T., and Andrus, R. D. (2000b). Risk-based liquefaction potential evaluation using standard penetration tests. *Canadian Geotechnical Journal*, 37(6):1195–1208.

Juang, C. H., Fang, S. Y., and Khor, E. H. (2006). First-order reliability method for probabilistic liquefaction triggering analysis using cpt. *Journal of Geotechnical and Geoenvironmental Engineering*, 132(3):337–350.

Juang, C. H., Fang, S. Y., and Li, D. K. (2008). Reliability analysis of liquefaction potential of soils using standard penetration test. *In: Phoon, K.K (Ed.), Reliability-based Design in Geotechnical Engineering, Computation and Applications*, pages 497–526.

Juang, C. H., Jiang, T., and Andrus, R. D. (2002). Assessing probability-based methods for liquefaction potential evaluation. *Journal of Geotechnical and Geoenvironmental Engineering*, 128(7):580–589.

Juang, C. H., Rosowsky, D. V., and Tang, W. H. (1999). Reliability-based method for assessing liquefaction potential of soils. *Journal of Geotechnical and Geoenvironmental Engineering*, 125(8):684–689.

Lee, T.-E. and Lee, Y.-D. (2002). An extended maximum entropy method for estimation of rare event probabilities. *European transactions on telecommunications*, 13(4):399–407.

Liao, S. S., Veneziano, D., and Whitman, R. V. (1988). Regression models for evaluating liquefaction probability. *Journal of Geotechnical Engineering*, 114(4):389–411.

Liu, P.-L. and Der Kiureghian, A. (1991). Optimization algorithms for structural reliability. *Structural Safety*, 9(3):161–177.

Low, B. and Tang, W. H. (1997). Efficient reliability evaluation using spreadsheet. *Journal of Engineering Mechanics*, 123(7):749–752.

Low, B. K. (2014). Practical reliability approach using spreadsheet. In *Reliability-Based Design in Geotechnical Engineering*, pages 146–180. CRC Press.

Low, B. K., Baecher, G., Bathurst, R., Bolton, M., Boothroyd, P., Chen, Z., Ching, J., Day, P., De Koker, N., Duncan, M., et al. (2017). Excel-based direct reliability analysis and its potential role to complement eurocodes. *Final Report of the Joint TC205/TC304 Working Group on Discussion of Statistical/Reliability Methods for Eurocodes"*, pages 79–101.

Martin, J. R., Olgun, C. G., Mitchell, J. K., and Durgunoğlu, H. T. (2006). Closure to high-modulus columns for liquefaction mitigation by james r.

martin ii, c. guney olgun, james k. mitchell, and h. turan durgunoğlu. *Journal of Geotechnical and Geoenvironmental Engineering*, 132(7):950–953.

Melchers, R., Ahammed, M., and Middleton, C. (2003). Form for discontinuous and truncated probability density functions. *Structural Safety*, 25(3):305–313.

Moss, R. E. (2003). CPT-Based Probabilistic Assessment of Seismic Soil Liquefaction Initiation. *Dissertation - University of California, Berkeley*.

Muduli, P. K. and Das, S. K. (2015). Model uncertainty of spt-based method for evaluation of seismic soil liquefaction potential using multi-gene genetic programming. *Soils and Foundations*, 55(2):258–275.

Muñoz-Cobo, J.-L., Mendizábal, R., Miquel, A., Berna, C., and Escrivá, A. (2017). Use of the principles of maximum entropy and maximum relative entropy for the determination of uncertain parameter distributions in engineering applications. *Entropy*, 19(9):486.

National Academies of Sciences, E., Medicine, et al. (2016). State of the art and practice in the assessment of earthquake-induced soil liquefaction and its consequences. *Washington, DC: The National Academies Press. doi*, 1017226:23474.

Phoon, K.-K. and Kulhawy, F. (2005). Characterisation of model uncertainties for laterally loaded rigid drilled shafts. *Geotechnique*, 55(1):45–54.

Rackwitz, R. and Fiessler, B. (1978). Structural reliability under combined random load sequences. *Computers & Structures*, 9(5):489–494.

Robertson, P. and Wride, C. (1998). Evaluating cyclic liquefaction potential using the cone penetration test. *Canadian Geotechnical Journal*, 35(3):442–459.

Robertson, P. K. and Campanella, R. G. (1985). Liquefaction potential of sands using the CPT. *Journal of Geotechnical Engineering*, 111(3):384–403.

Samui, P. and Sitharam, T. (2011). Machine learning modelling for predicting soil liquefaction susceptibility. *Natural Hazards and Earth System Sciences*, 11(1):1–9.

Seed, H., Tokimatsu, K., Harder, L., and Chung, R. (1984). The influence of SPT procedures in evaluating soil liquefaction resistance. *Report, UCB/EERC-84*, 15.

Seed, H. B. and Idriss, I. M. (1967). Analysis of soil liquefaction: Niigata earthquake. *Journal of the Soil Mechanics and Foundations Division*, 93(3):83–108.

Seed, H. B. and Idriss, I. M. (1971). Simplified procedure for evaluating soil liquefaction potential. *Journal of Soil Mechanics & Foundations Div*, pages 1249–1273.

Seed, H. B. and Idriss, I. M. (1982). Ground motion and soil liquefaction during earthquakes. *Earthquake Engineering Research Institute,Berkeley, California*.

Seed, H. B., Idriss, I. M., and Arango, I. (1983). Evaluation of liquefaction potential using field performance data. *Journal of Geotechnical Engineering*, 109(3):458–482.

Seed, H. B., Tokimatsu, K., Harder, L., and Chung, R. M. (1985). Influence of SPT procedures in soil liquefaction resistance evaluations. *Journal of Geotechnical Engineering*, 111(12):1425–1445.

Shinozuka, M. (1983). Basic analysis of structural safety. *Journal of Structural Engineering*, 109(3):721–740.

Singh, S. (2018). Quantile-Based Reliability Analysis and Design in Slope Stability. *Master's Thesis - Lakehead University, Thunder Bay, Canada*.

Terzaghi, K., Peck, R. B., and Mesri, G. (1996). *Soil Mechanics in Engineering Practice*. John Wiley & Sons.

Toprak, S., Holzer, T., Bennett, M. J., and Tinsley III, J. C. (1999). CPT and SPT-based probabilistic assessment of liquefaction. In *Proc., 7th US–Japan Workshop on Earthquake Resistant Design of Lifeline Facilities and Countermeasures against Liquefaction*, pages 69–86. Multidisciplinary Center for Earthquake Engineering Research Buffalo, NY.

Vukobratovic, V. and Ladjinovic, D. (2013). Liquefaction assessment according to eurocode 8. In *Proceedings of the 15th International Symposium of MASE: Struga (Macedonia), Macedonian Association of Structural Engineers*.

Wächter, A. and Biegler, L. T. (2006). On the implementation of an interior-point filter line-search algorithm for large-scale nonlinear programming. *Mathematical programming*, 106(1):25–57.

Wang, W. (1979). Water conservancy and hydroelectric power scientific research institute, beijing. *Some findings in soil liquefaction*.

Whitman, R. V. (1971). Resistance of soil to liquefaction and settlement. *Soils and Foundations*, 11(4):59–68.

Youd, T. L., Idriss, I. M., Andrus, R. D., Arango, I., Castro, G., Christian, J. T., Dobry, R., Finn, W. D. L., Harder, L. F., Hynes, M. E., Ishihara, K., Koester, J. P., Liao, S. S. C., Marcuson, W. F., Martin, G. R., Mitchell, J. K., Moriwaki, Y., Power, M. S., Robertson, P. K., Seed, R. B., and Stokoe, K. H. (2001). Liquefaction resistance of soils: Summary report from the 1996 NCEER and 1998 NCEER/NSF workshops on

evaluation of liquefaction resistance of soils. *Journal of Geotechnical and Geoenvironmental Engineering*, 127(10):817–833.

Youd, T. L. and Noble, S. K. (1997). Liquefaction criteria based on statistical and probabilistic analyses. Technical report, NCEER Workshop on Evaluation of Liquefaction Resistance of Soils.

Appendix A

Truncated based FORM Sample Output

The MATLAB programming script for reliability analysis based on truncated distribution is presented below

```
clc;
clear all;
close all;
global mu sigmaX;
mu=[10.29,12.0]; % Define the mean of the distribution
sigmaX=[ 0.794,1.5]; % Define the standard deviation of the distribution
rng default % For reproducibility
gs = GlobalSearch; %defining of global problem
[f,g]=constraint(mu);

options = optimoptions(@fmincon,'Algorithm','interior-point','Display',....

'iter-detailed',...

    'ScaleProblem','obj-and-constr',...
    'MaxIterations',1500,'MaxFunctionEvaluations',2000);

options.ConstraintTolerance = 1.000000e-4;
```

```
%Tolerance level of the constraint can be increased here

options.OptimalityTolerance = 1.000000e-4;
%Tolerance level of the objective finction can be increased here

problem = createOptimProblem('fmincon','x0',mu,...
    'objective',@object,'lb',[9,0],'nonlcon',@constraint ,'options',options);
    %lb stands for lower bound, assign the truncation conditions here.
xopt = run(gs,problem);
r_index=object(xopt);
if g>0
   reliability_index=r_index
else
    reliability_index=-r_index
end
probability_of_failure=normcdf(-reliability_index)
% probability of failure is calculated
G=g % prints the value of performance function at the design points
%% OBJECTIVE
function d=object(x)
X=transformation_of_variables(x);
d=sqrt(X*X');
end
%% CONSTRAINT
function [c,ceq]=constraint(x)
ceq =performancefunc1(x);
c=[];
end
%% Performance function
function z = performancefunc1(x)
z=5*x(1)+3*x(1)*x(2)-240;
end
function X1= transformation_of_variables(x)
global mu sigmaX;
SigmaX1=sigmaX;
muX1=mu;
X1=(x-muX1)./SigmaX1;
```

```
end

%%
% In case the random variables are correlated
function d=object(x)
X=transformation_of_variables(x);
R=[1 0.5
  0.5 1]; % R is the correlation matrix
L=chol(R,'lower'); % cholesky decomposition
Z=L\X.';
d=sqrt(Z.'*Z);
end
```

```
                                          First-order      Norm of
 Iter F-count            f(x)  Feasibility   optimality         step
    0       3    0.000000e+00    1.819e+02    1.481e-01
    1       6    1.736951e+00    1.035e+02    1.019e+00    1.599e+00
    2       9    3.642112e+00    2.442e+00    6.730e-01    4.115e+00
    3      12    3.589166e+00    3.553e-03    5.640e-02    7.508e-02
    4      15    3.588111e+00    3.192e-04    2.066e-02    1.461e-02
    5      18    3.579706e+00    3.809e-02    5.238e-03    1.595e-01
    6      21    3.576779e+00    7.951e-03    1.387e-03    7.280e-02
    7      24    3.576001e+00    1.584e-03    4.345e-04    3.250e-02
    8      27    3.575812e+00    1.697e-04    2.249e-04    1.064e-02
    9      30    3.575678e+00    1.695e-04    6.505e-05    1.063e-02

Optimization completed: The relative first-order optimality measure, 6.504818e-05,
is less than options.OptimalityTolerance = 1.000000e-04, and the relative maximum↙
constraint
violation, 9.317344e-07, is less than options.ConstraintTolerance = 1.000000e-04.

Optimization Metric                                      Options
relative first-order optimality =   6.50e-05       OptimalityTolerance =   1e-04↙
(selected)
relative max(constraint violation) =   9.32e-07    ConstraintTolerance =   1e-04↙
(selected)

Your initial point x0 is not between bounds lb and ub; FMINCON
shifted x0 to strictly satisfy the bounds.

                                          First-order      Norm of
 Iter F-count            f(x)  Feasibility   optimality         step
    0       3    2.994766e+00    3.604e+01    1.578e-01
    1       6    3.570360e+00    1.167e+00    1.617e-01    8.967e-01
    2       9    3.604641e+00    1.492e-02    1.022e-01    1.068e-01
    3      13    3.590742e+00    2.677e-04    2.258e-02    1.370e-01
    4      17    3.579297e+00    6.710e-04    5.976e-03    1.831e-01
    5      21    3.576995e+00    3.245e-05    2.017e-03    6.677e-02
    6      25    3.576434e+00    1.352e-06    1.121e-03    2.317e-02
    7      28    3.575946e+00    1.149e-03    3.716e-04    2.768e-02
    8      31    3.575691e+00    4.745e-04    7.196e-05    1.779e-02

Optimization completed: The relative first-order optimality measure, 7.196141e-05,
is less than options.OptimalityTolerance = 1.000000e-04, and the relative maximum↙
constraint
violation, 1.316797e-05, is less than options.ConstraintTolerance = 1.000000e-04.

Optimization Metric                                      Options
relative first-order optimality =   7.20e-05       OptimalityTolerance =   1e-04↙
(selected)
relative max(constraint violation) =   1.32e-05    ConstraintTolerance =   1e-04↙
(selected)
```

```
                                          First-order      Norm of
 Iter F-count            f(x)  Feasibility   optimality         step
    0       3    3.621046e+00    6.422e-01    7.671e-02
    1       6    3.630088e+00    3.831e-05    7.290e-02    2.477e-02
    2       9    3.607349e+00    4.269e-02    5.345e-02    1.693e-01
    3      12    3.582576e+00    1.920e-01    4.077e-03    3.584e-01
    4      15    3.576817e+00    5.085e-03    2.327e-03    5.852e-02
    5      18    3.576394e+00    2.999e-04    1.046e-03    1.414e-02
    6      21    3.575930e+00    1.041e-03    3.539e-04    2.635e-02
    7      24    3.575800e+00    8.580e-05    2.126e-04    7.563e-03
    8      27    3.575652e+00    2.279e-04    3.569e-05    1.233e-02
    9      30    3.575617e+00    1.270e-05    3.858e-06    2.909e-03

Optimization completed: The relative first-order optimality measure, 3.858002e-06,
is less than options.OptimalityTolerance = 1.000000e-04, and the relative maximum↙
constraint
violation, 1.269583e-05, is less than options.ConstraintTolerance = 1.000000e-04.

Optimization Metric                                          Options
relative first-order optimality =   3.86e-06       OptimalityTolerance =   1e-04↙
(selected)
relative max(constraint violation) =   1.27e-05    ConstraintTolerance =   1e-04↙
(selected)

                                          First-order      Norm of
 Iter F-count            f(x)  Feasibility   optimality         step
    0       3    3.625167e+00    4.930e-01    7.742e-02
    1       6    3.631008e+00    2.835e-04    7.372e-02    2.425e-02
    2       9    3.603611e+00    6.671e-02    4.935e-02    2.116e-01
    3      12    3.582100e+00    1.392e-01    5.272e-03    3.051e-01
    4      15    3.577034e+00    6.908e-03    2.292e-03    6.795e-02
    5      18    3.576428e+00    5.957e-04    1.090e-03    1.993e-02
    6      21    3.575939e+00    1.107e-03    3.642e-04    2.717e-02
    7      24    3.575801e+00    9.554e-05    2.140e-04    7.981e-03
    8      27    3.575653e+00    2.300e-04    3.600e-05    1.238e-02
    9      30    3.575617e+00    1.290e-05    3.889e-06    2.933e-03

Optimization completed: The relative first-order optimality measure, 3.888646e-06,
is less than options.OptimalityTolerance = 1.000000e-04, and the relative maximum↙
constraint
violation, 1.290471e-05, is less than options.ConstraintTolerance = 1.000000e-04.

Optimization Metric                                          Options
relative first-order optimality =   3.89e-06       OptimalityTolerance =   1e-04↙
(selected)
relative max(constraint violation) =   1.29e-05    ConstraintTolerance =   1e-04↙
(selected)

                                          First-order      Norm of
 Iter F-count            f(x)  Feasibility   optimality         step
```

```
    0       3    3.635407e+00    1.948e-01    8.054e-02
    1       6    3.634103e+00    1.182e-03    7.660e-02    2.972e-02
    2       9    3.595272e+00    1.683e-01    4.365e-02    3.362e-01
    3      12    3.580980e+00    4.927e-02    6.993e-03    1.812e-01
    4      15    3.577337e+00    8.733e-03    2.261e-03    7.630e-02
    5      18    3.576489e+00    1.130e-03    1.168e-03    2.745e-02
    6      21    3.576359e+00    3.704e-05    1.005e-03    4.969e-03
    7      24    3.575922e+00    9.694e-04    3.447e-04    2.542e-02
    8      27    3.575799e+00    7.744e-05    2.113e-04    7.185e-03
    9      30    3.575652e+00    2.260e-04    3.576e-05    1.228e-02
   10      33    3.575617e+00    1.252e-05    6.044e-06    2.889e-03

Optimization completed: The relative first-order optimality measure, 6.044410e-06,
is less than options.OptimalityTolerance = 1.000000e-04, and the relative maximum↙
constraint
violation, 1.251583e-05, is less than options.ConstraintTolerance = 1.000000e-04.

Optimization Metric                                          Options
relative first-order optimality =   6.04e-06       OptimalityTolerance =   1e-04↙
(selected)
relative max(constraint violation) =   1.25e-05    ConstraintTolerance =   1e-04↙
(selected)

                                          First-order      Norm of
 Iter F-count            f(x)  Feasibility   optimality         step
    0       3    3.623836e+00    7.106e-01    8.052e-02
    1       6    3.632521e+00    3.904e-04    7.545e-02    3.285e-02
    2       9    3.605229e+00    6.318e-02    5.150e-02    2.059e-01
    3      12    3.582329e+00    1.566e-01    4.992e-03    3.235e-01
    4      15    3.576984e+00    6.545e-03    2.423e-03    6.619e-02
    5      18    3.576419e+00    5.195e-04    1.079e-03    1.861e-02
    6      21    3.575937e+00    1.091e-03    3.615e-04    2.697e-02
    7      24    3.575801e+00    9.301e-05    2.136e-04    7.875e-03
    8      27    3.575653e+00    2.294e-04    3.592e-05    1.237e-02
    9      30    3.575617e+00    1.285e-05    3.881e-06    2.927e-03

Optimization completed: The relative first-order optimality measure, 3.880673e-06,
is less than options.OptimalityTolerance = 1.000000e-04, and the relative maximum↙
constraint
violation, 1.284994e-05, is less than options.ConstraintTolerance = 1.000000e-04.

Optimization Metric                                          Options
relative first-order optimality =   3.88e-06       OptimalityTolerance =   1e-04↙
(selected)
relative max(constraint violation) =   1.28e-05    ConstraintTolerance =   1e-04↙
(selected)

                                          First-order      Norm of
 Iter F-count            f(x)  Feasibility   optimality         step
    0       3    3.644595e+00    3.177e-01    9.021e-02
```

```
    1       6    3.641127e+00    3.679e-03    8.316e-02    5.223e-02
    2      10    3.591758e+00    3.759e-03    4.990e-02    3.793e-01
    3      14    3.579907e+00    6.243e-04    7.023e-03    1.801e-01
    4      18    3.577150e+00    4.575e-05    2.270e-03    7.523e-02
    5      22    3.576465e+00    2.221e-06    1.169e-03    2.739e-02
    6      25    3.575955e+00    1.224e-03    3.828e-04    2.857e-02
    7      28    3.575804e+00    1.140e-04    2.167e-04    8.719e-03
    8      31    3.575653e+00    2.340e-04    3.659e-05    1.249e-02
    9      34    3.575617e+00    1.331e-05    6.045e-06    2.978e-03

Optimization completed: The relative first-order optimality measure, 6.044801e-06,
is less than options.OptimalityTolerance = 1.000000e-04, and the relative maximum↙
constraint
violation, 1.330600e-05, is less than options.ConstraintTolerance = 1.000000e-04.

Optimization Metric                                          Options
relative first-order optimality =   6.04e-06       OptimalityTolerance =   1e-04↙
(selected)
relative max(constraint violation) =   1.33e-05    ConstraintTolerance =   1e-04↙
(selected)

                                          First-order      Norm of
 Iter F-count            f(x)  Feasibility   optimality         step
    0       3    3.623640e+00    1.043e+00    3.811e-02
    1       6    3.613717e+00    9.315e-03    4.827e-02    9.023e-02
    2      10    3.592755e+00    3.595e-04    3.115e-02    1.879e-01
    3      14    3.579829e+00    7.868e-04    6.812e-03    1.942e-01
    4      18    3.577117e+00    4.462e-05    2.216e-03    7.460e-02
    5      22    3.576458e+00    2.013e-06    1.159e-03    2.650e-02
    6      25    3.575953e+00    1.207e-03    3.803e-04    2.837e-02
    7      28    3.575804e+00    1.115e-04    2.163e-04    8.624e-03
    8      31    3.575653e+00    2.334e-04    3.651e-05    1.248e-02
    9      34    3.575617e+00    1.325e-05    5.304e-06    2.972e-03

Optimization completed: The relative first-order optimality measure, 5.303948e-06,
is less than options.OptimalityTolerance = 1.000000e-04, and the relative maximum↙
constraint
violation, 1.270190e-05, is less than options.ConstraintTolerance = 1.000000e-04.

Optimization Metric                                          Options
relative first-order optimality =   5.30e-06       OptimalityTolerance =   1e-04↙
(selected)
relative max(constraint violation) =   1.27e-05    ConstraintTolerance =   1e-04↙
(selected)

                                          First-order      Norm of
 Iter F-count            f(x)  Feasibility   optimality         step
    0       3    3.588584e+00    5.334e-01    3.818e-02
    1       6    3.610260e+00    1.324e-02    4.552e-02    9.508e-02
    2      10    3.591249e+00    7.035e-04    2.550e-02    1.780e-01
```

```
    3      14    3.579716e+00    6.317e-04    6.777e-03    1.792e-01
    4      18    3.577115e+00    4.066e-05    2.213e-03    7.217e-02
    5      22    3.576458e+00    2.009e-06    1.158e-03    2.647e-02
    6      25    3.575953e+00    1.207e-03    3.802e-04    2.837e-02
    7      28    3.575804e+00    1.114e-04    2.163e-04    8.619e-03
    8      31    3.575653e+00    2.334e-04    3.651e-05    1.248e-02
    9      34    3.575617e+00    1.325e-05    3.939e-06    2.972e-03

Optimization completed: The relative first-order optimality measure, 3.939058e-06,
is less than options.OptimalityTolerance = 1.000000e-04, and the relative maximum↙
constraint
violation, 1.324966e-05, is less than options.ConstraintTolerance = 1.000000e-04.

Optimization Metric                                          Options
relative first-order optimality =   3.94e-06       OptimalityTolerance =   1e-04↙
(selected)
relative max(constraint violation) =   1.32e-05    ConstraintTolerance =   1e-04↙
(selected)

                                        First-order      Norm of
 Iter F-count            f(x)  Feasibility   optimality         step
    0       3    3.608391e+00    2.918e-01    4.010e-02
    1       6    3.612804e+00    9.884e-03    4.839e-02    8.267e-02
    2      10    3.590322e+00    8.845e-04    2.660e-02    2.094e-01
    3      14    3.579953e+00    4.685e-04    7.135e-03    1.627e-01
    4      18    3.577168e+00    4.666e-05    2.298e-03    7.571e-02
    5      22    3.576469e+00    2.332e-06    1.175e-03    2.784e-02
    6      25    3.575957e+00    1.232e-03    3.841e-04    2.867e-02
    7      28    3.575804e+00    1.153e-04    2.169e-04    8.769e-03
    8      31    3.575653e+00    2.343e-04    3.664e-05    1.250e-02
    9      34    3.575617e+00    1.333e-05    5.751e-06    2.982e-03

Optimization completed: The relative first-order optimality measure, 5.750813e-06,
is less than options.OptimalityTolerance = 1.000000e-04, and the relative maximum↙
constraint
violation, 1.333480e-05, is less than options.ConstraintTolerance = 1.000000e-04.

Optimization Metric                                          Options
relative first-order optimality =   5.75e-06       OptimalityTolerance =   1e-04↙
(selected)
relative max(constraint violation) =   1.33e-05    ConstraintTolerance =   1e-04↙
(selected)

                                        First-order      Norm of
 Iter F-count            f(x)  Feasibility   optimality         step
    0       3    3.606152e+00    1.891e-01    4.016e-02
    1       6    3.612599e+00    1.006e-02    4.825e-02    8.276e-02
    2      10    3.590156e+00    9.508e-04    2.661e-02    2.098e-01
    3      14    3.579949e+00    4.527e-04    7.142e-03    1.607e-01
    4      18    3.577169e+00    4.646e-05    2.300e-03    7.559e-02
```

```
    5      22    3.576469e+00    2.342e-06    1.175e-03    2.788e-02
    6      25    3.575957e+00    1.233e-03    3.842e-04    2.867e-02
    7      28    3.575804e+00    1.155e-04    2.169e-04    8.773e-03
    8      31    3.575653e+00    2.343e-04    3.664e-05    1.250e-02
    9      34    3.575617e+00    1.334e-05    5.562e-06    2.982e-03

Optimization completed: The relative first-order optimality measure, 5.562345e-06,
is less than options.OptimalityTolerance = 1.000000e-04, and the relative maximum↙
constraint
violation, 1.333701e-05, is less than options.ConstraintTolerance = 1.000000e-04.

Optimization Metric                                        Options
relative first-order optimality =   5.56e-06       OptimalityTolerance =   1e-04↙
(selected)
relative max(constraint violation) =   1.33e-05    ConstraintTolerance =   1e-04↙
(selected)

                                          First-order      Norm of
 Iter F-count            f(x)  Feasibility   optimality         step
    0       3    3.582569e+00    8.636e-01    3.996e-02
    1       6    3.610179e+00    1.152e-02    4.621e-02    9.173e-02
    2      10    3.592351e+00    5.535e-04    3.086e-02    1.648e-01
    3      14    3.579476e+00    8.451e-04    6.357e-03    1.976e-01
    4      18    3.577053e+00    3.532e-05    2.111e-03    6.881e-02
    5      22    3.576445e+00    1.649e-06    1.139e-03    2.477e-02
    6      25    3.575949e+00    1.176e-03    3.757e-04    2.801e-02
    7      28    3.575803e+00    1.069e-04    2.157e-04    8.441e-03
    8      31    3.575653e+00    2.324e-04    3.636e-05    1.245e-02
    9      34    3.575617e+00    1.315e-05    3.925e-06    2.961e-03

Optimization completed: The relative first-order optimality measure, 3.924602e-06,
is less than options.OptimalityTolerance = 1.000000e-04, and the relative maximum↙
constraint
violation, 1.314976e-05, is less than options.ConstraintTolerance = 1.000000e-04.

Optimization Metric                                        Options
relative first-order optimality =   3.92e-06       OptimalityTolerance =   1e-04↙
(selected)
relative max(constraint violation) =   1.31e-05    ConstraintTolerance =   1e-04↙
(selected)


GlobalSearch stopped because it analyzed all the trial points.

All 12 local solver runs converged with a positive local solver exit flag.

reliability_index =

    3.5756
```

```
probability_of_failure =

   1.7470e-04

>>
```

Appendix B

Data Collection

The field performance post-liquefaction SPT-N database is extracted from the published works of Çetin et al. (2004) and Çetin et al. (2016). In spite of several SPT-based databases available, these databases are considered because of the availability of standard deviation values for various input variables. Also, the historical cases are well categorized based on the quality of the available information. The database compiles details of 213 post-liquefaction historical cases out of which, there are 117 liquefaction cases and 96 non-liquefaction cases shown in Table B.1. It includes the earthquake events of Tohnankai, Fukui, Niigata, San Fernando, Haicheng, Guatemala, Tangshan, Argentina, Miyagiken, Imperial Valley, Mid-chba, West Morland, Nihonkai-Chhubu, Loma Prieta, Elmore Ranch, Superstition Hills, Luzon, Kushiro-Oki, Northridge and Hyogoken-Nambu, etc. The details include the year of earthquake took place, name of the earthquake event, name of the site where the sampling was taken, magnitude of the earthquake, the total pressure, effective pressure, peak ground motion, stress reduction factor, fineness content of the soil and corrected and normalized SPT-N count with respect to the critical depth. The units for total pressure and effective pressure are converted from psf to kN/m^2 for convenient calculation and

representation.

1 2

Table B.1: Field performance post liquefaction database

Case No.	Year	Liq.	σ_v	σ_v*	σ'_v	σ'_v*	$\frac{amax}{g}$	$\frac{amax}{g}*$	r_d	r_d*	M	$F.C$	$F.C*$	$(N_1)_{60}$	$(N_1)_{60}*$
1	1944	Yes	65.12	10.00	47.19	5.36	0.2	0.06	0.83	0.068	8	25	3	2.2	0.8
2	1944	Yes	53.06	8.32	38.20	4.69	0.2	0.06	0.93	0.057	8	13	1	9.4	2.9
3	1944	Yes	30.93	7.95	16.28	4.16	0.2	0.06	0.89	0.036	8	27	3	3.6	1.6
4	1948	Yes	53.17	11.92	32.21	5.63	0.4	0.12	0.95	0.055	7.3	0	0	6.6	2.2
5	1948	Yes	132.21	25.99	90.83	12.95	0.35	0.105	0.79	0.115	7.3	4	1	21.5	3.5
6	1964	Yes	130.52	17.82	61.06	9.82	0.16	0.024	0.65	0.116	7.5	8	2	12	3.1
7	1964	No	135.64	16.18	80.04	8.66	0.18	0.027	0.75	0.11	7.5	8	2	22.7	0.7
8	1964	No	211.04	11.31	116.23	7.93	0.18	0.027	0.55	0.158	7.5	8	2	27.1	3.3
9	1964	Yes	122.27	15.12	57.71	8.76	0.16	0.024	0.78	0.11	7.5	8	2	13	1.6
10	1964	No	171.36	10.37	82.30	9.30	0.16	0.024	0.65	0.14	7.5	2	2	18.8	2.5
11	1964	Yes	139.26	25.25	61.82	11.49	0.16	0.024	0.6	0.122	7.5	0	0	11.1	4.3
12	1964	No	106.43	15.09	67.22	7.98	0.18	0.027	0.78	0.097	7.5	0	0	15.1	3.9
13	1964	Yes	61.59	13.20	24.99	5.77	0.16	0.024	0.86	0.061	7.5	10	3	7.5	0.6
14	1964	No	108.31	7.16	61.45	4.76	0.18	0.027	0.87	0.91	7.5	0	0	43	3.4
15	1968	No	104.38	16.17	71.51	8.76	0.23	0.025	0.93	0.084	7.9	5	2	37.4	2.8
16	1968	No	41.90	9.36	26.96	5.06	0.23	0.025	0.96	0.042	7.9	5	2	26	2.6
17	1968	Yes	65.91	12.06	32.15	6.79	0.23	0.025	0.89	0.065	7.9	5	2	7.6	0.9
18	1968	Yes	45.74	10.91	25.71	5.31	0.2	0.04	0.95	0.05	7.9	20	3	10.4	1.4
19	1971	Yes	81.54	5.99	70.93	6.11	0.45	0.045	0.81	0.082	6.6	55	5	4.1	1
20	1971	Yes	94.92	6.81	84.47	6.47	0.45	0.045	0.86	0.094	6.6	50	5	8.2	2.8

[1] liq. denotes liquefied

[2] * denotes standard deviation of particular input variable

Table B.1: Field performance post liquefaction database

Case No.	Year	Liq.	σ_v	σ_v*	σ'_v	σ'_v*	$\frac{amax}{g}$	$\frac{amax}{g}*$	r_d	r_d*	M	$F.C$	$F.C*$	$(N_1)_{60}$	$(N_1)_{60}*$
21	1975	Yes	129.56	25.10	66.05	11.16	0.13	0.026	0.79	0.116	7.3	67	7	8.2	1.2
22	1975	Yes	137.81	14.47	69.39	7.58	0.1	0.02	0.77	0.122	7.3	5	2	11.1	1.8
23	1975	Yes	117.37	12.68	63.66	7.59	0.2	0.04	0.83	0.103	7.3	48	5	14.9	1.1
24	1975	Yes	121.32	16.96	62.70	8.13	0.2	0.04	0.74	0.11	7.3	5	2	12.5	4
25	1976	Yes	122.09	28.99	47.40	9.65	0.14	0.015	0.46	0.117	7.5	3	1	4.6	1.5
26	1976	No	53.15	7.43	32.23	2.98	0.14	0.015	0.75	0.065	7.5	3	1	8.5	1.1
27	1976	No	124.25	18.47	60.01	7.12	0.14	0.015	0.47	0.125	7.5	3	1	14.1	1.8
28	1976	Yes	72.31	8.55	40.16	4.73	0.13	0.026	0.92	0.064	8	12	3	13.2	3.2
29	1976	Yes	83.30	7.93	47.19	4.77	0.2	0.04	0.94	0.067	8	12	3	12.8	2.6
30	1976	Yes	97.24	6.74	52.15	4.63	0.35	0.07	0.92	0.076	8	20	3	23.2	2.6
31	1976	No	75.40	6.70	60.70	4.20	0.5	0.1	0.96	0.064	8	10	2	33.7	5.8
32	1976	Yes	71.87	4.85	40.01	3.79	0.2	0.04	0.92	0.061	8	5	3	11.9	5.3
33	1977	Yes	131.43	4.14	95.58	4.39	0.2	0.015	0.78	0.107	7.4	20	3	6.7	1.5
34	1977	Yes	181.77	9.54	133.22	6.65	0.2	0.015	0.56	0.144	7.4	20	3	7.3	1
35	1977	No	39.26	7.14	27.31	3.95	0.2	0.015	0.97	0.038	7.4	4	1.5	14.8	0.6
36	1977	No	45.61	4.90	38.14	3.25	0.2	0.015	0.98	0.044	7.4	3	1	14.5	0.1
37	1977	Yes	73.26	5.74	46.37	3.69	0.2	0.015	0.94	0.065	7.4	50	5	5.7	0.2
38	1978	No	84.96	17.49	44.91	8.31	0.1	0.02	0.91	0.07	6.7	0	0	14.1	2.7
39	1978	No	52.33	4.67	44.37	3.57	0.14	0.028	0.96	0.048	6.7	20	3	12.5	2.5
40	1978	No	58.83	12.76	36.28	5.96	0.12	0.024	0.89	0.054	6.7	10	2	6.2	0.5
41	1978	No	53.41	3.49	48.51	2.57	0.14	0.028	0.85	0.052	6.7	5	2	13.5	2.5
42	1978	No	71.34	11.28	53.42	5.99	0.14	0.028	0.92	0.061	6.7	3	1	12.6	5.3
43	1978	Yes	65.19	5.95	30.88	4.03	0.12	0.024	0.97	0.058	6.7	5	1	8.7	0.7

Table B.1: Field performance post liquefaction database

Case No.	Year	Liq.	σ_v	σ_v*	σ'_v	σ'_v*	$\frac{amax}{g}$	$\frac{amax}{g}*$	r_d	r_d*	M	$F.C$	$F.C*$	$(N_1)_{60}$	$(N_1)_{60}*$
44	1978	No	53.57	3.81	33.26	3.26	0.12	0.024	0.96	0.05	6.7	4	1	10.3	2
45	1978	No	91.33	10.91	74.90	8.51	0.14	0.024	0.73	0.081	6.7	5	3	9.8	1.8
46	1978	No	73.93	9.00	53.72	5.14	0.14	0.024	0.92	0.064	6.7	10	2	9.7	2.3
47	1978	No	54.89	3.21	37.35	3.16	0.12	0.024	0.94	0.051	6.7	5	1	4.1	1.8
48	1978	No	38.17	3.56	27.02	3.05	0.12	0.024	0.98	0.038	6.7	7	1	19.7	2.8
49	1978	No	49.07	5.77	22.22	3.09	0.12	0.024	0.96	0.045	6.7	12	2	12	2.1
50	1978	No	57.37	10.31	39.24	5.09	0.12	0.024	0.92	0.053	6.7	60	5	2.8	1.2
51	1978	No	60.52	9.82	32.09	5.01	0.12	0.024	0.95	0.055	6.7	0	0	13.3	5.2
52	1978	Yes	71.34	11.28	53.42	5.99	0.24	0.048	0.92	0.061	7.4	3	1	12.6	5.3
53	1978	Yes	84.96	17.49	44.91	8.31	0.2	0.04	0.91	0.07	7.4	0	0	13.1	3.6
54	1978	Yes	52.33	4.67	44.37	3.57	0.24	0.048	0.97	0.048	7.4	20	3	12.5	2.7
55	1978	Yes	58.83	12.76	36.28	5.96	0.2	0.04	0.89	0.054	7.4	10	2	6	0.7
56	1978	No	133.39	16.26	105.94	7.67	0.2	0.04	0.95	0.06	7.4	10	2	25.2	2.4
57	1978	Yes	53.41	3.49	48.51	2.57	0.28	0.056	0.85	0.052	7.4	5	2	13.5	2.9
58	1978	No	66.67	7.67	54.66	7.74	0.28	0.056	0.96	0.061	7.4	0	0	18.9	7.3
59	1978	No	76.85	9.55	55.93	5.40	0.24	0.048	0.93	0.065	7.4	26	5	15.4	3.1
60	1978	No	49.72	5.98	29.14	3.66	0.32	0.064	0.98	0.045	7.4	4	1	26.8	7.2
61	1978	Yes	65.19	5.95	30.88	4.03	0.32	0.064	0.97	0.058	7.4	5	1	8.7	0.7
62	1978	Yes	53.57	3.81	33.26	3.26	0.32	0.064	0.96	0.05	7.4	7	2	10.3	2
63	1978	Yes	91.33	10.91	74.90	8.51	0.24	0.048	0.74	0.081	7.4	5	3	9.8	2.2
64	1978	Yes	73.93	9.00	53.72	5.14	0.24	0.048	0.92	0.064	7.4	10	2	9.7	2.3
65	1978	Yes	54.89	3.21	37.35	3.16	0.24	0.048	0.95	0.051	7.4	5	1	4.1	1.8
66	1978	Yes	38.17	3.56	27.02	3.05	0.24	0.048	0.98	0.038	7.4	7	1	19.7	2.8

Table B.1: Field performance post liquefaction database

Case No.	Year	Liq.	σ_v	σ_v*	σ'_v	σ'_v*	$\frac{amax}{g}$	$\frac{amax}{g}*$	r_d	r_d*	M	$F.C$	$F.C*$	$(N_1)_{60}$	$(N_1)_{60}*$
67	1978	Yes	49.07	5.77	22.22	3.09	0.24	0.048	0.96	0.045	7.4	12	2	12	2.1
68	1978	No	131.40	10.83	70.63	7.48	0.24	0.048	0.86	0.099	7.4	17	3	26.3	8.6
69	1978	Yes	57.37	10.31	39.24	5.09	0.24	0.048	0.92	0.053	7.4	60	5	2.8	1.2
70	1978	Yes	60.52	9.82	32.09	5.01	0.24	0.048	0.95	0.055	7.4	0	0	13.3	5.2
71	1978	No	101.64	9.49	63.90	5.37	0.24	0.048	0.91	0.082	7.4	0	0	27.3	2.5
72	1979	No	35.74	2.82	30.83	3.16	0.16	0.019	0.99	0.02	6.5	30	5	17	2.8
73	1979	No	59.69	11.18	44.01	7.66	0.47	0.05	0.82	0.01	6.5	25	4	45.2	3.6
74	1979	Yes	46.64	7.05	32.72	8.70	0.47	0.05	0.78	0.02	6.5	29	4.5	3.8	2.4
75	1979	No	52.43	8.77	37.24	8.42	0.47	0.05	0.75	0.025	6.5	37	5	19.5	6.1
76	1979	No	59.79	7.38	48.59	4.26	0.13	0.01	0.83	0.03	6.5	92	10	7.2	3.5
77	1979	Yes	41.90	6.51	29.94	3.85	0.51	0.05	0.95	0.042	6.4	31	3	8.5	4.2
78	1979	Yes	61.85	6.50	39.80	3.96	0.18	0.019	0.97	0.03	6.5	75	10	6.8	5.2
79	1979	Yes	15.47	3.75	8.14	1.94	0.16	0.045	0.99	0.015	6.5	80	10	4	3.4
80	1979	No	72.78	11.45	35.43	6.69	0.17	0.045	0.67	0.035	6.5	40	3	12.8	5.7
81	1980	No	90.00	8.57	45.05	4.92	0.1	0.001	0.75	0.076	6.1	13	1	6.3	0.6
82	1980	No	238.45	10.48	105.28	7.78	0.1	0.001	0.33	0.149	6.1	27	1	3.7	0.6
83	1981	Yes	59.79	7.38	48.59	4.26	0.19	0.025	0.83	0.012	5.9	92	10	7.2	3.5
84	1981	Yes	61.85	6.45	39.80	3.87	0.17	0.02	0.89	0.012	5.9	75	10	6.8	5.2
85	1981	No	35.74	2.69	30.83	3.05	0.16	0.02	0.98	0.01	5.9	30	5	17	2.8
86	1981	No	15.47	3.75	8.14	1.94	0.17	0.02	0.99	0.003	5.9	80	10	4	3.4
87	1981	No	72.78	5.85	33.94	3.53	0.17	0.02	0.97	0.01	5.9	18	3	20.2	7.7
88	1981	Yes	72.78	10.67	35.43	5.25	0.23	0.02	0.89	0.013	5.9	40	3	12.8	5.7
89	1981	No	41.90	1.72	29.94	3.85	0.09	0.023	0.93	0.01	5.9	31	3	8.5	4.2

Table B.1: Field performance post liquefaction database

Case No.	Year	Liq.	σ_v	σ_v*	σ'_v	σ'_v*	$\frac{amax}{g}$	$\frac{amax}{g}*$	r_d	r_d*	M	$F.C$	$F.C*$	$(N_1)_{60}$	$(N_1)_{60}*$
90	1964	Yes	52.82	7.05	30.77	4.21	0.09	0.018	0.9	0.054	7.5	5	2	4.8	2.6
91	1964	Yes	85.16	10.50	42.66	6.24	0.16	0.024	0.78	0.081	7.5	8	2	12	2.1
92	1968	Yes	94.84	10.29	38.48	5.88	0.21	0.03	0.8	0.087	7.8	3	1	16.3	1.6
93	1976	No	61.66	12.73	38.13	6.51	0.22	0.044	0.96	0.052	8	5	3	26.5	3.6
94	1976	Yes	56.00	11.13	32.48	5.38	0.22	0.044	0.96	0.052	8	3	2	8.8	0.9
95	1983	No	69.32	18.00	37.46	8.04	0.15	0.03	0.84	0.061	7.1	15	4	8.9	4.9
96	1983	No	158.26	8.91	77.40	6.58	0.15	0.03	0.63	0.118	7.1	0	1	17.7	4.5
97	1983	Yes	73.95	11.30	33.27	5.86	0.12	0.022	0.8	0.064	7.1	0	1	14.6	1.6
98	1983	Yes	94.84	10.29	38.48	5.88	0.12	0.018	0.8	0.079	7.7	3	1	16.3	1.6
99	1983	Yes	69.32	18.00	37.46	8.04	0.2	0.04	0.85	0.061	7.7	15	4	8.9	4.9
100	1983	Yes	123.10	27.86	53.40	12.28	0.23	0.035	0.74	0.099	7.7	1	1	12.3	2.9
101	1983	Yes	54.98	8.41	37.83	4.46	0.25	0.055	0.93	0.052	7.7	1	1	16.4	3.6
102	1983	Yes	73.95	11.30	33.27	5.86	0.28	0.04	0.81	0.064	7.7	0	1	14.6	1.6
103	1983	No	56.55	6.36	44.30	9.51	0.204	0.01	0.999	0.045	7.7	2.7	1.5	16	2.8
104	1983	Yes	195.62	47.32	107.11	23.04	0.2214	0.032	0.622	0.131	7.7	5.5	6.9	6.9	2.1
105	1983	No	98.96	17.38	63.19	12.36	0.051	0.003	0.917	0.073	7.7	66	45.3	5.2	2.1
106	1983	Yes	138.61	35.54	82.35	16.84	0.208	0.031	0.79	0.099	7.7	14.6	17.4	8.7	3
107	1983	Yes	106.86	23.00	67.16	11.68	0.207	0.031	0.904	0.076	7.7	2	1	6.6	2
108	1983	Yes	72.57	11.70	49.54	5.80	0.203	0.03	0.961	0.056	7.7	8	5.7	9	6.2
109	1983	Yes	38.99	8.11	30.95	3.67	0.207	0.031	0.952	0.037	7.7	3	2	5.4	0.2
110	1983	Yes	119.94	29.63	72.39	14.40	0.202	0.03	0.857	0.087	7.7	7.8	3	10.8	4.2
111	1983	Yes	115.51	26.36	56.40	11.72	0.204	0.031	0.728	0.09	7.7	1.1	0.5	7.3	4.6
112	1983	No	107.78	13.33	67.62	10.75	0.174	0.026	0.973	0.076	7.7	3	1	24	2.9

Table B.1: Field performance post liquefaction database

Case No.	Year	Liq.	σ_v	σ_v*	σ'_v	σ'_v*	$\frac{amax}{g}$	$\frac{amax}{g}*$	r_d	r_d*	M	$F.C$	$F.C*$	$(N_1)_{60}$	$(N_1)_{60}*$
113	1989	Yes	88.58	7.16	58.70	3.87	0.25	0.075	0.99	0.007	6.93	3	1.4	19.8	6.7
114	1989	No	97.63	17.43	67.29	9.89	0.25	0.075	0.98	0.007	6.93	5	2	25.8	6
115	1989	No	35.86	3.39	32.38	1.85	0.25	0.075	0.99	0.007	6.93	5	2	15.1	3
116	1987	No	61.85	6.45	39.80	3.87	0.09	0.025	0.97	0.032	6.2	75	10	6.8	5.2
117	1987	No	72.78	10.67	35.43	5.25	0.09	0.005	0.75	0.035	6.2	40	3	12.8	5.7
118	1987	No	61.85	6.45	39.80	3.87	0.2	0.04	0.94	0.032	6.6	75	10	6.8	5.2
119	1987	Yes	72.78	10.67	35.43	5.25	0.18	0.005	0.84	0.035	6.6	40	3	12.8	5.7
120	1987	No	59.69	11.18	44.01	7.66	0.16	0.02	0.82	0.022	6.7	25	4	44	3.6
121	1987	No	46.64	7.48	32.72	9.04	0.15	0.02	0.78	0.024	6.7	29	4.5	3.8	2.4
122	1987	No	52.43	8.77	37.24	8.42	0.13	0.02	0.75	0.025	6.7	37	5	19.5	6.1
123	1987	No	59.79	7.38	48.59	4.26	0.17	0.02	0.83	0.03	6.7	92	10	7.2	3.5
124	1987	No	41.90	6.51	29.94	3.85	0.16	0.02	0.95	0.025	6.7	31	3	8.5	4.2
125	1987	No	35.74	3.19	30.83	3.50	0.18	0.02	0.99	0.02	6.7	30	5	17	2.8
126	1987	No	15.47	3.76	8.14	3.07	0.19	0.02	0.99	0.01	6.7	80	10	4	3.4
127	1987	No	72.78	5.85	33.94	3.53	0.19	0.02	0.97	0.025	6.7	18	3	20.2	7.7
128	1989	No	125.28	4.43	90.97	8.89	0.24	0.024	0.95	0.087	7	7	2	42.6	1.8
129	1989	Yes	86.01	7.79	71.30	10.32	0.37	0.05	0.9	0.02	7	8	2	10.9	2.5
130	1989	No	68.04	6.76	57.01	5.68	0.14	0.013	0.72	0.013	7	30	7	5.3	3.7
131	1989	Yes	61.38	8.82	46.19	8.47	0.24	0.025	0.99	0.011	7	3	1	12.5	0.9
132	1989	No	39.27	3.60	34.37	2.68	0.24	0.025	0.99	0.007	7	1	2	23.9	3.5
133	1989	No	68.41	14.00	45.86	6.90	0.27	0.025	0.99	0.007	7	1	2	18.7	3.5
134	1989	Yes	42.37	5.28	32.06	3.49	0.26	0.025	0.99	0.008	7	2	2	16.1	1
135	1989	Yes	86.40	10.34	66.79	5.20	0.42	0.05	0.84	0.017	7	22	3	10	4.4

Table B.1: Field performance post liquefaction database

Case No.	Year	Liq.	σ_v	σ_v*	σ'_v	σ'_v*	$\frac{amax}{g}$	$\frac{amax}{g}*$	r_d	r_d*	M	$F.C$	$F.C*$	$(N_1)_{60}$	$(N_1)_{60}*$
136	1989	Yes	124.49	8.44	70.58	5.44	0.41	0.05	0.88	0.024	7	20	3	24	3.5
137	1989	Yes	96.57	6.84	87.50	7.42	0.46	0.05	0.83	0.019	7	27	5	11.6	4.1
138	1989	Yes	115.38	9.64	92.84	5.75	0.41	0.05	0.9	0.016	7	13	2	21.9	3.5
139	1989	Yes	98.26	8.50	82.57	5.18	0.46	0.05	0.73	0.013	7	15	2	10.3	1
140	1989	Yes	41.45	5.03	32.35	3.54	0.29	0.025	0.95	0.01	7	2	2	8.5	1.6
141	1989	Yes	75.77	11.10	56.35	5.62	0.24	0.025	0.99	0.013	7	1	2	19	2.5
142	1989	Yes	111.10	4.77	80.22	6.81	0.22	0.01	0.95	0.018	7	3	1	13	3.1
143	1989	Yes	117.42	4.18	83.12	4.38	0.22	0.01	0.83	0.018	7	5	1	13.2	4.1
144	1989	Yes	66.46	4.85	52.78	3.85	0.15	0.013	0.71	0.017	7	50	5	3.8	1.2
145	1989	Yes	117.81	5.65	85.96	4.87	0.27	0.01	0.77	0.013	7	8	3	8.1	2.2
146	1989	Yes	26.70	4.01	19.35	3.22	0.25	0.025	0.99	0.005	7	35	5	9.7	0.3
147	1989	Yes	53.89	3.07	44.04	3.19	0.26	0.025	0.99	0.008	7	3	1	15.9	3.5
148	1989	Yes	85.42	20.78	48.66	10.33	0.18	0.01	0.88	0.012	7	20	4	7.6	4.6
149	1990	No	85.81	15.52	59.83	7.78	0.25	0.025	0.91	0.069	7.6	19	2	26.2	5.3
150	1990	Yes	127.36	19.88	78.84	9.91	0.25	0.025	0.82	0.096	7.6	19	2	14	2.8
151	1993	Yes	383.92	15.20	198.66	12.99	0.4	0.04	0.47	0.149	8	10	3	7.2	1.9
152	1993	Yes	89.15	7.59	57.29	4.80	0.4	0.04	0.94	0.073	8	2	1	17.1	4.2
153	1993	No	200.13	21.24	110.44	11.68	0.4	0.04	0.79	0.134	8	0	1	30.3	3.6
154	1994	Yes	159.76	6.92	142.11	6.96	0.69	0.06	0.71	0.005	6.7	43	13	18.5	4
155	1994	Yes	172.44	7.79	120.00	5.76	0.51	0.06	0.7	0.006	6.7	25	5	24.4	2.7
156	1994	Yes	119.86	4.42	88.49	4.02	0.4	0.04	0.72	0.087	6.7	37	5	10.5	0.7
157	1994	Yes	112.59	4.48	93.48	4.08	0.54	0.04	0.86	0.04	6.7	38	23	11	1.6
158	1995	No	141.62	7.53	98.00	5.28	0.4	0.05	0.82	0.104	6.9	2	1	31.3	5.9

Table B.1: Field performance post liquefaction database

Case No.	Year	Liq.	σ_v	σ_v*	σ'_v	σ'_v*	$\frac{amax}{g}$	$\frac{amax}{g}*$	r_d	r_d*	M	$F.C$	$F.C*$	$(N_1)_{60}$	$(N_1)_{60}*$
159	1995	No	88.44	10.53	71.78	5.85	0.4	0.05	0.89	0.072	6.9	18	4	21.6	7.1
160	1995	Yes	152.57	8.52	101.11	5.82	0.4	0.05	0.64	0.113	6.9	2	1	12.9	3.1
161	1995	Yes	240.19	10.79	141.18	8.14	0.4	0.05	0.41	0.149	6.9	18	4	5.8	2.8
162	1995	Yes	146.52	35.22	94.08	18.06	0.34	0.01	0.71	0.101	6.9	20	5	6.9	1.7
163	1995	No	155.12	23.24	120.82	12.31	0.4	0.04	0.8	0.11	6.9	20	5	21.9	4.1
164	1995	No	184.58	33.03	135.57	17.13	0.4	0.04	0.73	0.126	6.9	20	5	18.6	3.3
165	1995	No	174.76	29.76	130.65	15.51	0.4	0.04	0.84	0.121	6.9	20	5	32.2	7
166	1995	Yes	183.79	25.59	115.18	13.22	0.34	0.04	0.67	0.126	6.9	20	5	10.8	1.8
167	1995	Yes	137.84	23.16	103.54	12.16	0.4	0.05	0.89	0.099	6.9	25	5	17.1	6.9
168	1995	Yes	210.50	47.43	136.98	23.38	0.34	0.04	0.59	0.142	6.9	20	5	12.2	3.5
169	1995	Yes	82.08	10.52	35.52	5.85	0.25	0.04	0.87	0.067	6.9	20	7	15.5	3.5
170	1995	No	104.70	6.63	68.92	4.62	0.4	0.06	0.93	0.082	6.9	4	1.5	57.7	3.2
171	1995	No	149.01	21.45	94.02	10.72	0.4	0.06	0.83	0.11	6.9	15	5	42.7	9.6
172	1995	No	95.43	12.30	66.02	6.53	0.4	0.06	0.91	0.076	6.9	4	1	54.2	7.2
173	1995	No	76.74	9.86	50.27	5.23	0.4	0.06	0.9	0.067	6.9	4	1	43.5	5.3
174	1995	Yes	155.70	14.15	99.53	7.91	0.35	0.045	0.71	0.113	6.9	2	1	6.9	1.6
175	1995	Yes	102.97	9.41	68.67	5.62	0.4	0.06	0.84	0.079	6.9	25	3	22.7	3.9
176	1995	Yes	111.33	12.37	80.55	6.76	0.4	0.06	0.81	0.085	6.9	0	0	27.3	1.7
177	1995	Yes	80.15	5.95	60.06	4.20	0.5	0.075	0.89	0.07	6.9	0	0	24.5	2.9
178	1995	Yes	73.33	6.36	58.33	4.22	0.5	0.075	0.89	0.061	6.9	3	1	12.1	5.3
179	1995	No	126.09	9.28	96.30	5.75	0.6	0.09	0.75	0.099	6.9	9	1	27.7	4.2
180	1995	Yes	110.20	16.85	58.25	8.02	0.5	0.075	0.7	0.09	6.9	5	1	8.3	2.3
181	1995	No	84.91	6.00	64.32	4.28	0.5	0.075	0.83	0.073	6.9	13	3	26.7	1.3

Table B.1: Field performance post liquefaction database

Case No.	Year	Liq.	σ_v	σ_v*	σ'_v	σ'_v*	$\frac{amax}{g}$	$\frac{amax}{g}*$	r_d	r_d*	M	$F.C$	$F.C*$	$(N_1)_{60}$	$(N_1)_{60}*$
182	1995	Yes	105.40	8.78	64.24	5.27	0.5	0.075	0.81	0.087	6.9	18	3	13.3	1.5
183	1995	No	76.74	3.54	60.08	3.71	0.5	0.075	0.84	0.068	6.9	18	3	22.5	2.3
184	1995	Yes	92.38	6.74	71.56	4.57	0.5	0.075	0.76	0.079	6.9	5	2	19.9	4.4
185	1995	No	72.30	3.41	52.20	3.58	0.6	0.09	0.93	0.064	6.9	5	1	26.1	1.5
186	1995	Yes	73.64	8.59	36.88	4.95	0.5	0.075	0.93	0.064	6.9	5	1	23.2	7.9
187	1995	No	183.67	10.39	155.74	7.14	0.7	0.105	0.62	0.131	6.9	0	0	38.6	4.1
188	1995	No	125.91	4.97	112.18	4.86	0.6	0.09	0.86	0.099	6.9	10	1	21.7	1
189	1995	No	105.25	12.38	66.04	6.67	0.55	0.09	0.93	0.082	6.9	0	0	64.3	2
190	1995	No	60.64	3.42	42.50	3.26	0.6	0.09	0.96	0.052	6.9	0	0	36.4	3.2
191	1995	No	104.62	12.36	69.33	6.64	0.6	0.09	0.86	0.082	6.9	6	2	40.8	12.2
192	1995	No	85.61	6.45	66.01	4.36	0.6	0.09	0.89	0.07	6.9	8	2	24.3	1
193	1995	Yes	59.53	3.46	48.26	3.30	0.5	0.075	0.96	0.052	6.9	0	0	25.3	1.4
194	1995	No	59.85	3.44	46.62	3.28	0.7	0.105	0.96	0.052	6.9	4	1	39.4	1.2
195	1995	No	59.77	3.37	34.29	3.48	0.6	0.09	0.97	0.052	6.9	0	0	43.1	6.8
196	1995	No	40.41	2.98	26.20	3.17	0.6	0.09	0.98	0.039	6.9	10	2	52.2	5.7
197	1995	Yes	72.85	3.44	45.89	3.61	0.4	0.06	0.93	0.064	6.9	10	2	26.3	4
198	1995	Yes	61.66	4.65	44.50	3.55	0.4	0.06	0.94	0.055	6.9	0	0	18.8	3.4
199	1995	No	139.02	9.40	70.41	6.24	0.6	0.09	0.73	0.11	6.9	10	1	43.4	6.6
200	1995	No	67.23	6.09	39.79	4.02	0.6	0.09	0.94	0.058	6.9	0	0	59.8	6.3
201	1995	No	53.88	8.02	33.30	4.33	0.5	0.09	0.94	0.052	6.9	6	2	32.2	3.5
202	1995	No	130.38	6.79	71.57	5.32	0.5	0.075	0.74	0.104	6.9	50	5	30.3	2.1
203	1995	Yes	114.05	16.85	63.07	8.02	0.4	0.06	0.73	0.093	6.9	9	1	25.8	3.7
204	1995	Yes	72.62	8.49	48.60	4.77	0.5	0.075	0.86	0.064	6.9	8	2	19	2.6

Table B.1: Field performance post liquefaction database

Case No.	Year	Liq.	σ_v	σ_v*	σ'_v	σ'_v*	$\frac{amax}{g}$	$\frac{amax}{g}*$	r_d	r_d*	M	$F.C$	$F.C*$	$(N_1)_{60}$	$(N_1)_{60}*$
205	1995	No	56.99	3.25	31.90	3.42	0.6	0.09	0.93	0.052	6.9	3	1	36.6	1.5
206	1995	Yes	62.83	11.28	62.83	5.81	0.35	0.05	0.92	0.058	6.9	0	0	22.3	3.1
207	1995	Yes	129.60	11.59	80.59	6.39	0.5	0.075	0.73	0.104	6.9	5	1	20.1	2.8
208	1995	No	77.21	3.66	58.59	3.50	0.6	0.09	0.96	0.064	6.9	0	0	66.1	4.4
209	1995	No	61.03	3.52	54.17	3.57	0.6	0.09	0.97	0.052	6.9	0	0	43.6	10.8
210	1995	Yes	69.71	10.96	48.88	5.72	0.4	0.06	0.93	0.059	6.9	0	0	14.7	2.9
211	1995	Yes	77.64	5.82	39.90	4.22	0.4	0.06	0.81	0.07	6.9	10	1	12.2	0.5
212	1995	Yes	75.01	3.45	50.50	3.62	0.35	0.05	0.91	0.066	6.9	20	2	15.2	0.3
213	1995	Yes	61.62	5.55	37.60	3.84	0.4	0.06	0.87	0.058	6.9	5	1	8	2

Appendix C

MATLAB Output for Neural Network Modelling

The MATLAB programming script for neural network modelling of LI function is presented below

```
clc;
clear all;
close all;
trainset=importdata('data set/trainingset.txt');
testset=importdata('data set/testset.txt');
traininput=trainset(:,1:4);
trainoutput=trainset(:,5);
testinput=testset(:,1:4);
testoutput=testset(:,5);
traininput=traininput';
trainoutput=trainoutput';
testinput=testinput';
testoutput=testoutput';
xr=minmax(traininput); b=ones(4,1);
for i=2:4
    a(i,1)=((xr(i,2))-(9*xr(i,1)))/8;
    b(i,1)=((xr(i,2))-(xr(i,1)))/0.8;
end
```

```
for i=1:163
    traininput(:,i)=((traininput(:,i)+a))./b;
end
xr=minmax(testinput);
for i=2:4
    a(i,1)=((xr(i,2))-(9*xr(i,1)))/8;
    b(i,1)=((xr(i,2))-(xr(i,1)))/0.8;
end
for i=1:50
    testinput(:,i)=((testinput(:,i)+a))./b;
end
net=newff(traininput,trainoutput,4);
numNN = 10;
NN = cell(1, numNN);
perfs = zeros(1, numNN);
for i = 1:numNN
  fprintf('Training %d/%d\n', i, numNN);
  net=configure(net,traininput,trainoutput);
net.layers{1}.transferFcn = 'logsig';
net.layers{2}.transferFcn = 'logsig';
net.divideFcn= 'divideind';
net.divideParam.trainInd=1:163;
net.trainFcn = 'trainlm';
net.inputs{1}.processFcns= {};
net.outputs{2}.processFcns={};
net.inputWeights{1,1}.learnParam.lr = 0.1;
net.biases{1,1}.learnParam.lr = 0.1;
net.trainParam.min_grad=1e-4;
net.trainParam.max_fail=100;
net.trainParam.goal=1e-3;
net.trainParam.epochs=1000;
  [NN{i}, tr(i)] = train(net,traininput,trainoutput);
  y1 = NN{i}(testinput);
  perfs(i) = mse(net,testoutput,y1)
end
```

```
>> perfs

perfs =

    0.1980    0.2132    0.1605    0.2400    0.2303    0.1906    0.2423    0.2200↙
0.2057    0.1558

>> [r,m,b]=regression(y1,testoutput)

r =

    0.6477


m =

    0.7983


b =

    0.0529

>> y1 = NN{10}(testinput);
>> [r,m,b]=regression(y1,testoutput)

r =

    0.6477


m =

    0.7983


b =

    0.0529

>> NN{3}(testinput)'

ans =

    1.0000
    1.0000
    1.0000
         0
    1.0000
    1.0000
```

```
    1.0000
    1.0000
    0.0000
    1.0000
    1.0000
    1.0000
    1.0000
    1.0000
    1.0000
         0
    1.0000
    1.0000
    1.0000
    1.0000
         0
         0
         0
         0
    1.0000
    1.0000
    1.0000
    1.0000
    1.0000
    1.0000
    1.0000
    1.0000
    1.0000
    1.0000
    0.1518
    1.0000
    0.0000
    1.0000
         0
    0.0000
         0
    1.0000
    1.0000
    0.0000
    0.0000
         0
    1.0000
    1.0000
         0

>> y1 = NN{3}(testinput);
>> plotregression(testoutput,y1)
>> y2 = NN{3}(traininput);
>> plotregression(trainoutput,y2)
>> completeinput=traininput;
```

```
>> completeoutput=trainoutput;



>> for i=164:213   completeinput(:,i)=testinput(:,i-163); end
>> for i=164:213   completeoutput(:,i)=testoutput(:,i-163); end
>> y2 = NN{3}(completeinput);
>> [r,m,b]=regression(y2,completeoutput)

r =

    0.8906


m =

    0.9085


b =

   -0.0016

>> plotregression(y2,completeoutput)
>> tr(3)

ans =

  struct with fields:

        trainFcn: 'trainlm'
      trainParam: [1×1 struct]
       performFcn: 'mse'
     performParam: [1×1 struct]
         derivFcn: 'defaultderiv'
        divideFcn: 'divideind'
       divideMode: 'sample'
      divideParam: [1×1 struct]
         trainInd: [1×163 double]
           valInd: [0×1 double]
          testInd: [0×1 double]
             stop: 'Minimum gradient reached.'
       num_epochs: 228
        trainMask: {[1×163 double]}
          valMask: {[1×163 double]}
         testMask: {[1×163 double]}
       best_epoch: 228
             goal: 1.0000e-03
```

```
          states: {'epoch'  'time'  'perf'  'vperf'  'tperf'  'mu'  'gradient'↙
'val_fail'}
           epoch: [1×229 double]
            time: [1×229 double]
            perf: [1×229 double]
           vperf: [1×229 double]
           tperf: [1×229 double]
              mu: [1×229 double]
        gradient: [1×229 double]
        val_fail: [1×229 double]
       best_perf: 0.0245
      best_vperf: NaN
      best_tperf: NaN

>> plotperform(tr(3))
>> plottrainstate(tr(3))
>> genFunction(NN{3},'LI')

MATLAB function generated: LI.m
To view generated function code: edit LI
For examples of using function: help LI

>> NN{3}.IW

ans =

  2×1 cell array

    [4×4 double]
    []

>> NN{3}.IW{1}

ans =

   -2.0249   -0.7516   21.9303    0.9669
  188.2523   52.6672   64.8545   54.0202
   44.3555   -7.0789  -33.1357    8.8690
  -89.1416   18.7082  112.4106  -20.7840

>> NN{3}.LW{2}

ans =

   1.0e+03 *

   -2.5534    0.4192    1.9627    1.2375

>> NN{3}.b{1}
```

```
ans =

   -8.4126
  -88.6730
    1.0270
  -12.8847

>> NN{3}.b{2}

ans =

  -1.6250e+03

>>
```